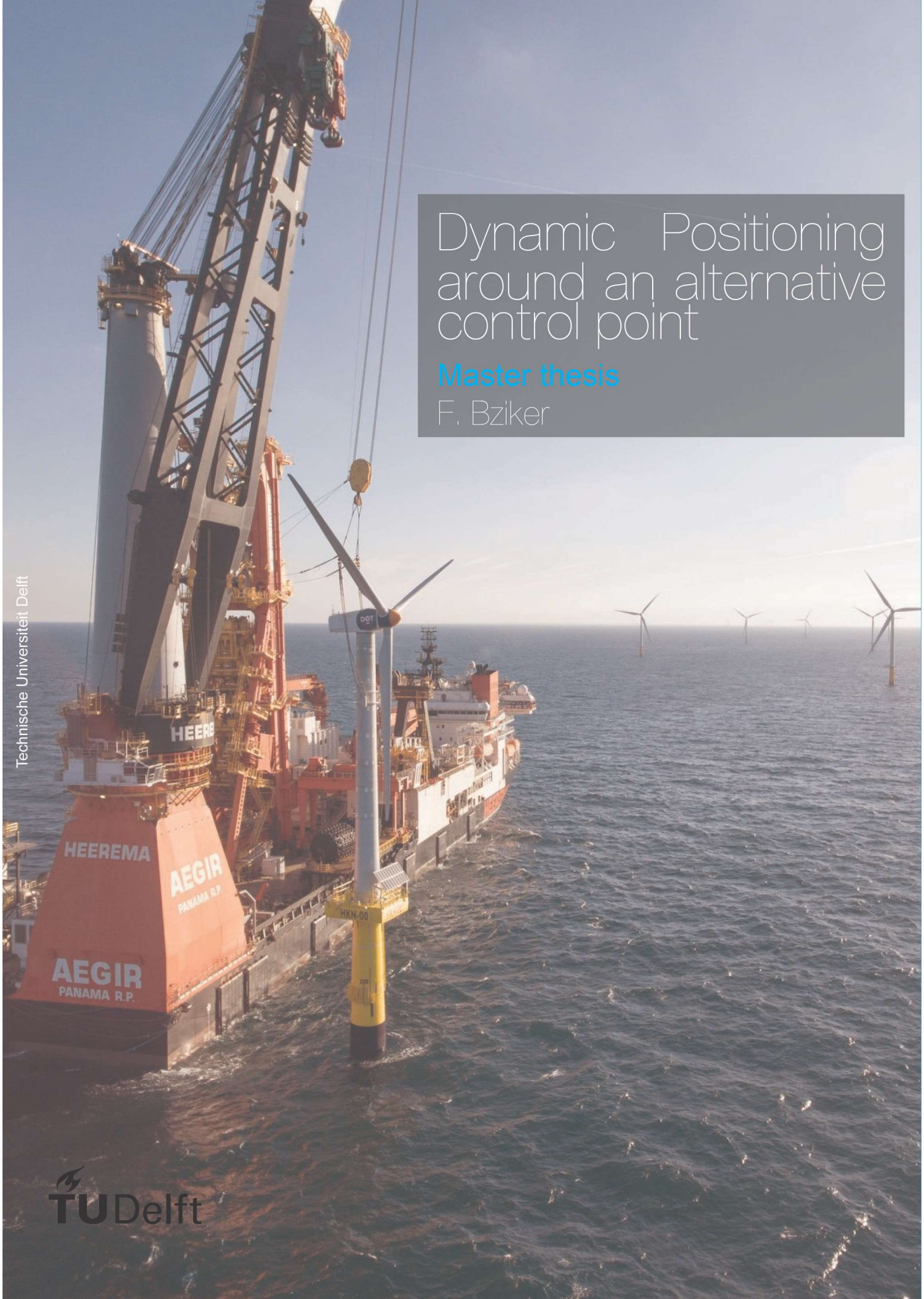

Dynamic Positioning around an alternative control point

Master thesis

F. Bziker

Technische Universiteit Delft

TU Delft

Dynamic Positioning around an alternative control point

Master thesis

by

F. Bziker

to obtain the degree of Master of Science
at the Delft University of Technology,
to be defended publicly on 8th of June at 10:00.

Student number:	5069327	
Project duration:	December 15th, 2021 - June 8th, 2023	
Thesis committee:	Ir. K. Visser	TU Delft, chairman
	Dr. H. Seyffert	TU Delft, supervisor
	Dr. V. Reppa	TU Delft, committee
	Ir. Y. Rentoulis	Heerema Engineering Solutions, committee
	Dr. A. Pistidda	Heerema Engineering Solutions, committee

An electronic version of this thesis is available at http://repository.tudelft.nl/.

TU Delft

Abstract

Traditionally, the control point (CP) of a dynamically positioned vessel is located around its center of gravity (CoG). However, during offshore operations, other locations, such as the crane tip or gripper position, become more critical due to the load being located there. This thesis proposes shifting the control point from the CoG to an alternative location, specifically the gripper position, to minimize the DP footprint at this location. Minimizing the DP footprint at the gripper location could lead to smaller motion deviations at this critical point. Consequently, this could potentially improve the workability of the vessel, which in turn could lead to higher operational yields. Additionally, the risk of potential damage and unsafe situations offshore is mitigated.

The conventional DP system contains a Kalman Filter, to filter out the first-order motions, a P(I)D controller that calculates the demanded forces to keep the vessel in place, and a thruster allocation algorithm that distributes the demanded forces to all the thrusters in an optimized way.

A new design for a DP system with the control point at the gripper position for the Deepwater Construction Vessel (DCV) Aegir is presented and evaluated. Time domain simulations were performed with the Aegir containing its conventional DP system and with the Aegir containing the newly designed DP system. These time domain simulations were performed using Orcaflex, which contains a model of the Aegir. This model of the vessel is connected to an external Python code, that contains the DP system, including a thruster allocation.

As the new DP system at the gripper location has to cope with coupled equations of motion, it is equipped with a new Multiple-Input-Multiple-Output (MIMO) PD controller, that consists of a decoupling module and separate PD controllers for each DOF. To obtain state estimates for the second-order motions at the gripper location, the state estimates calculated by the Kalman Filter are translated to the gripper location.

The effects on DP performance were assessed by evaluating and comparing the motion responses in the horizontal plane and DP footprint at the gripper location of both models. Also, the thruster behavior and energy consumption of both models are compared. This was done for an incoming wave direction of 135 degrees, a peak period (Tp) of 8 seconds, and significant wave heights (Hs) from 1.0 m to 2.0 m with increments of 0.5 m. The wave spectrum used is a JONSWAP spectrum. Three-hour simulations are performed for the so-called 'base case' sea state with Hs = 1.5m. However, due to the extensive simulation time only one-hour simulations were performed for the cases with Hs = 1.0m and 2.0m.

When comparing the motion responses, differences are considered marginal. Lower responses were found for the yaw motion in all tested sea states. Further on, the motion responses for sway appeared to be bigger for the gripper control point compared to the center control point in Hs = 1.5m and Hs = 1.0 m. However, the differences in sway are observed to be marginal for Hs = 2.0m.

The results show that the DP footprint has slightly improved in the x-direction for the gripper control point model compared to the center control point model for the base case. The same observation is done for Hs = 2.0m, but the differences found between the models in Hs = 1.0m are marginal. Also, the DP footprint was observed to be slightly larger in the y-direction for Hs = 1.0m and Hs = 1.5m for the gripper control point.

The total thrust outputs as delivered by the DP system during the simulations were converted to power and energy consumption. From these results, it became clear that the gripper point control model consumes less energy in all tested sea states compared center control point model.

From the results presented in this study, it is concluded that the system itself has potential, but no hard conclusions can be drawn for the system in its current form. In summary, based on the tests performed, responses of interest were quite comparable between the two models and therefore it cannot be concluded whether controlling around the alternative point provides an advantage or not. It is recommended to look into the response of the system in more sea states. Since in this thesis, only the responses to waves are checked, it is recommended to look into the responses to more sudden excitations too. Problems were observed with the current thruster allocation algorithm from HES, which need to be explored in more detail and resolved.

Preface

This Master's thesis is the final part to obtain the Master of Science degree in Marine Technology at the Delft University of Technology. The work was performed at the Delft University of Technology, in the Department of Ship Hydromechanics, and in cooperation with Heerema Engineering Solutions.

I would like to send my special thanks to my supervisor Harleigh Seyffert for her encouragement, advice and help when things got tough, and for her guidance through the process. I would also like to extend my appreciation to all other faculty members who shared their knowledge and insights during discussions. I would like to thank Klaas Visser for being the chairman of my committee, for his suggestions, and for always bringing his enthusiasm to the meetings and discussions. I would also like to thank Vasso Reppa for joining the committee and bringing her expertise from the Control Theory perspective.

I would like to thank Heerema Engineering Solutions for giving me the opportunity to explore the subject of Dynamic Positioning. Special thanks to Yannis Rentoulis and Alessio Pistidda for their help and patience. Their contributions enriched my understanding of the field of Dynamic Positioning and provided me with a broader perspective on the subject matter.

Finally, I would like to thank my dad, Soufiane, and all of my friends for their support during the process. Special thanks to my friend Stan Zwinkels, for studying together during the thesis and the insightful discussions we had along the process.

I wish you all a very pleasant read.

F. Bziker
Rotterdam, May 2023

Contents

List of Figures

List of Tables

Abbreviations

CoG Center of Gravity

CP Control Point

DCV Deep Water Construction Vessel

DNV Det Norske Veritas

DOF Degrees Of Freedom

DP Dynamic Positioning

HES Heerema Engineering Solutions

IMO International Maritime Organisation

JONSWAP Joint Northsea Wave Project

LF Low frequency

MARIN Maritime Research Institute Netherlands

MIMO Multiple-Input-Multiple-Output

PID Proportional-Integral-Derivative

QTF Quadratic Transfer Function

RAO Response Amplitude Operator

RMSE Root Mean Square Error

WF Wave frequency

Nomenclature

$\hat{\mathbf{x}}_k$	A posteriori estimates
$\hat{\mathbf{x}}_k$	A priori estimates
$\mathbf{K}_k$	Kalman Gain Matrix
$\mathbf{P}_k$	A posteriori estimate covariance matrix
$\mathbf{P}_k$	A priori estimate covariance matrix
$\mathbf{Q}_k$	Process noise covariance matrix
$\mathbf{R}_k$	Measurement noise covariance matrix
$\mathbf{z}_k$	Measurements
ω	Circular frequency in rad/s
$\overline{T}_i$	Total deliverable force per thruster, for $i = 1, ..6$
ψ	Yaw motion
$\tilde{F_T}$	Total thruster force when thrusters are saturated
ζ	Wave elevation
ζ_a	Amplitude of the wave elevation
A	Added mass
B	Damping
b_{ij}	Hydrodynamic damping coefficient for $i = 1, 2, 6 \wedge j = 1, 2, 6$
C	Spring stiffness
F	Force
f	Frequency in Hz
F_i^D	Drift force in the surge, sway and yaw direction respectively for $i = 1, 2, 6$
f_p	Peak frequency in Hz
F_T	Total thruster force when thrusters are not saturated
$f_{x,i}$	Thruster forces in the x-direction for thruster $i = 1, .., 6$
$f_{y,i}$	Thruster forces in the y-direction for thruster $i = 1, .., 6$
H_s	Significant wave height
I_{zz}	Moment of inertia around the z-axis
k	Wave number
K_i^D	Derivative gain for the surge, sway and yaw motion respectively for $i = 1, 2, 6$
K_i^I	Integral gain for the surge, sway and yaw motion respectively for $i = 1, 2, 6$

K_i^P	Proportional gain for the surge, sway and yaw motion respectively for $i = 1, 2, 6$
M	Solid mass of a vessel
P	Power
$S(f)$	Wave spectrum
T	Period
T_i	Total force per thruster for $i = 1, .., 6$
T_p	Peak period
x_p	Distance in x-direction from center to gripper location
y_p	Distance in y-direction from center to gripper location

1 Introduction

The offshore wind market is growing at a rapid pace as offshore wind energy has emerged as a significant source of renewable power generation globally. As many oil and gas fields are becoming superannuated and will eventually cease production as they are reaching the end of their life cycles, the decommissioning market for the oil and gas infrastructure will grow as well. The installation and removal of the above-mentioned offshore facilities often happen using either a Dynamic Positioning (DP) system or a mooring configuration. As a DP system has proven to save a lot of time, and thus money, it is usually the preferred choice against the conventional mooring system. Since offshore operations become increasingly complex and demanding, there is a growing need to enhance DP performance.

Conventionally, the Control Point (CP) of a dynamically positioned vessel lies around its Center of Gravity (CoG), which is an obvious choice since the vessel dynamically moves around this point. Besides, it is the most straightforward to choose this point in order to prevent the system from having to cope with coupled equations of motion, which could make calculations more complex. However, the CoG is often not the point of highest interest. During offshore operations, it is often found that locations such as the crane tip are of greater importance than the CoG since that is where the load is located. Therefore, Heerema Engineering Solutions (HES) proposed the idea of shifting the control point from the CoG to an alternative location in order to minimize the DP footprint at this location. Minimizing the DP footprint at another location means that the motion deviations at this location ought to be minimized. Smaller motion deviations of the location of interest could lead to higher workability of the vessel and the prevention of potential damage and/or unsafe situations for the crew. This thesis aims to present the design of this newly proposed system and explore whether implementing this method, can potentially improve the DP footprint at the desired location of interest.

1.1. Motivation

The Aegir is one of the Deep Water Construction Vessel (DCV) within the Heerema fleet, which is one of the world's largest monohull crane vessels [1]. It is mainly used for offshore construction installations and a model of this vessel will be used in this study for dynamic simulations. The cover of this thesis shows the Aegir vessel in action and as can be seen its crane is located on the starboard side of the vessel. To install a monopile, the Aegir will be equipped with a motion-compensated gripper frame, or *the gripper*. The gripper is a claw-like structure attached to the vessel, that catches the pile when the crane brings the pile in front of the gripper. Once the gripper catches the pile, the crane and gripper are vertically aligned. An example of such gripper is displayed in Figure 1.1.

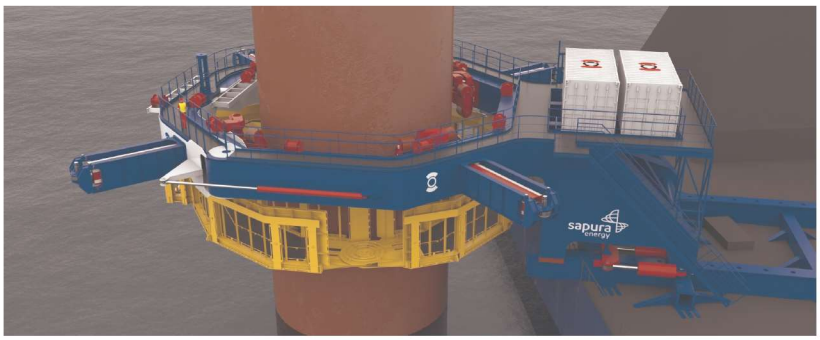

Figure 1.1: Example of a gripper in action

During offshore heavy lifting, the gripper location (located at coordinates [30.8 m, -37.1 m, 21.26 m] w.r.t. stern, centerline, and keel) is of greater importance than the CoG of the vessel since that is where the most critical activities happen. Consequently, HES would like to minimize the DP footprint at the gripper location instead of at the center location.

HES researched the motion responses of different points on the vessel. The absolute vessel motion responses differ when measured at points further away from the CoG. Results of the difference in motion responses at the different locations of interest found by HES are shown in Figure 1.2. The figure shows a time trace of the Aegir in a quartering sea state with a DP setup as it is programmed aboard the existing vessel. The vessel is currently equipped with a conventional DP system, with a control point at the center. The blue line indicates measurements of the surge and sway motions in the CoG, and the red line indicates measurements of the motions at the crane tip/gripper location. As shown in the figure, the results deviate from each other.

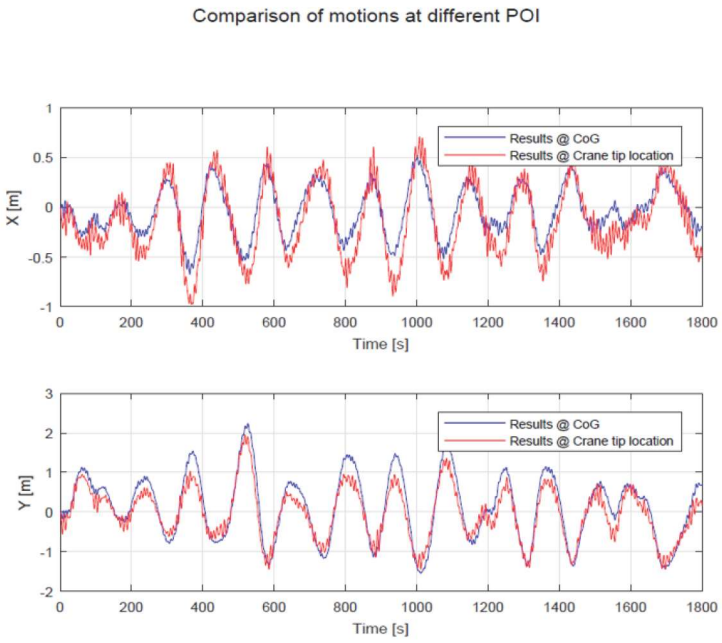

Figure 1.2: Comparison of motion responses at different Point of Interest: CoG vs. gripper location.

This difference in responses is due to motion coupling, which is induced by the yaw motion in quartering waves. This coupling can be considered negligible in the center but gets more severe at points far away from the center. This phenomenon will concisely be discussed hereafter.

In Figure 1.3, the grey-filled vessel with the solid line represents the starting position, and the vessel with the dashed line indicates the vessel at rest with only a yaw motion. The conventional control point controls the DP system around point A, while for this thesis, it will be designed to control the vessel around point B; where the crane and gripper are located. Point A will be referred to as the *center of the vessel* or the *center* in this study, Point B will be referred to as *gripper position* or the *gripper location*. x_p and y_p are the distances from point A to B in the x and y direction, respectively.

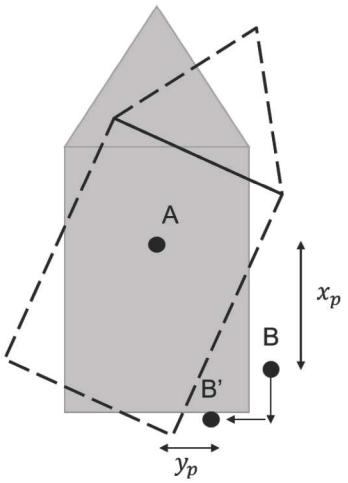

Figure 1.3: Shifting of the control point; wherein A is the conventional control point, and B is the location of the gripper where the control point will be shifted to in this study.

Consider the vessel in Figure 1.3 rotating from its resting position (grey-filled vessel with the solid line) to the vessel's position with the dashed line. No motion responses are observed when measuring the translations in the horizontal plane locally in point A. However, when we measure the translations locally in point B, motion responses are observed as point B shifted to point B' due to the rotating of the vessel as indicated by the arrows. Because the influences of motion coupling can't be neglected anymore in point B, it is evident that the equations of motions in that point differ from the ones in point A. As some components of the DP system work with a dynamic model of the vessel and the hydrodynamic parameters (such as added mass) would differ in point B compared to point A, a new DP system is needed in order to account for these.

In practice, a vessel won't be able to maintain a perfect position and heading. Although, the aim is to minimize the deviations from the setpoint as much as possible. For example, when considering Figure 1.2 it is intended to design a DP system such that the responses at the gripper location (red line) are as small as possible.

The design of the new proposed DP system holds significant promise for several reasons. Firstly, implementing this system could lead to a smaller DP footprint at the gripper location, resulting in reduced deviations at this critical point. This, in turn, has the potential to improve the workability of the vessel, leading to higher operational yields, while mitigating potential damage and unsafe situations during offshore operations. Secondly, given that the vessel is currently equipped with a conventional DP system controlling responses around the vessel's center, a new DP system that accounts for the equations of motion at the gripper location is essential to deliver a proof of concept for this new proposed method.

1.2. Literature review

A broad amount of work was already done in the field of DP improvement. The first DP vessel was introduced in the 1960s and consisted of single-input and single-output PID controllers, with a low-pass filter for wave filtering [2][3]. In the 1970s, the first DP system with a Kalman filter was introduced by Balchen, Jenssen and Saelid [4]. In general, this is the filtering technique that is still used in DP nowadays.

The Kalman Filter will function as a motion estimator in DP, and for this study the motion estimation should be done at a point away from the CoG. Seung-Min and Johnsson describe a relative motion estimator for unmanned aerial vehicles flying in a formation, using an Unscented Kalman Filter [5]. The paper describes the implementation of the relative position, the relative velocity, the size, and the lateral and longitudinal acceleration components of a leader object in the Unscented Kalman Filter, to determine the position of a following object. The paper describes the dynamic behaviour of an object relative to another object, but in this study one needs to describe the dynamic behaviour of a point on the *same* body, far away from its CoG.

Ye et al.[6] introduced a method to jointly estimate the position and horizontal crane force, as induced at the crane position. In order to prevent an unstable DP control system, Ye proposes a solution based on force feedforward control. It describes how the low-frequency horizontal component of the crane force is forwarded to the DP system, by introducing a joint-parameter state observer. The outcomes of this work are helpful in improving the state estimations during offshore operations but didn't include the motions at the actual crane position.

When considering a control point close to the vessel's center, the motion coupling can often be neglected. By shifting the control point of a DP system to a location far away from the center, the assumption of decoupled equations of motion is not valid anymore [7]. Hence, the ship dynamics the controller has to deal with have to change too. Under the assumption of neglected motion coupling, the PID controller, as proposed by Balchen et al.[4] is often implemented. To cope with the motion coupling a way must be created to decouple the now Multiple-Input-Multiple-Output (MIMO) system. Liyun et al.[8] proposed a method to decouple the sway and yaw motions in order to feed them into a controller. However, the controller mentioned in this paper is not a PID controller. Astrom, Johansson and Wang [9] propose a method for the design of decoupled PID controllers for MIMO systems, which is similar to the method applied in this study.

A repeatedly researched problem seems to be the DP instabilities due to uncertainties, as discussed in this section. Crane loads have a significant impact on a vessel's dynamic behavior [10][11]. Those instabilities mainly arise from an operating crane, often connected to another structure. Some studies proposed a solution for this problem in the form of setpoint adaptation, where the ideal DP setpoint is calculated and automatically set into the controller [12] [13]. However, none of them involved the use of a different control point.

From the literature, it became clear that much is done in the field of improving the station keeping on a vessel on DP, and several researchers mentioned the design of components that deal with the coupled behavior of the system. None of them, however, mentioned the control and optimized station keeping around a point far away from the vessel's center nor a complete DP system at a different control point. This research contributes to the field of DP by demonstrating the potential benefits of changing the control point location.

1.3. Problem statement

In this thesis, it was intended to design a DP system around the gripper location, in order to find out whether this could lead to better station keeping at this point; i.e. we tried to minimize the DP footprint at the gripper location. The remaining challenge was to simulate the vessel close to reality, with a renewed DP system with its control point at the gripper location. To achieve this, the following research question is formulated for the thesis:

What are the effects of changing the control point of a vessel's DP system from its center to an alternative point on the DP performance?

This has led to the following sub-questions:

- *What does the DP system with the new proposed control point look like?*
- *What are the motion responses for a DP vessel model with the conventional control point and a vessel model with the new proposed control point?*
- *How is the DP footprint at the location of interest affected by the new proposed control point?*
- *What is the influence of changing the control point on the demanded power and behavior of the thrusters of the DP system?*

1.4. Report outline

This thesis consists of 8 chapters, of which the upcoming 7 consists of the following:

- **Chapter 2** starts with an introduction to Dynamic Positioning and explains the most relevant subsystems in a DP system that were used for this study. The chapter also explains some of the background theories of DP and the hydromechanics as used by the software.
- **Chapter 3** discusses the methods and approach used for this thesis and presents the models as provided by the company.
- **Chapter 4** explains the design process of the new DP system.
- **Chapter 5** discusses the motion response results from time-domain simulations and compares the conventional DP model to the new DP model.
- **Chapter 6** discusses the behavior of the thrusters and the energy consumption during the time-domain simulations for both models.
- **Chapter 7** concerns the discussion of the results.
- **Chapter 8** presents the overall conclusion and gives recommendations for further research.

*In this version of the thesis, confidential information is left out and replaced by '***'.*

2
Background

This chapter provides a summary of the relevant knowledge available in the existing literature. It starts with explaining the working principle and background theories of a Dynamic Positioning system. Hereafter, the hydromechanics as used by the software in this thesis are discussed.

2.1. Dynamic Positioning

A Dynamically Positioned vessel is defined by the International Maritime Organisation (IMO) and the certifying class societies as a vessel that maintains its position and heading (fixed location or predetermined track) exclusively by means of active thrusters [2]. As for today speaking, it is widely used for offshore operations. The following section gives an introduction on the concept of dynamic positioning and background on literature used in this thesis.

2.1.1. DP system overview

A DP system includes different control functions for the automatic positioning of vessels, using thruster and propeller actions. Position reference sensors, combined with wind sensors, motion sensors, and gyro compasses, provide information to the controller related to the vessel's position and environmental forces affecting its position [14][15].

The vessel position and orientation are estimated based on a mathematical vessel model (that uses Kalman Filtering technique), the forces acting on the vessel, and on the position and orientation measurements. Based on the difference between the desired position/orientation and the estimated position/orientation, the control command to the thruster system is calculated in the PID controller and allocated to the appropriate thrusters. The thrusters (actuators) then provide the necessary forces to counter the external forces and moment acting on the vessel and maintain the vessel on location (with the desired heading), using the power coming from the power system [16]. Generally speaking, a DP system consists of the blocks displayed in Figure 2.1. The most important components of the DP system will be discussed in the upcoming section.

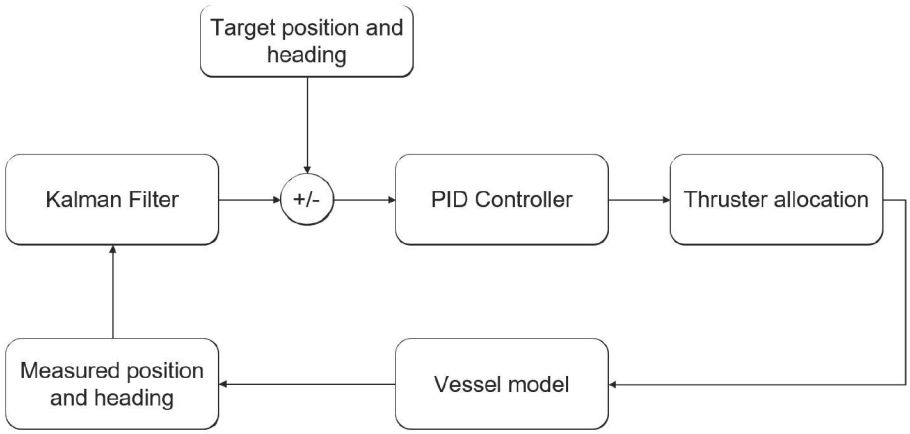

Figure 2.1: Overview of a Dynamic Positioning system

The DP set point and control point

The control point is a point in the local, body-fixed frame of the vessel. It is the point that the DP system needs to keep in place and where the DP controller bases its position and orientation errors during DP operations. The set point of the DP system is defined as a point in the global, earth-fixed frame where the control point should be pinned to or the required position of the control point. The difference between the set point and the control point is the position error.

2.1.2. Kalman filter

One of the most challenging problems for the DP system is to prevent first-order wave-induced forces to enter the feedback loop, as a DP system would be unable to correct for those high frequent forces. The Kalman Filter is a state observer, which has the purpose of separating the Low frequency (LF) and Wave frequency (WF) motion components such that only feedback from the LF motion components is used [17]. The difference between LF and WF motion components will be discussed in more detail in Chapter 2.2. The Kalman filter 'estimates' the low-frequency motions of the vessel and feeds this signal to the PID controller.

A *state observer* (or state estimator) is a system that provides an estimate of the internal state of an existing system by use of measurements of the input and output.

The Kalman Filter contains a hydrodynamic description of the vessel and is used to predict how the vessel would respond when certain forces and moments are applied to it. The state that is predicted in DP is typically the vessel's position and heading in the horizontal plane and the associated velocities [16].

The DP model provided by HES for the dynamic simulations is equipped with a discrete Kalman Filter, which will be discussed hereafter. The discrete Kalman Filter assumes linear dynamics, while the DP system has to cope with the low-frequency, non-linear behavior of the vessel. However, according to the paper of Vaerno et al [18], it was found that the DP system behaved mostly linearly, meaning that the relationship between the control inputs and the vessel's position and heading was close enough to a linear relationship that linear control models could be used with reasonable accuracy. Hence, a discrete Kalman Filter will be used in this study. The theory on the Kalman Filter discussed in this section is obtained from the paper of Welch & Bishop [19].

The process to be estimated can be described by the following equation:

$$\mathbf{x_k} = \mathbf{A}\mathbf{x}_{k-1} + \mathbf{B}\mathbf{u}_{k-1} + \mathbf{w}_{k-1} \tag{2.1}$$

Wherein $\mathbf{A}$ is a nxn matrix that relates the state in timestep $k-1$ to timestep k, also called the *state-transition matrix*. In this study, $\mathbf{A}$ consists of a $6x6$ matrix corresponding to the positions and velocities in the horizontal plane. $\mathbf{B}$ is the control vector, which is a $nx1$ vector that relates the control input $\mathbf{u}_k$ to the state $\mathbf{x}_k$ and are both assumed to be zero for this study. $\mathbf{w}_k$ represents the *process noise* or *model uncertainty* [16] [19]. As mentioned before, measurements of the position and orientation are fed into the DP system and compared with the estimates. These measurements can be defined mathematically as:

$$\mathbf{z}_k = \mathbf{H}\mathbf{x}_k + \mathbf{v}_k \tag{2.2}$$

Wherein $\mathbf{H}$ is a mxn matrix that relates the state to the measurement (for scaling, unit conversion), and $\mathbf{v}_k$ represents the measurement noise. $\mathbf{w}_k$ and $\mathbf{v}_k$ are random variables, which are considered to be independent of each other and white noises, with normal probability distributions and covariance matrices $\mathbf{Q}$ and $\mathbf{R}$ respectively [16][19]:

$$p(\mathbf{w}) \sim N(\mathbf{0}, \mathbf{Q}) \tag{2.3}$$

$$p(\mathbf{v}) \sim N(\mathbf{0}, \mathbf{R}) \tag{2.4}$$

$\mathbf{Q}$ is here defined as the process noise covariance and $\mathbf{R}$ is defined as the measurement noise covariance. Both these covariance matrices are $6x6$ matrices in this study, corresponding to the positions and velocities in the horizontal plane.

The Kalman Filter estimates the process state at a time and obtains feedback in the form of measurements. Hence, the algorithm can be divided into two groups: *time update* equations and *measurement*

update equations. The first step for the Kalman Filter is to predict the state at the next timestep based on the current state and the vessel model. This step is called the *prediction step* and corresponds to the time update equations and the *a priori* estimate is obtained. The a priori estimate is the estimate of the vessel states at timestep k given the knowledge of the process prior to step k [16][19], and is denoted by the bar. The a priori state estimate is defined as:

$$\hat{\mathbf{x}}_k^- = \mathbf{A}\hat{\mathbf{x}}_{k-1} + \mathbf{B}\mathbf{u}_k \tag{2.5}$$

Wherein $\hat{\mathbf{x}}_k^-$ is the a priori estimate at time step k, $\mathbf{A}$ is the state-transition matrix and $\hat{\mathbf{x}}_{k-1}$ is the *a posteriori* estimate or updated estimate at time step $k-1$. Simultaneously, the Kalman Filter calculates the a priori estimate error covariance, $\mathbf{P}_k^-$:

$$\mathbf{P}_k^- = \mathbf{A}\mathbf{P}_{k-1}\mathbf{A}^T + \mathbf{Q} \tag{2.6}$$

Wherein $\mathbf{P}_{k-1}$ is the a posteriori estimate covariance at timestep $k-1$. The next step is called the update step and corresponds to the measurement update equations, obtaining the a *a posteriori* estimate. The a posteriori estimate, $\hat{\mathbf{x}}_k$ is the state estimate at step k based on the actual measurements ($\mathbf{z}_k$). In this step, the Kalman Filter corrects or updates its first prediction made in the prediction step. The *a posteriori* estimate, is in fact nothing but the *a priori* estimate plus a correction factor which is proportional to the difference between the actual measurements and the prediction:

$$\hat{\mathbf{x}}_k = \hat{\mathbf{x}}_k^- + \mathbf{K}_k(\mathbf{z}_k - \mathbf{H}\hat{\mathbf{x}}_k^-) \tag{2.7}$$

Wherein $\mathbf{K}_k$ is the Kalman Gain Matrix. At this step, the error covariance is updated too:

$$\mathbf{P}_k = (\mathbf{I} - \mathbf{K}_k \cdot \mathbf{H})\mathbf{P}_k^- \tag{2.8}$$

Simultaneously, the Kalman gain matrix is calculated:

$$\mathbf{K}_k = \mathbf{P}_k^-\mathbf{H}^T(\mathbf{H}\mathbf{P}_k^-\mathbf{H}^T + \mathbf{R})^{-1} \tag{2.9}$$

The Kalman Gain Matrix is calculated by the Kalman Filter in such way that the *a posteriori* error covariance is minimized. The Kalman Gain Matrix is based on how much the measurements are weighted versus how much the vessel model is weighted [16]. Which comes from the process noise and measurement noise covariance matrices, $\mathbf{Q}$ and $\mathbf{R}$.

2.1.3. PID Controller

In its simplest and earliest form, the DP system contained a PID controller already, and it is still widely used [2][3]. The controller measures the vessel's position with respect to the intended position, which is called the position error $e(t)$. Due to this error, power is directed to the thrusters to correct for this error. The overall control function is mathematically defined as [20]:

$$u(t) = K_P e(t) + K_I \int_{t_0}^{t_1} e(t)\,dt + K_D \dot{e}(t) \tag{2.10}$$

Wherein K_P, K_I and K_D are the proportional, integral and derivative gains respectively. In the horizontal plane, little to none stiffness and damping is present, which would lead to the vessel drifting away over time when its operating at sea. A DP system is able to correct for the motions in the horizontal plane: surge, sway and yaw. And, the PID controller serves as a spring and damper for these motions in the horizontal plane. For each of these motions, the required force to correct for the position or heading deviations is calculated by the PID controller. The proportional gain P multiplies the error signal, it is simply proportional to the position error with an amplifier.:

$$P = K_p \cdot e(t) \tag{2.11}$$

The proportional gain, P, serves as the spring stiffness. The integrator I integrates the error over time:

$$I = K_I \int_{t_0}^{t_1} e(t)\,dt \tag{2.12}$$

Hence, when a certain error is measured for a long time, the output signal gradually increases. As a result of this, the thrusters will provide more thrust force until steady state errors are eliminated [20]. The differentiator D differentiates the error with respect to time:

$$D = K_D \cdot \dot{e}(t) \tag{2.13}$$

The differentiator measures the rate of change of the error. When the rate of change becomes smaller, it reduces the thruster action to prevent overshoot (i.e. the differentiator works as a damper) [20]. The PID-gains as discussed in this section need to be well chosen, in order to have a properly ”tuned” DP system.
For a dynamically positioned vessel, the Proportional and Derivative term respond to the oscillating low-frequency wave drift forces, the Integral term should respond to the mean wave drift forces. Wave loads are discussed more in detail in section 2.2.

2.1.4. Thruster allocation

After the PID controller calculates the required forces and moments for the vessel to maintain its position and heading, these need to be converted to signals that tell each actuator the demanded thrust and angle. In the DP system, those actuators are thrusters and/or the vessel’s main propulsion system combined with its rudders [21]. The thrust allocation determines the configuration of which thrusters could be used to move the ship to the desired position. It takes into account the limit for the thruster rpm, angles, and power [22]. The allocation system can be translated into a constrained optimization problem. The objective function and its constraints as used in this thesis are introduced in this section.

The objective function

The objective function is an equation that describes a function that is to be optimized. It is typically used in optimization problems, where the goal is to maximize or minimize the value of the objective function. The objective function is usually composed of decision variables and a measure of performance. The general objective function can be written in mathematical notation using the following equation [23]:

$$\text{Objective} = f(x_1, x_2, \dots, x_n) \tag{2.14}$$

where $x_1, x_2, \dots, x_n$ are the decision variables and f is the measure of performance. The objective is to find the values of the decision variables that will maximize or minimize the value of the objective function.

To obtain the thruster allocation algorithm for the dynamically positioned vessel in this thesis, an objective function is set up for the DP vessel. This objective function is based on the approach as presented by the Maritime Research Institute Netherlands (MARIN) [24] and it can be written as:

$$F_T = \sum_{i=1}^{N} (f_{x,i}^2 + f_{y,i}^2) \tag{2.15}$$

Wherein F_T is the total thruster force in a given timestep (the measure of performance), $f_{x,i}$ and $f_{y,i}$ are the thruster forces in the x-direction and y-direction (the decision variables), and $i = 1, \dots, N$ indicates the thruster number, in this study: $i = 1, .., 6$. At each time step, the allocation algorithm checks whether the minimization satisfies the force equilibrium as well as the limiting criteria for each thruster. These criteria, or constraints, are discussed hereafter.

Constraints

In Dynamic Positioning, maximum efficiency and minimum fuel consumption are considered important parameters. Hence, the optimization problem concerns a minimization problem and Equation 2.15 should be minimized subject to the constraints mentioned hereafter. The first set of constraints that needs to be satisfied is a so-called *equality constraint*, which follows from the need to generate the required forces and moments in order to keep the vessel in place [24]:

$$F_x = \sum_{i=1}^{N} f_{x,i}, \tag{2.16}$$

$$F_y = \sum_{i=1}^{N} f_{y,i}, \tag{2.17}$$

$$M_z = \sum_{i=1}^{N} x_i f_{y,i} - y_i f_{x,i} \tag{2.18}$$

The second constraint follows from the vessel's physical limitations and is an *inequality constraint*. The thrusters may have a limited capacity, $\overline{T}_i$, which can lead to the demanded forces not equaling the obtained forces, resulting in the thrusters becoming saturated. This constraint is defined as follows, for $i = 1, \ldots, N$:

$$\overline{T}_i \geq T_i = \sqrt{f_{x,i}^2 + f_{y,i}^2} \tag{2.19}$$

Wherein T_i is the total force per thruster and $\overline{T}_i$ is the total deliverable force per thruster. Note that in this thesis the so-called forbidden zones and any other interaction effects are neglected, such as thruster-thruster interactions and thruster-hull interactions.

The thruster allocation algorithm as provided by HES contains two additional constraints on top of the above-mentioned constraints of MARIN. Both are inequality constraints. The first additional constraint arises from the maximum ramp-up speed of the thrusters, i.e. the ability of a thruster to generate a certain amount of thrust within a time step. For each thruster, it applies that the rate of change of the applied force per time step must not exceed the ramp-up force limit. The rate of change of the azimuth per time step must not exceed the azimuth speed limit. The limits used in this study are discussed in subsection 3.1.1.

Saturated thrusters

In some situations, the thrusters cannot produce the requested forces. In this case, the minimization cannot satisfy all constraints anymore and the system should prioritize station keeping over energy consumption. If the capacity of the thrusters is insufficient, the approach as described in the paper of MARIN [24] is used. The approach describes that in the event of thruster saturation, a modified objective function should be used:

$$\tilde{F_T} = w_1(\Delta_{F_x}^2 + \Delta_{F_y}^2) + w_2\Delta_{M_z}^2 \tag{2.20}$$

Wherein w_1 and w_2 are weight factors, and:

$$\Delta_{F_x} = F_x - \sum_{i=1}^{N} f_{x,i}, \tag{2.21}$$

$$\Delta_{F_y} = F_y - \sum_{i=1}^{N} f_{y,i}, \tag{2.22}$$

$$\Delta_{M_z} = M_z - \sum_{i=1}^{N} (x_i f_{y,i} - y_i f_{x,i}). \tag{2.23}$$

Thus, when the thrusters have insufficient capacity, the optimisation problem is to minimize Equation 2.20, subject to the constraints mentioned in Equations 2.21, 2.22 and 2.23. The weights in the thruster allocation used in this study are chosen such that force and moment are equally treated at each timestep.

2.2. Hydromechanics

The field of hydromechanics is concerned with the behavior of (structures in) fluids in motion and at rest. A vessel in waves gets moving due to external influences of for example waves, wind, and/or current. To get insights into the vessel's dynamic behavior due to these external influences, one aims to define the vessel and the external forces mathematically. By doing this, insights can be gathered in the vessel's expected responses. This chapter discusses the background theories used in this thesis for the dynamic simulations. To prevent the problem from becoming too complex to analyze, wind and current are neglected in this thesis. Hence, only wave theory will be discussed in this chapter in terms of environmental forces.

2.2.1. Axis-conventions and definition of motions

To interpret the eventual results in the right way, it is important to define the axis-systems and motions first. The motions of a vessel can be split into three translations of the center of gravity and three rotations around the center of gravity. Generally speaking, a vessel has six Degrees Of Freedom (DOF). An example of the DOF is given in Figure 2.2.

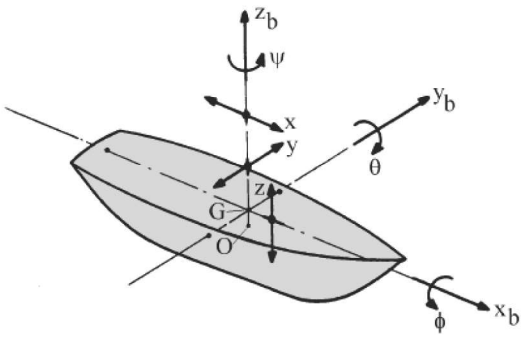

Figure 2.2: Definition of the vessel's Degrees Of Freedom in the **V** frame [7]

These motions are defined in the *vessel-fixed frame* as:

- **Surge** (x), in the longitudinal x-direction, positively forwards.
- **Sway** (y), in the lateral y-direction, positive to portside.
- **Heave**(z), in the vertical z-direction, positive upwards.
- **Roll** $(\phi \ or \ rx)$, rotation about the x-axis, positive right-turning.
- **Pitch** $(\theta \ or \ ry)$, rotation about the y-axis, positive right-turning.
- **Yaw** $(\psi \ or \ rz)$, rotation about the z-axis, positive right turning.

A DP system only corrects for the motions in the *horizontal plane*, which are surge, sway and yaw. Hence, these motions will be of greatest interest for this study.

In this study, 2 frames of reference are used to describe the vessel its motions: the (earth-fixed) inertial frame, **G** $= [X, Y, Z]^T$ and a vessel-fixed frame, **V** $= [x, y, z]^T$. All the coordinate systems are right-handed, and positive rotations are clockwise when looking in the direction of the axis of rotation. This aligns with the axis-conventions of the used software packages for time-domain simulations [25]. An example of the coordinate systems is given in Figure 2.3.

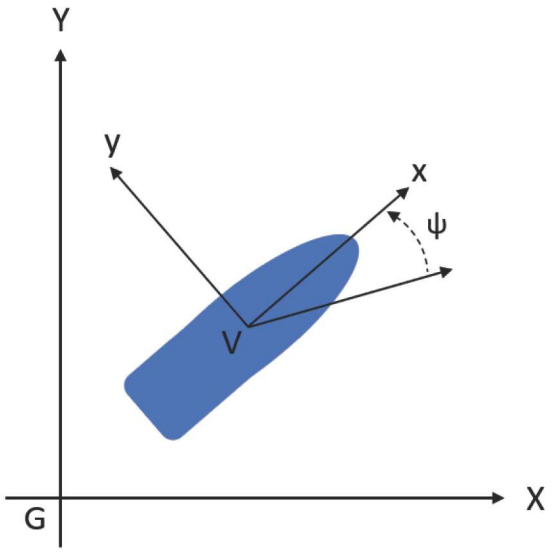

Figure 2.3: Frames of references used for this study; wherein **G** is the earth-fixed inertial frame and **V** is the vessel-fixed frame.

The calculations for the center position will be performed in the center (point A), where a local vessel-fixed frame is placed. Calculations for the gripper location are considered at the gripper position (point B), where again a local vessel-fixed axis is placed in point B (see Figure 1.3).

2.2.2. Ocean waves

As mentioned before, wind and currents are neglected in this study, hence the only environmental forces applied on the vessel come from waves. In this section, background information is provided on the generation of a wave train and the relevant statistics. In a time record, the surface elevation is the instantaneous elevation of a sea surface relative to a reference level. In such a record, a wave is defined as the profile of the surface elevation, between two successive downward zero-crossing of the elevation.

Wave energy spectra

For this study, the vessel will operate in ocean waves (i.e. deep waters). To obtain ocean waves in the time domain, wave records are generated from wave energy spectra. These wave energy spectra come from actual wave measurements over long periods of time at sea. The waves at sea are considered irregular waves, which can be defined as the sum of a large number of harmonic wave components (a Fourier series) [26] [7]:

$$\zeta(t) = \sum_{i=1}^{N} \zeta_{an} cos(k_n x - \omega_n + \epsilon_n) \tag{2.24}$$

Wherein ζ is the the wave elevation, ζ_{an} is the wave amplitude component, k_n is the wave number component, ω_n is the circular frequency component and ϵ_n is the random phase angle component. Note that the elevation is only considered in the x-direction here. With a Fourier analysis, the values of the amplitude and phase can be determined at each frequency, which would give an amplitude and phase spectrum for a given wave record. However, most ocean wave records have a value between 0 and 2π without any preferred value. Hence, the phase spectrum (and thus ϵ_n) is ignored and one is left with only the wave amplitude spectrum to characterize the wave record [26].
For several reasons, it is more relevant to present a wave energy spectrum in stead of a wave amplitude spectrum. To get to the actual wave energy spectrum, one should consider the variance instead of just the amplitude. According to the book of Journée and Massie [7] and the book of L. Holthuijsen [26],the

variance of the signal mentioned in Equation 2.24 is defined as:

$$\sigma_\zeta^2 = \sum_{n=1}^{N} \frac{1}{2}\zeta_{an}^2 \tag{2.25}$$

Which can be expressed in a wave spectrum as:

$$S_\zeta(\omega_n) = \sum_{\omega_n}^{\omega_n+\omega} \frac{1}{2}\zeta_{an}^2(\omega) \tag{2.26}$$

Letting $\Delta\omega \to 0$:

$$S_\zeta(\omega_n)d\omega = \frac{1}{2}\zeta_{an}^2 \tag{2.27}$$

As recommended by HES, the Joint North Sea Wave Project (JONSWAP) spectrum is used for the calculations in this study. Orcaflex generates waves from this given spectrum.
This spectrum is derived in the same way as mentioned above and is defined as follows by the Orcaflex manual[27]:

$$S(f) = \frac{\alpha g^2}{16\pi^4} f^{-5} exp\left[-\frac{5}{4}\frac{f}{f_p}^{-4}\right]\gamma^b \tag{2.28}$$

Wherein α is a spectral energy parameter, g is the acceleration due to the gravitation, f is the frequency in Hz, f_p is the peak frequency in Hz and γ is the peak enhancement factor, which is defined as 3.3 for a JONSWAP spectrum. b is:

$$b = exp\left[-\frac{1}{-2\sigma^2}\left(\frac{f}{f_p} - 1\right)^2\right] \tag{2.29}$$

Wherein σ is the spectral width parameter; which is defined for JONSWAP as:

$$\begin{aligned} &if\ f < f_p\ then : \sigma = 0.07 \\ &if\ f > f_p\ then : \sigma = 0.09 \end{aligned} \tag{2.30}$$

Note that the wave energy spectrum given by the Orcaflex manual is in Hertz and that: $f = 1/T$ and $\omega = 2\pi f$.
As stated in subsection 3.1.3, the significant wave heights used for this study concern 1.0 meters, 1.5 meters and 2.0 meters, the peak period considered in this thesis is 8 seconds. The wave energy spectra used for this study are displayed in Figure 2.4.

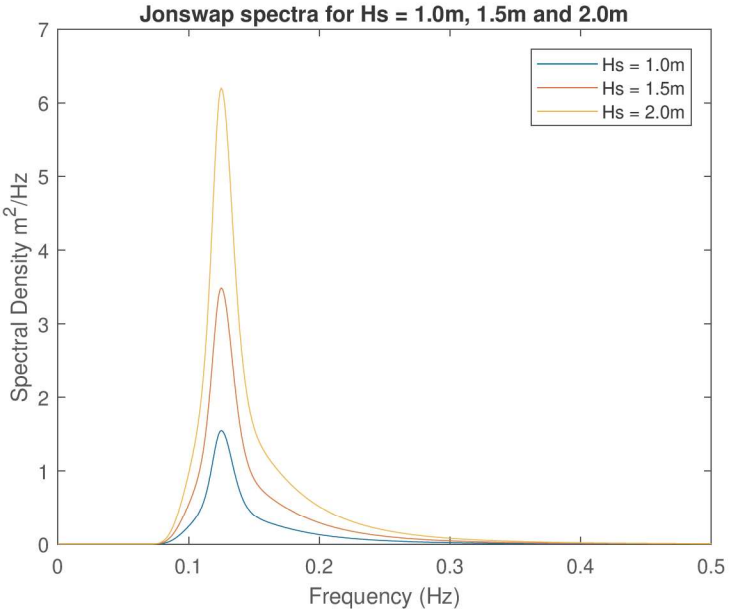

Figure 2.4: JONSWAP spectra as calculated by Orcaflex for Hs = 1.0m, 1.5m and 2.0m, with Tp = 8s.

The given spectra are transformed to time series by doing the inverse from what was discussed in the beginning of this section; by filling in Equation 2.24, with the necessary constants. The variance of the water surface elevation, is equal to the area of the spectrum:

$$\sigma_\zeta^2 = \int_o^\infty S(\omega) d\omega \tag{2.31}$$

Hence, the amplitudes, ζ_{an} can be obtained by:

$$\zeta_{an} = 2\sqrt{S_\zeta(\omega)\Delta\omega} \tag{2.32}$$

The wave number k_n (see Equation 2.24) can be obtained at each frequency ω_n using the dispersion relation. The phase angles ϵ_n are chosen to be random values between 0 and 2π. An example of a part of the wave record for the base case as produced by Orcaflex is shown in Figure 2.5.

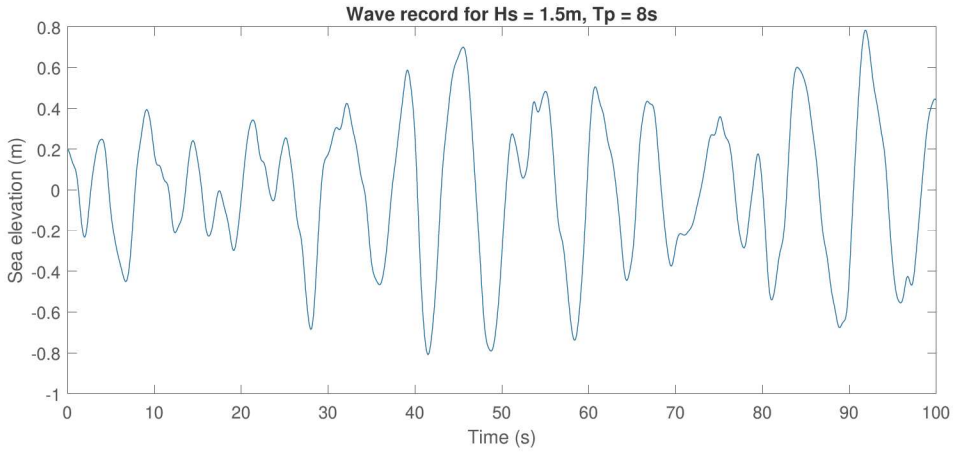

Figure 2.5: Example of wave record for Hs = 1.5m, Tp = 8s between t = [0s 100s]

Wave directions

Due to the OrcaFlex manual [27], the direction in which the wave progresses in the software is measured positive counter-clockwise from the global X-axis when viewed from above. So, for example, 0 degrees means a wave traveling in the positive X-direction, and 90° means a wave traveling in the positive Y-direction. These directions are relative to the global axis. For clarity, an example is shown below in Figure 2.6.

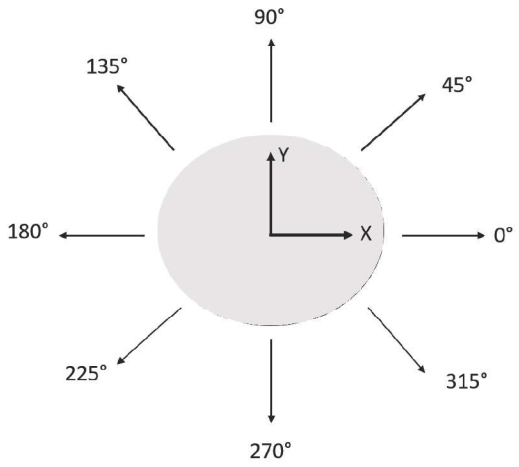

Figure 2.6: Definition of wave directions in Orcaflex

2.2.3. Wave loads

The vessel will be excited due to external forces and moments. In this study, those external forces and moments are only due to waves, since winds and currents are neglected. The wave loads on a vessel can be expressed as the sum of first-order, second-order and higher-order terms.

In this thesis, the second-order motions and wave drift loads are of higher importance than the first-order motions and loads, since a DP system would be unable to correct for the first-order (highly frequent) motions [7]. However, first-order wave loads are still briefly discussed since the time domain simulations include first and second-order wave loads.

Figure 2.7 illustrates the difference between the first-order motion or wave frequent motion and second-order motion or low-frequency motion. The lower wave record in this figure is an example of the superposition of the upper two wave signals, wherein the red line indicates a second-order, low-frequency wave and the blue line indicates a first-order, wave frequent wave.

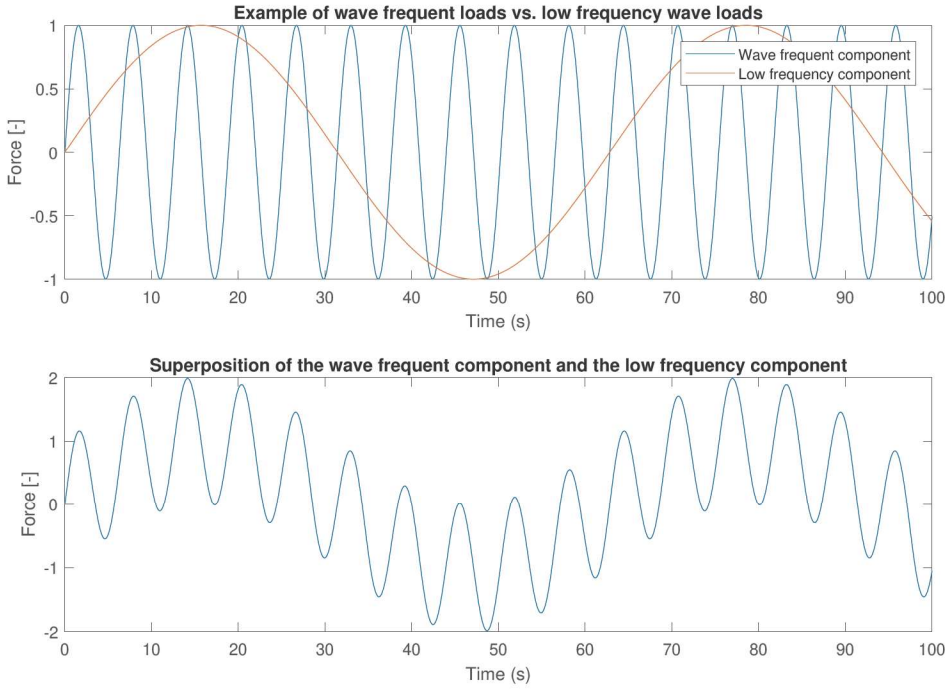

Figure 2.7: Example of waves superposition; showing superposed waves in the lower graph and an example of the first and second order waves it is composed of in the upper graph.

The first-order loads are linear with the wave amplitude, and composed of contributions from each individual wave component in the sea state, which excite the vessel's first-order motions. These first-order motions are modeled in Orcaflex using displacement Response Amplitude Operator (RAO) or load RAOs. These RAOs are transfer functions, relating the response amplitudes to the wave amplitudes or the wave force amplitudes linearly.

Second-order loads are quadratic with the wave amplitude and consist of contributions from each pair of wave components in the sea state and are modeled in Orcaflex using Quadratic Transfer Function (QTF) [28]. Within the second-order loads for a vessel operating on DP, a distinction can be made between two components: the mean wave drift force and the low-frequency wave drift forces. Wherein the mean wave drift force is a constant load and the low-frequency wave drift force is an oscillating load. The mean wave drift forces determine the vessel its new equilibrium position and the low-frequency wave drift forces lead to an oscillating displacement of the vessel at the low-frequency region. The second-order motions are the ones to be compensated for by the DP system and therefore the most important for this thesis.

The first and second-order wave loads and the hydrodynamic coefficients are computed using WAMIT [1] software, which is a software package based on the linear and second order potential theory for analyzing floating or submerged bodies in the presence of ocean waves. For more extensive background theory on potential theory is referred to Appendix G and the book of Journée and Massie [7].

[1] https://www.wamit.com/

2.2.4. Motions in the time domain

The equation of motion that is used to obtain an adequate model of the motions of a vessel in waves, comes from Newton's second law. The vessel can be considered as a linear spring-damper system, and for each degree of freedom the (uncoupled) equation of motion that will be solved at each time step in the time domain is:

$$(M + A)\ddot{x}(t) + B\dot{x}(t) + Cx(t) = F(t) \tag{2.33}$$

Wherein M is the vessel's solid mass, A is the hydrodynamic mass coefficient, B is the hydrodynamic damping coefficient, c is the restoring spring coefficient and F are the external forces working on the vessel. In this equation, the added mass and damping are frequency dependent.

In time-domain simulations, hydrodynamic coefficients (e.g. mass, damping, stiffness) are evaluated at each time step, keeping into account the variation of geometry. To implement the frequency-dependent added mass and damping in the time domain, a method as proposed by Ogilvie [29][7] is used by Orcaflex. With this method, the impulse response function is calculated for the vessel and then that impulse response function is applied at each time step, using a convolution integral to account for the past motion of the vessel [7][28][30]. The hydrodynamic force (or moment) becomes:

$$F = A \cdot \ddot{x}(t) + \int_{-\infty}^{t} B(t - \tau) \cdot \dot{x}(t) d\tau \tag{2.34}$$

Together with a linear restoring spring term $C \cdot x$ and a linear external load, $X(t)$, a linear equation of motion is obtained. This equation is also often referred to as the Cummins equation and is written as follows:

$$(M + A) \cdot \ddot{x}(t) + \int_{0}^{\infty} B(\tau) \cdot \dot{x}(t - \tau)\, d\tau + C \cdot x(t) = X(t) \tag{2.35}$$

3
Methodology and case study

The eventual goal of this thesis is to design a new DP system that aims to minimize the footprint around the gripper location of the vessel. In the previous chapters, developments of dynamic positioning were discussed and an overview of relevant background theories was given for a clearer understanding of the problem. The models as provided by the company are discussed in this chapter, as well as the approach for this study. Also, the assumptions made will be discussed in this chapter.

3.1. Simulation model

To gather insights into the dynamic behavior of the DP vessel, hydrodynamic simulations will be performed in the time domain using Orcaflex[1]. An existing model for time-domain simulations of the Heerema vessel Aegir in Orcaflex is provided by HES. The vessel model consists of a dynamic model of the Aegir vessel with an external code that mimics the DP system similar to the one described in Section 2.1.

The setup of the Orcaflex model will be discussed hereafter. An example of the model setup is shown in Figure 3.1 below.

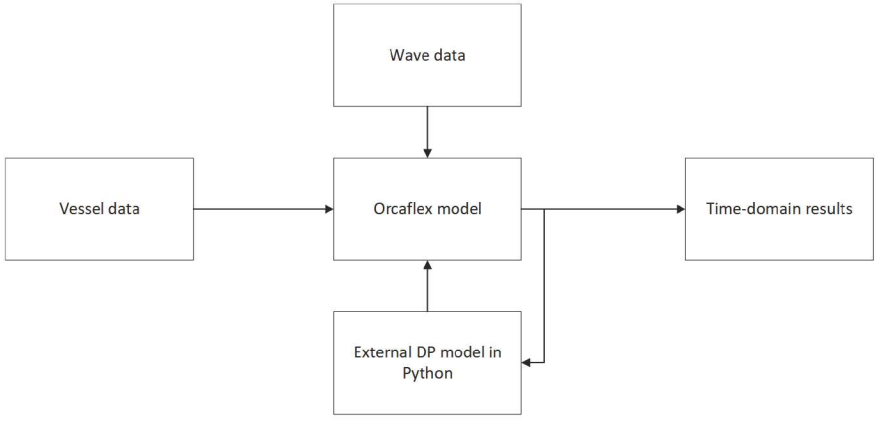

Figure 3.1: Setup of Orcaflex model

Before simulations, environmental conditions were defined in Orcaflex. Based on user-defined wave parameters, such as significant wave height (Hs), wave direction, and Peak period (Tp), Orcaflex generates a wave train for a user-defined period of time. This wave train comes from a wave spectrum. The vessel data consists of the vessel's RAOs, QTFs, hydrodynamic coefficients, and general vessel characteristics. These concepts were explained in section 2.2.

At each time step, the Orcaflex model works together with an external code in Python, that contains a Kalman Filter, PD controller, and thruster allocation algorithm. Motion responses are fed into this external function, which filters the responses in order to only correct for the second-order motions, calculates the forces that are needed to keep the vessel in position, and then sends this to the thruster allocation, which applies counter-acting forces on the vessel to keep its position. All components and characteristics of the simulation model will be discussed hereafter.

[1] Orcaflex

3.1.1. Vessel data

As mentioned in the introduction, the vessel model used for this study is based on Heerema's DCV Aegir. This section presents all characteristics of the vessel that were made available by HES and were relevant to perform the eventual dynamic analyses.

Main characteristics

Table 3.1 displays the main characteristics of the vessel, all characteristics are given for 9 meters draught, which is the operating draught of the vessel.

Table 3.1: Main characteristics of Aegir at 9 m draught

Displacement	(t)	***
Length overall	(m)	***
Width	(m)	***
Operating draught	(m)	***
Transit draught	(m)	***

The coordinates of the Points Of Interest for this study are displayed in Table 3.3 below. All coordinates are given with respect to the stern, center line, and keel. The hydrodynamic origin is the point where the calculations are performed by the WAMIT software.

The solid mass of the vessel for surge, sway, and heave is equal to the displacement of *** t and, the moment of inertia tensor is defined for the ***-meter draft and around the CoG as:

Table 3.2: Moment of inertia tensor in $t \cdot m^2$ for Aegir vessel

X [m]	Y [m]	Z [m]
***	***	***
***	***	***
***	***	***

Table 3.3: POI of Aegir for this study

	X [m]	Y [m]	Z [m]
Center of Gravity (CoG)	***	***	***
Hydrodynamic Origin	***	***	***
Gripper location	***	***	***

3.1.2. External DP model in Python

The DP model of the Aegir vessel as provided by HES consists of the same components as presented in Figure 2.1 in section 2.1. It is equipped with a discrete Kalman Filter as explained in section 2.1, that feeds estimated states to the PID controllers, which calculate the demanded forces to keep the vessel in position. Although a model for the Kalman Filter was provided by HES, the tuning parameters were not predetermined and the tuning process will be discussed in section 4.1. The initial setup of the external DP module is shown in Figure 3.2. The provided PID settings will be discussed hereafter.

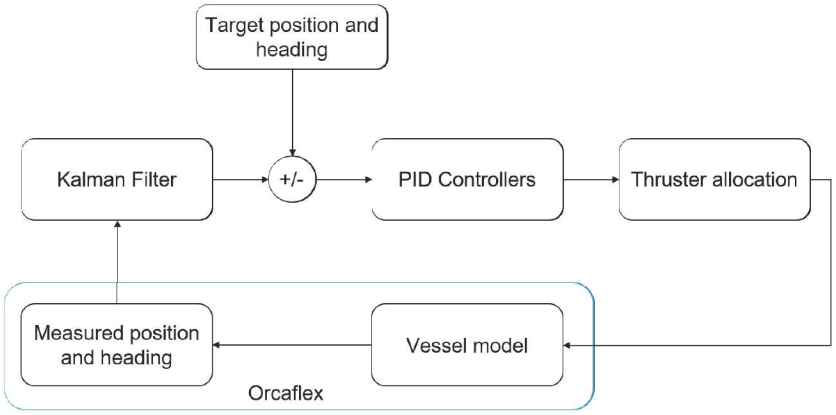

Figure 3.2: External DP module setup for time domain simulations - center control point (conventional) model

The Aegir vessel is currently equipped with three separate PID controllers: one for each DOF. An example is shown in Figure 3.3 below:

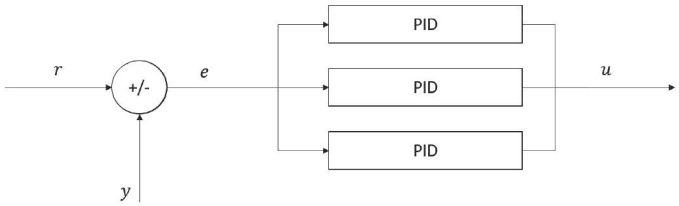

Figure 3.3: Original PID controller setup

Wherein r is the reference signal, which in this case consists of the set point, y is the measured position and heading, and u is the control vector, which here consists of the demanded forces in the x direction and y direction and a moment about the body-bound z-axis. The PID controller as presented here was implemented for the center control point model and used as a starting point for the tuning of the gripper control point model. It is programmed with predefined settings from HES for the center control point, which are shown in Table 3.4.

Table 3.4: Aegir PID-controller parameters

	X-gain	Y-gain	Rz-gain
P	***	***	***
I	***	***	***
D	***	***	***

As mentioned in section 2.1, for this study only a PD controller will be used. Hence, the I terms were neglected. The allocation is an important part of any DP system, as the thrusters must be properly allocated in order to ensure safe and efficient vessel operation.

Propulsion system and thruster allocation settings

The Aegir vessel is currently equipped with a DP3 dynamic positioning that is tuned for optimal response at the center of the vessel. To obtain such a DP3 system, multiple thrusters are needed. Hence, the vessel is equipped with 7 thrusters: 1 tunnel thruster and 6 azimuth thrusters. The tunnel thruster will not be used for this thesis, as its behavior was found to be different to others and therefore complex to implement in the current thruster allocation algorithm. An overview of the thruster capacities of the thrusters that are used for this study are given in Table 3.5. Coordinates of the thrusters are given in Table 3.7 and an overview of the thruster locations is given in Figure F.1 in Appendix F. All coordinates are w.r.t. stern, centerline and keel. The thrusters itself have limits, which will be taken into account during simulations. The limits are displayed in Table 3.6. The allocation algorithm was previously discussed in subsection 2.1.4.

Table 3.5: Aegir Thruster Data

Thruster	Type	Power [kW]
T01 - T04	Azimuth	3200
T05 & T06	Azimuth	6500

Table 3.6: Thruster limits per thruster of the Aegir vessel

	Thruster 1	Thruster 2	Thruster 3	Thruster 4	Thruster 5	Thruster 6
Maximum thrust (94.4% eff) [kN]	***	***	***	***	***	***
Force ramp-up time [s]	***	***	***	***	***	***
Ramp-up force limit [kN/s]	***	***	***	***	***	***
Azimuth speed [deg/s]	***	***	***	***	***	***

Table 3.7: Thruster coordinates per thruster of Aegir vessel, coordinates w.r.t. stern, centerline and keel

	Thruster 1	Thruster 2	Thruster 3	Thruster 4	Thruster 5	Thruster 6
x-coordinate [m]	***	***	***	***	***	***
y-coordinate [m]	***	***	***	***	***	***

3.1.3. Wave data

Prior to the time domain analyses, the environmental conditions that were used for the simulations were determined. The conditions were chosen to be as equal as possible to the Aegir's common working conditions. These environmental conditions were defined based on experience with offshore operations of HES. For the sake of simplicity, wind and current are neglected for this study. Also, the crane of the vessel is considered rigid for this study and has no influence on the vessel.

Base case

A detailed analysis of the responses of the vessel in the 'base case' sea state as defined by HES will be presented in this thesis in chapter 5. This base case consists of bow quartering waves since the yaw motion that induces the coupling would only be present in quartering waves. The wave parameters for the 'base case' are defined as:

- Assuming a Joint Northsea Wave Project (JONSWAP)
- A significant wave height of 1.5 meters,
- A peak period of 8 seconds,
- Waves propagating in the 135 degrees direction, without spreading

Most results presented in this thesis correspond to the 'base case' as mentioned above, unless stated otherwise. According to Det Norske Veritas (DNV) RP-H103 [31], the duration of the time domain simulation should be sufficient to provide adequate statistics. It is therefore recommended to perform 3-hour simulations, which is done for the base case sea state of this study.

Wave height variations

To get insights into whether the system works in different sea states, variations of the base case simulations were performed, wherein the wave heights were varied to a lower and higher Hs. Due to the extensive simulation time, the wave height variation simulations were performed for only one hour. In order to get an as equal as possible comparison of results, the same wave trains are applied for both the center control point model and the gripper control point model. The set of variations consists of the following:

- Significant wave heights of 1.0 meters and 2.0 meters,
- Assuming a JONSWAP spectrum for all simulations,
- A peak period of 8 seconds for all simulations,
- Waves propagating in the 135 degrees direction, without spreading

By a set is meant: one simulation for the center control point model and one simulation for the gripper control point model. No wave spreading was used for any simulation in this thesis.

3.2. Research approach

The remaining challenge for this study was to develop a new DP model that regulates the vessel its motions around the gripper position. To draw a conclusion on the performance of the newly proposed method, comparisons should be made with the original model that regulates the vessel its motions around the center. In this section, the steps taken to get to the eventual results are explained.

1. Evaluate the current DP model for time-domain simulations

The first step was to evaluate the DP model from HES. Emphasis in this phase was on getting a proper understanding of the current model and, on identifying and implementing the required modifications to the existing model, in order to make the DP model for the gripper location. During this phase, it became clear that the Kalman Filter, the P(I)D-controller, and the thruster allocation needed modifications for the new proposed model. These modifications are mostly due to the motion coupling that becomes larger at the gripper control point and the equations of motions the system has to handle which therefore change.

2. Create, evaluate, and test the new DP model for time-domain simulations

As stated in the previous subsection, it was found that the new DP system needed a new Kalman Filter, a new PD controller, and some modifications in the thruster allocation algorithm. All of these components of the DP system were tested separately before they were implemented in the eventual DP model in Python.

First, a new Kalman Filter was developed that takes into account the motions at the alternative location. The new design was tested in a separate MATLAB module first, before adding it to the external Python code in Orcaflex. The new PD controller was also first tested separately in MATLAB, before implementing it in the loop.

The design decisions taken for the design of the above-mentioned components are discussed thoroughly in chapter 4. An overview of the steps taken to obtain the new DP model design is given in Figure 3.4.

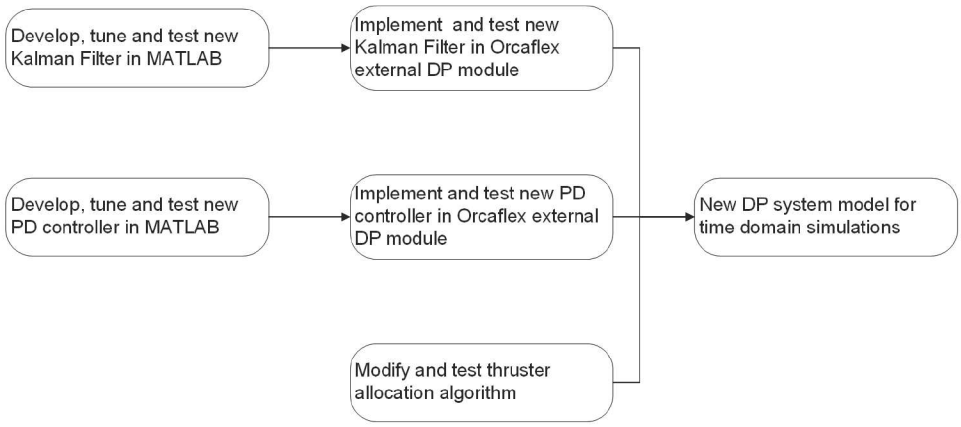

Figure 3.4: Step-by-step approach for new DP model design

By completing this step, an answer can be formulated to the first sub-question about how the new DP system looks.

3. Perform time-domain simulations

In order to draw a conclusion on the performance of the new system, simulations were done for both a model of the vessel with its existing, conventional DP system (with a control point at center position) and the same vessel with the new DP model (with a control point at gripper location). A step-by-step approach of this approach is given in Figure 3.5

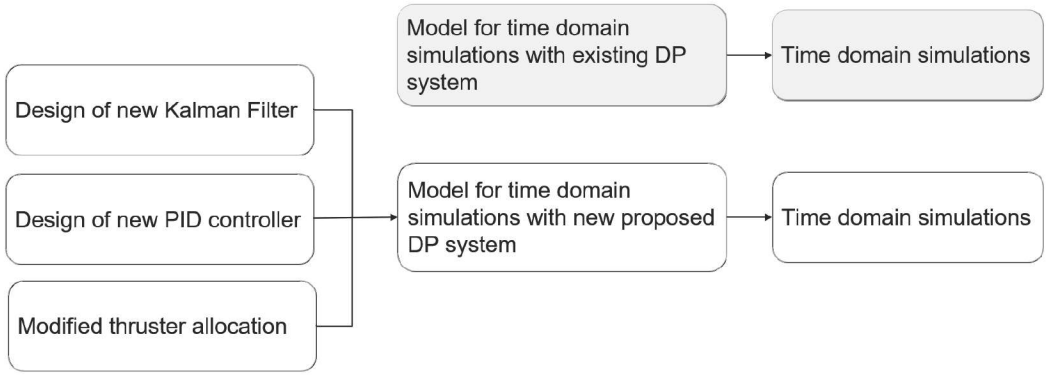

Figure 3.5: Step-by-step approach for performing simulations with both models

In this thesis, the new (proposed) DP system refers to the DP system with the gripper control point and the existing, or conventional, DP system refers to the DP system with the center control point. During the study, the vessel motions are assessed under several sea states, which are specified in subsection 3.1.3. While doing this, outcomes were validated and verified.

4. Analyze time-domain results

With the outcomes of the time domain simulations, a comparison can be made between both models. With the help of Python[2] and MATLAB[3], large amounts of results can be processed into useful graphs. The results of interest that are meaningful to the performance are the DP footprint, the total motion responses in the horizontal plane at the center and at the point of interest, the behavior of the thrusters, and energy consumption. A schematic overview of result processing is shown in Figure 3.6.

[2]Python
[3]MATLAB

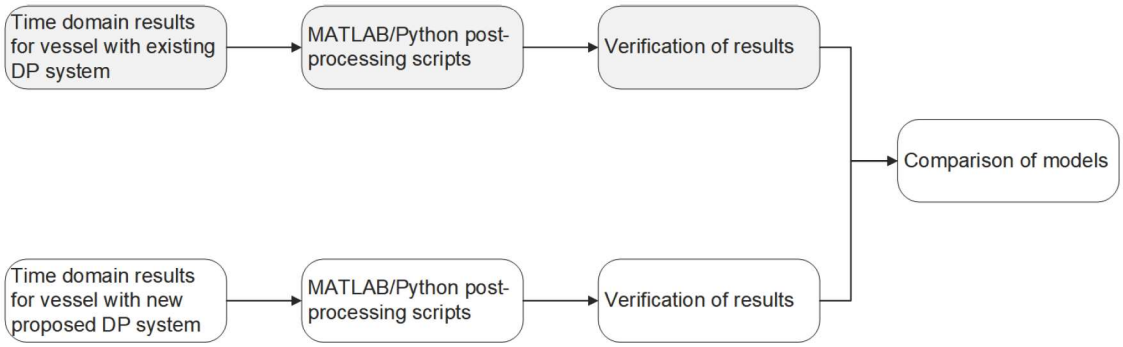

Figure 3.6: Step-by-step comparison methods

By completing steps 3 and 4, an answer can be given to the remaining sub-questions about the performance of the new model.

5. Conclude on the performance of new model

The final task is to draw conclusions on the results obtained at the fourth step. Roughly, it can be stated that the performance of the system improved when the DP footprint is smaller than the conventional DP footprint. The results found at the fourth step will be evaluated based on the same criteria as found in papers about the performance of DP systems, like the paper of Park, Jo and Choi [32] and Martelli, Fagionni and Donnarumma [33]. Such papers assess a DP system based on: the environment, control deviation, and fuel consumption. In this study, those parameters will be assessed based on the DP footprints around the gripper location, the motion statistics at the gripper location, and the energy consumption per simulation. The energy consumption is calculated using the propeller diagrams of the six thrusters mentioned in subsection 3.1.1. The DP module that is provided by HES calculates the total delivered thrust per thruster during simulations. The propeller diagrams relate the thrust to the input powers. Consequently, by finalizing this last step, an answer can be given to the main question of this thesis.

4

Design and implementation of the new DP system

The first sub-question concerned the design of the new DP system. As mentioned in the previous chapter, the new model was implemented in the external DP module. After a thorough analysis of the existing DP model, it was found that the new DP system required a new Kalman Filter and PD controller. This chapter discusses the design, tuning, testing, and implementation of the new Kalman Filter and PD controller. Also, the existing components of the conventional DP model are discussed to give insights into the DP model with the conventional control point.

4.1. Design and implementation of the Kalman Filter

This section explains how the Kalman Filter was designed and implemented for both the center location and the gripper location. First, the models and equations for both the center position and gripper position are explained. Although the model itself for the Kalman Filter was provided by the company, the appropriate tuning was still to be found for this study. After that, implementation and testing for the center point are discussed. Based on the behavior of the Kalman Filter for the center, the new Kalman Filter for the gripper position was designed and implemented. The design of the Kalman Filter at the gripper location will also be discussed in this chapter. The Kalman Filter settings and modifications mentioned in this chapter were eventually adopted in the external DP function in Python of HES.

4.1.1. State-transition matrices for the Kalman Filter

State-space representation is a way of representing a dynamical system as a set of states, inputs, and outputs. The variables include the system its states, input, and output. It can be used to describe and analyze the behavior of a system. The equation for the states to be estimated as presented in subsection 2.1.2 in the Kalman filter is nothing more than the regular EOM, written in a state-space form. In general, a state space is introduced into a system description without examining its specific physical meaning [34], just like for the Kalman Filter.

State-space representation for the Kalman Filter with center control point

As mentioned in Chapter 2.1, the states to be estimated in the Kalman Filter are the position and the velocity, which will be estimated based on the vessel properties. As mentioned in subsection 2.1.2, the state-transition matrix ($\mathbf{A}$) relates the states at time step $k-1$ to time step k. For the vessel, this relation comes from the kinematic equations, here presented for a single uncoupled DOF:

$$x_k = x_{k-1} + \Delta t v_{k-1} \tag{4.1}$$

and for the velocity:

$$v_k = v_{k-1} + \Delta t a_{k-1} \tag{4.2}$$

Wherein x_{k-1} is the position at the previous timestep, v_{k-1} is the velocity at the previous timestep and a_{k-1} is the acceleration at the previous time-step. State-space representations can also be used as a method to replace an n_{th}-order differential equation with a system of lower-order differential equations. To simplify the equations, the Kalman Filter in this study is reduced to a first-order system of equations. In order to do so, the acceleration term is isolated and expressed in terms of position and velocity. These terms are obtained from the equations of motion for the vessel. As stated before, motion coupling in

the center of the vessel can be assumed negligible. Hence, the equations of motion in the horizontal plane at the center of the vessel, assuming the vessel is at rest, are defined as:

$$\begin{bmatrix} M_{11} & 0 & 0 \\ 0 & M_{22} & 0 \\ 0 & 0 & M_{66} \end{bmatrix}\begin{bmatrix} \ddot{x} \\ \ddot{y} \\ \ddot{\psi} \end{bmatrix} + \begin{bmatrix} B_{11} & 0 & 0 \\ 0 & B_{22} & 0 \\ 0 & 0 & B_{66} \end{bmatrix}\begin{bmatrix} \dot{x} \\ \dot{y} \\ \dot{\psi} \end{bmatrix} + \begin{bmatrix} C_{11} & 0 & 0 \\ 0 & C_{22} & 0 \\ 0 & 0 & C_{66} \end{bmatrix}\begin{bmatrix} x \\ y \\ \psi \end{bmatrix} = \begin{bmatrix} 0 \\ 0 \\ 0 \end{bmatrix} \tag{4.3}$$

Wherein M_{ij} are the total masses for each DOF (mass + hydrodynamic mass or), B_{ij} are the hydrodynamic damping coefficients, and C_{ij} are the restoring spring coefficients, for $(i = j = 1, 2, 6)$.

The hydrodynamic coefficients are frequency dependent, but in the dynamic model for the Kalman Filter, the hydrodynamic coefficients are assumed constant and are obtained at a higher period of 83.78 seconds (= lower frequency). Since the DP system operates in the lower-frequency region and, since it was found that the hydrodynamic coefficients don't differ much in this region, a linearization was made around this operating point. Isolating the acceleration terms gives:

$$\begin{bmatrix} \ddot{x} \\ \ddot{y} \\ \ddot{\psi} \end{bmatrix} = -[M]^{-1}[C]\begin{bmatrix} x \\ y \\ \psi \end{bmatrix} - [M]^{-1}[B]\begin{bmatrix} \dot{x} \\ \dot{y} \\ \dot{\psi} \end{bmatrix} \tag{4.4}$$

Substituting this into equation 4.2 for all degrees of freedom in the horizontal plane, at the center of the vessel and bringing the position and velocity terms to the left-hand side of the equations, relating the current timestep k to the previous timestep $k-1$ gives the following system of equations:

$$\begin{bmatrix} x_k \\ y_k \\ \psi_k \\ \dot{x}_k \\ \dot{y}_k \\ \dot{\psi}_k \end{bmatrix} = \begin{bmatrix} 1 & 0 & 0 & \Delta t & 0 & 0 \\ 0 & 1 & 0 & 0 & \Delta t & 0 \\ 0 & 0 & 1 & 0 & 0 & \Delta t \\ & -[M]_{3x3}^{-1}[C]_{3x3}\Delta t & & & [I]_{3x3} - [M]_{3x3}^{-1}[B]_{3x3}\Delta t & \end{bmatrix}\begin{bmatrix} x_{k-1} \\ y_{k-1} \\ \psi_{k-1} \\ \dot{x}_{k-1} \\ \dot{y}_{k-1} \\ \dot{\psi}_{k-1} \end{bmatrix} \tag{4.5}$$

Wherein the $6x6$ matrix on the right-hand side of the equation is the *state-transition matrix*. Since there is little to no hydrodynamic stiffness (restoring term), nor hydrodynamic damping in the horizontal plane, these parameters are added by the DP system (see section 2.1 for an extensive explanation of this concept).

The values for the stiffness consist of the proportional gains of the PD controller and the values for the damping consist of the derivative gains of the PD controller. The PD controller gains for the center control point were provided by HES, and already defined in subsection 3.1.1 in Table 3.4.

For clarity, an example derivation for 1 DOF is written out for the surge motion hereafter. From Equation 4.1 and Equation 4.2 it follows that:

$$x_k = x_{k-1} + \Delta t \dot{x}_{k-1} \tag{4.6}$$

$$\dot{x}_k = \dot{x}_{k-1} + \Delta t \ddot{x}_{k-1} \tag{4.7}$$

Isolating the acceleration gives:

$$\ddot{x} = -\frac{b_{11}}{M_{11}}\dot{x} - \frac{c_{11}}{M_{11}}x \tag{4.8}$$

And, when substituting this back into equation 4.7 and filling in equation 4.6 gives:

$$\begin{bmatrix} position \\ velocity \end{bmatrix} = \begin{bmatrix} 1 & \Delta t \\ -\frac{C_{11}}{M_{11}}\Delta t & (1 - \frac{B_{11}}{M_{11}})\Delta t \end{bmatrix}\begin{bmatrix} x_{k-1} \\ v_{k-1} \end{bmatrix} \tag{4.9}$$

for the surge motion at the center of the vessel.

Using the same approach, this gives the following system of equations for all DOF in the horizontal plane:

$$\begin{bmatrix} x_k \\ y_k \\ \psi_k \\ \dot{x}_k \\ \dot{y}_k \\ \dot{\psi}_k \end{bmatrix} = \begin{bmatrix} 1 & 0 & 0 & \Delta t & 0 & 0 \\ 0 & 1 & 0 & 0 & \Delta t & 0 \\ 0 & 0 & 1 & 0 & 0 & \Delta t \\ -\frac{C_{11}}{M_{11}}\Delta t & 0 & 0 & 1-\frac{B_{11}}{M_{11}}\Delta t & 0 & 0 \\ 0 & -\frac{C_{22}}{M_{22}}\Delta t & 0 & 0 & 1-\frac{B_{22}}{M_{22}}\Delta t & 0 \\ 0 & 0 & -\frac{C_{66}}{M_{66}}\Delta t & 0 & 0 & 1-\frac{B_{66}}{M_{66}}\Delta t \end{bmatrix} \begin{bmatrix} x_{k-1} \\ y_{k-1} \\ \psi_{k-1} \\ \dot{x}_{k-1} \\ \dot{y}_{k-1} \\ \dot{\psi}_{k-1} \end{bmatrix} \tag{4.10}$$

Wherein: $C_{11}, C_{22}\ and\ C_{66}$ equal the proportional gains (K_1^P, K_2^P and K_6^P) from Table 3.4 for surge, sway and yaw respectively, and $B_{11}, B_{22}\ and\ B_{66}$ equal the derivative gains (K_1^D, K_2^D and K_6^D) from Table 3.4. $M_{11}, M_{22}\ and\ M_{66}$ are the solid mass + the added mass for the corresponding DOF.

State-space representation for the Kalman Filter with the control point at the gripper location

As the gripper is located far away from the center motion coupling becomes more severe and cannot be neglected anymore. When considering the gripper location, the equations of motion for the vessel at rest for surge, sway, and yaw are defined as follows, assuming we are only taking into account motion coupling in the horizontal plane:

$$\begin{bmatrix} M_{11} & 0 & M_{16} \\ 0 & M_{22} & M_{26} \\ M_{16} & M_{26} & M_{66} \end{bmatrix} \begin{bmatrix} \ddot{x} \\ \ddot{y} \\ \ddot{\psi} \end{bmatrix} + \begin{bmatrix} B_{11} & 0 & B_{16} \\ 0 & B_{22} & B_{26} \\ B_{16} & B_{26} & B_{66} \end{bmatrix} \begin{bmatrix} \dot{x} \\ \dot{y} \\ \dot{\psi} \end{bmatrix} + \begin{bmatrix} C_{11} & 0 & C_{16} \\ 0 & C_{22} & C_{26} \\ C_{16} & C_{26} & C_{66} \end{bmatrix} \begin{bmatrix} x \\ y \\ \psi \end{bmatrix} = \begin{bmatrix} 0 \\ 0 \\ 0 \end{bmatrix} \tag{4.11}$$

Hence, the state-space transition matrix for the Kalman Filter as previously presented for the center position, is not valid anymore at this point. Therefore, the estimated motions from the center are translated to the gripper position using a method for motion superposition as described in the book of Journee and Massie [7]. The method is explained hereafter. Knowing the motions of and about the center of the vessel, one can easily calculate the motions at any point of the vessel (staying in the same frame of reference) using motion superposition. Assuming small angles, it accounts that:

$$sin\phi \approx \phi \quad and, \quad cos\phi \approx 1.0 \tag{4.12}$$

Hence, the absolute motions for surge and sway in point B, with distances x_p and y_p relative to the center, become:

$$x_B = x_A - y_p\psi \tag{4.13}$$

$$y_B = y_A + x_p\psi \tag{4.14}$$

Wherein x_A and y_A are the motions in the CoG of the vessel, in the vessel-fixed frame **V**. x_B and y_B are the motions at the gripper location. Note that heave motions, as proposed in the book of Journee and Massie, are neglected here due to the fact that the DP controller is not able to correct for those. To use this method, the yaw angles should be defined in *radians*.

To get an estimate at the gripper location of the low-frequency motions, the state estimates of the Kalman Filter for the center control point, are translated to the alternative location using Equation 4.13 and Equation 4.14. The setup of this new filtering method is displayed in Figure 4.1.

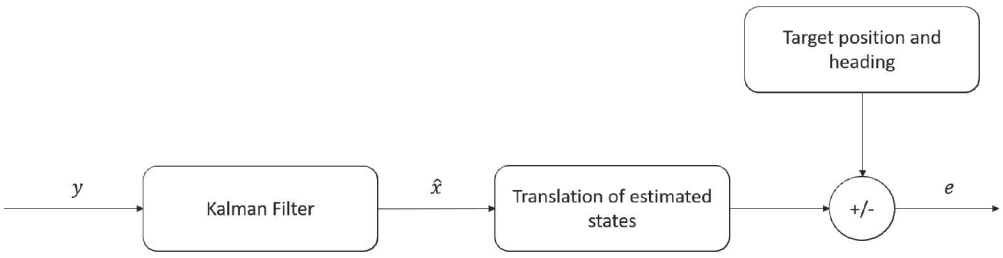

Figure 4.1: New Kalman Filter setup for gripper control point model

Wherein y is the input for the Kalman Filter, which are the measurements. $\hat{x}$ are the estimated states at the center position, of which the position estimates are then translated to the gripper position with Equation 4.13 and Equation 4.14. Hereafter, the translated position estimate is compared to the target position and heading of the gripper location, resulting in an error (e) that is sent to the PD controller. The design and implementation of the PD controller will be discussed in section 4.3.

4.1.2. Kalman Filter tuning and implementation

For the prediction step of the Kalman Filter, the state-transition matrix was established in the previous subsection. To update the prediction with the measurements, Equation 2.7 is solved by the Kalman Filter. For clarity, the equation is repeated here:

$$\hat{\mathbf{x}}_k = \hat{\mathbf{x}}_k^- + \mathbf{K}_k(\mathbf{z}_k - \mathbf{H}\hat{\mathbf{x}}_k^-) \tag{4.15}$$

The Kalman Gain in this equation, $\mathbf{K}_k$, is dependent on the tuning of the process noise covariance ($\mathbf{Q}$) and measurement noise covariance ($\mathbf{R}$) matrices. As stated before, the primary purpose of the Kalman Filter is to filter out the first-order motion responses. To do so, a proper tuning must be found. The tuning process for the Kalman Filters for both models is explained hereafter.

Kalman Filter tuning and implementation for the center control point

Kalman Filter tuning is the process of adjusting the parameters of a Kalman filter to optimize its performance. The parameters that need to be adjusted are specific to each application and typically include the process noise covariance matrix ($\mathbf{Q}$) and the measurement noise covariance matrix ($\mathbf{R}$). From tuning the $\mathbf{Q}$ and $\mathbf{R}$ matrices, it is determined how much the Kalman Filter relies on either the measurements or the dynamic model; i.e. it gives weights on whether it should trust the dynamic model or the measurements more.

Tuning a Kalman filter involves adjusting these parameters to minimize the filter's error in estimating the actual state of the system, which in this case would be the low-frequency motions. The tuning process is an iterative process that involves trial and error [35].

HES provided a model of the Kalman Filter in MATLAB. The Kalman Filter was tested as a single module before being implemented in the loop. Hence, the first step was to find the desired tuning in the MATLAB model. Figure 4.2 shows an example of the experimental setup.

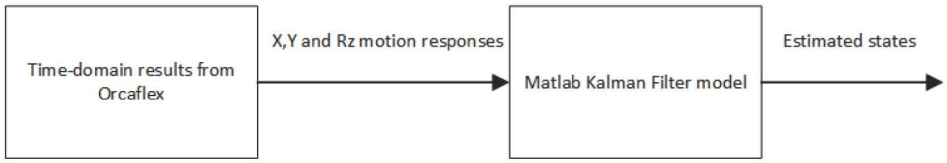

Figure 4.2: Kalman Filter setup for MATLAB tests

The Kalman Filter in this MATLAB setup was tuned by applying the filtering on time traces of the motions, which are obtained from simple time-domain simulations in Orcaflex. For the time-domain results from Orcaflex, the Aegir vessel was modelled with a constraint that only allows motions in the horizontal plane. For the motions allowed in the horizontal plane, stiffness and damping constraints were added to mimic an actual DP system. The stiffness and damping values for the constraints had equal values as the P and D gains as stated in Table 3.4.

The $\mathbf{Q}$ matrix was iteratively changed until the desired behavior was found. The design requirement for the filter was to give a balanced output between filtering the noise whilst taking into account all of the low-frequency motions. The output signal should show similar behavior as the second order signal as mentioned in section 2.2. The measurement noise covariance can be measured from simulations. Hence, values for the measurement noise covariance matrix $\mathbf{R}$ were provided by HES based on their previous work.

The final process noise covariance matrix and measurement noise covariance matrix for the Kalman

Filter at the center position are displayed in equations 4.16 and 4.17.

$$\mathbf{Q} = \begin{bmatrix} Q_x & 0 & 0 & 0 & 0 & 0 \\ 0 & Q_y & 0 & 0 & 0 & 0 \\ 0 & 0 & Q_{rz} & 0 & 0 & 0 \\ 0 & 0 & 0 & Q_x & 0 & 0 \\ 0 & 0 & 0 & 0 & Q_y & 0 \\ 0 & 0 & 0 & 0 & 0 & Q_{rz} \end{bmatrix} \tag{4.16}$$

With:

$$[Q_x, Q_y, Q_{rz}] = [***, ***, ***]$$

$$\mathbf{R} = \begin{bmatrix} \sigma_x & 0 & 0 & 0 & 0 & 0 \\ 0 & \sigma_y & 0 & 0 & 0 & 0 \\ 0 & 0 & \sigma_{rz} & 0 & 0 & 0 \\ 0 & 0 & 0 & \sigma_{vx} & 0 & 0 \\ 0 & 0 & 0 & 0 & \sigma_{vy} & 0 \\ 0 & 0 & 0 & 0 & 0 & \sigma_{vrz} \end{bmatrix} = \begin{bmatrix} R_x & 0 & 0 & 0 & 0 & 0 \\ 0 & R_y & 0 & 0 & 0 & 0 \\ 0 & 0 & R_{rz} & 0 & 0 & 0 \\ 0 & 0 & 0 & R_{vx} & 0 & 0 \\ 0 & 0 & 0 & 0 & R_{vy} & 0 \\ 0 & 0 & 0 & 0 & 0 & R_{vrz} \end{bmatrix} \tag{4.17}$$

With:

$$[R_x, R_y, R_{rz}, R_{vx}, R_{vy}, R_{vrz}] = [***, ***, ***, ***, ***, ***]$$

Results of implementing the tuning parameters as mentioned in Equation 4.16 and Equation 4.17 are displayed in Figure 4.3 for the MATLAB model. In this figure, the blue lines indicate the actual measured motion response of the vessel in the surge, sway, and yaw direction. The red lines indicate the output of the Kalman Filter, which is the signal that will eventually be sent to the PD controller. As can be seen in Figure 4.3, the vast majority of the noise is filtered out.

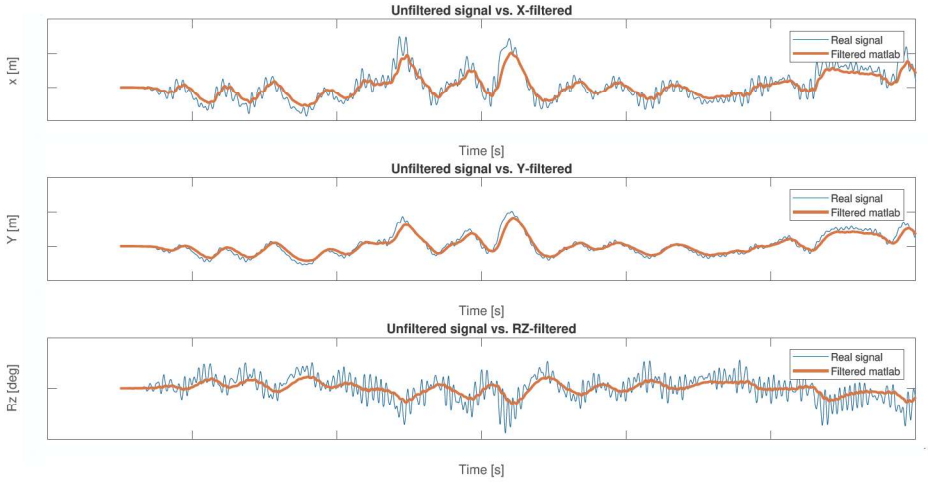

Figure 4.3: Tuned Kalman Filter output at center position

Kalman Filter tuning and implementation for the gripper control point

As the equations of motions changed for the gripper control point, a translation of the states estimated by the Kalman Filter in the center of the vessel was applied. The full approach was already explained in subsection 4.1.1. An equal testing setup was used as for the Kalman Filter at the center, using a time trace from Orcaflex and applying the filtering through MATLAB afterward. For clarity, an overview of the setup for testing the Kalman Filter for the alternative location is displayed in Figure 4.4.

Figure 4.4: Kalman Filter setup for MATLAB tests - Gripper CP model

The center DP control point is located at [95.3 m, 0.0m, 9.0 m] with respect to the stern, center line, and keel. The gripper location is located at [30.8 m, -37.1 m, 9.0 m] with respect to the stern, center line, and keel. This means that:

$$x_p = 95.3 - 30.8 = 64.5\ m$$
$$y_p = 0 - (-37.1) = 37.1\ m$$

As the Kalman Filter itself is still located at the center, the tuning parameters remained equal. Filtering results from the MATLAB model setup for the gripper location, as displayed in Figure 4.4, are displayed in Figure 4.5. Again the blue lines represent the measurements and the red lines indicate the translated Kalman Filter outputs. Note that the measurements presented here are obtained at the gripper location.

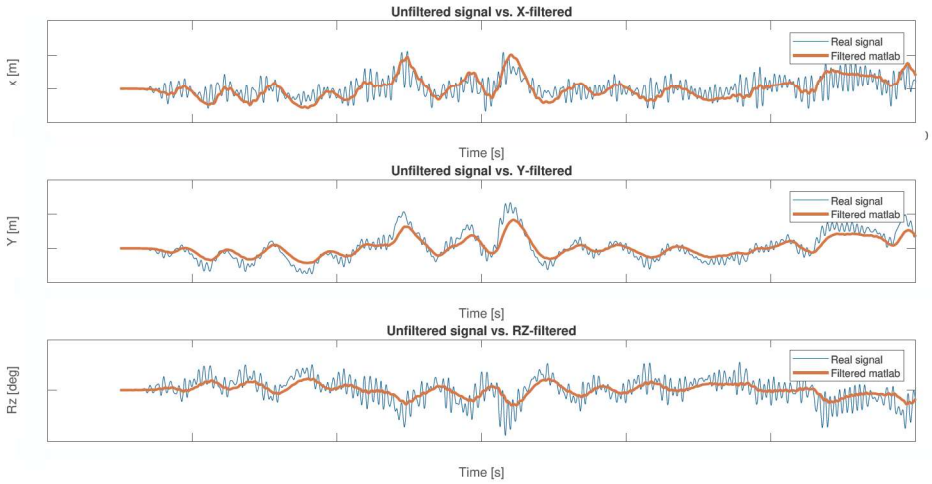

Figure 4.5: Tuned Kalman Filter output at gripper location

4.2. System verification

Eventually, the Kalman Filter needs to work in harmony with the PD controller and the thruster allocation, as programmed in the external DP function in Python of HES. Hence, after implementing the Kalman Filters as discussed in the previous sections of this chapter, the PD controllers as discussed in section 4.3 and, the thruster allocation algorithm in the external DP function in Python, the Kalman Filter outputs were checked after the first time-domain simulations were performed in Orcaflex. The results in this section are the filtering results for a 3-hour simulation, under the vessel its normal working conditions (the 'base case') as mentioned in subsection 3.1.3. The setup for the time domain simulations was shown in Figure 3.2 for the center and will be presented at the end of this chapter in Figure 4.14 for the new proposed DP system.

The difference between the time domain model presented here and the MATLAB model in the previous section is that for the time domain model the filtering was applied at every time step, while for the MATLAB model, the filtering was applied afterward.

4.2.1. Filtering during time domain simulations

Figure 4.6 shows the behavior of the Kalman Filter at the center position during the time-domain simulations on the left side. As can be seen in the Figures, the filter in the Orcaflex model shows equal behavior to the model used for tuning in MATLAB (see subsection 4.1.2) and filters out the wave frequent motions. Therefore, the model is assumed to be valid for the rest of the study.

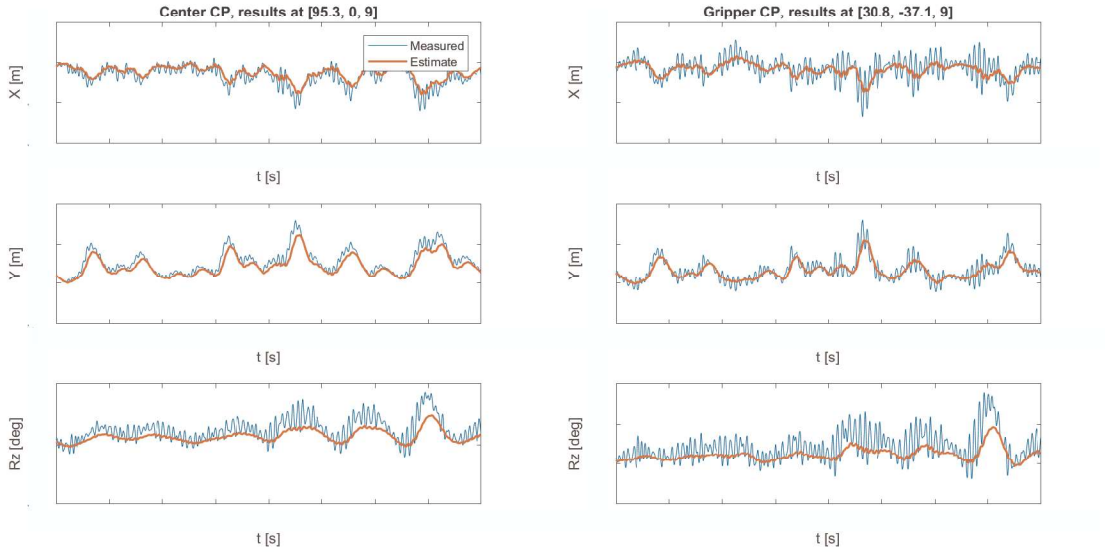

Figure 4.6: Time-domain results for Kalman Filter; center control point vs. gripper control point

As stated before, the Kalman Filter for the gripper location consists of the same Kalman Filter for the center, plus a translation. Results from time domain simulations at the gripper location are plotted and displayed in Figure 4.6 on the right side. In order to eventually make a fair comparison between both models, the filtering of the two models should be as equal as possible. The filtering behavior at the gripper location was assumed equal enough to the center location.

4.2.2. Comparison of filtering

To make an even more extensive comparison between the Kalman Filters, the Kalman Filter outputs were compared to the 'ideal filter' outputs. By using a bandpass filter function in MATLAB, developed by Heerema, the motion signals from simulations were obtained and the low-frequency motions were filtered out without any phase lag. The cut-off frequency of the bandpass filter was set on 0.2 rad/s.

The second-order motions are compared with the Kalman Filter outputs for both models and in order to draw a conclusion on their performance relative to each other, the Root Mean Square Error (RMSE) were calculated between the low-frequency signal and the Kalman Filter outputs for both models. The RMSE is a measure of the differences between values predicted by a model or an estimator and the values observed; here: the Kalman Filter (estimator) and the actual low-frequency motions (values observed). The RMSE is calculated as:

$$RMSE = \sqrt{\frac{\sum_{n=1}^{N}(x_i - \hat{x}_i)^2}{N}} \tag{4.18}$$

Wherein x_i is the actually observed time series, here: bandpass filter signal, or 'ideal signal', and $\hat{x}_i$ is the estimated time series, here: Kalman Filter output signal. N is the number of data points, which is the total amount of timesteps here. The results are displayed in Figure 4.7. The RMSE are displayed in Table 4.1

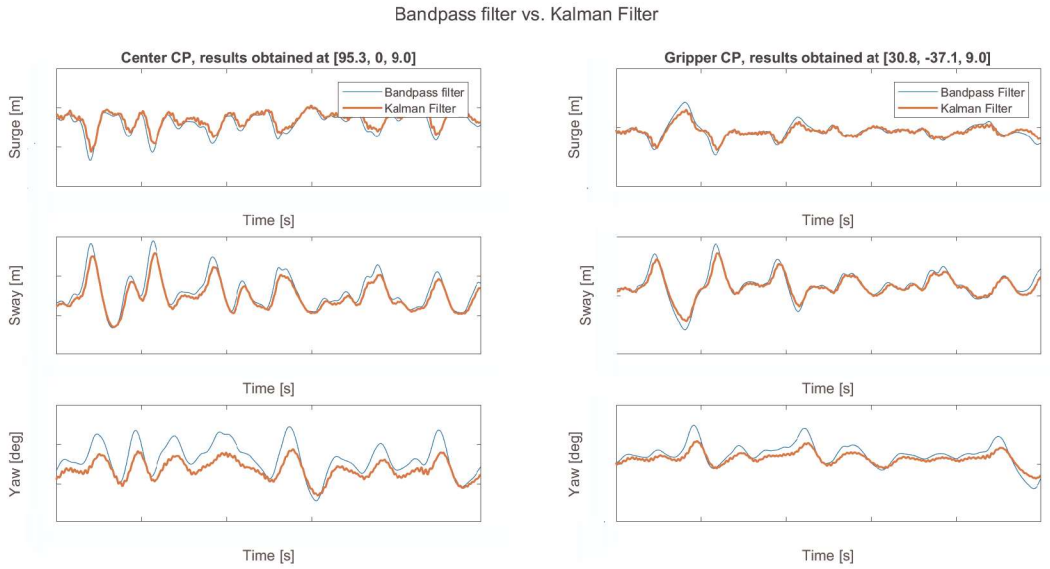

Figure 4.7: Testing of Kalman Filter performance: Low-frequency motions vs. Kalman Filter output signals

As can be seen in Table 4.1, the performance of the Kalman Filter for the gripper control point is slightly better, but the differences are marginal. Hence, the performances of the Kalman Filter are assumed to be equal enough to do a comparison study.

Table 4.1: RMSE for Kalman Filter tests

	RMSE Center CP	RMSE Gripper CP
Surge [m]	0.022	0.021
Sway [m]	0.074	0.060
Yaw [deg]	0.083	0.061

4.3. Controller design and implementation

The PD controller in a DP system is used to monitor and control the positioning of the vessel. It receives the filtered position and heading in the horizontal plane, and compares this to the desired position and heading. The controller then calculates the necessary changes in the vessel's speed and heading in order to maintain this position. As stated before, the integral term is left out in this thesis.

This section discusses the design of the new PD controller. After that, the dynamic models for both control points are presented. These will be used for the testing of the systems. Thereafter, the implementation, verification, and testing of the new system for the gripper control point will be discussed.

4.3.1. PD controller design for the gripper location

The setup in the conventional DP system was presented in Figure 3.3. The conventional controller consisted of three separate PID controllers, one for each DOF, and was already implemented in the external DP module that communicates with the Orcaflex software. As stated before, the equations of motion will change at the gripper location, and as discussed in section 4.1, the estimated states at the gripper location consist of coupled responses as they are translated. Due to this coupling, the signal that is fed into the PD controllers contains coupling too. When sending coupled signals into the PD controller, the applied PD actions could affect one another which could potentially lead to difficulties. Consequently, the control parameters were modified and a decoupling module was added to account for such coupling at the gripper position. This can help prevent unwanted interactions between different states that might otherwise interfere with the controller's ability to accurately control the system. The model presented here is based on an example on the Mathworks[1] website, and an equal method is described in the paper of Astrom, Johansson, and Wang [9]. The new proposed controller for the alternative location consists of Multiple-Input-Multiple-Output (MIMO) PD controller setup and an example is shown in Figure 4.8.

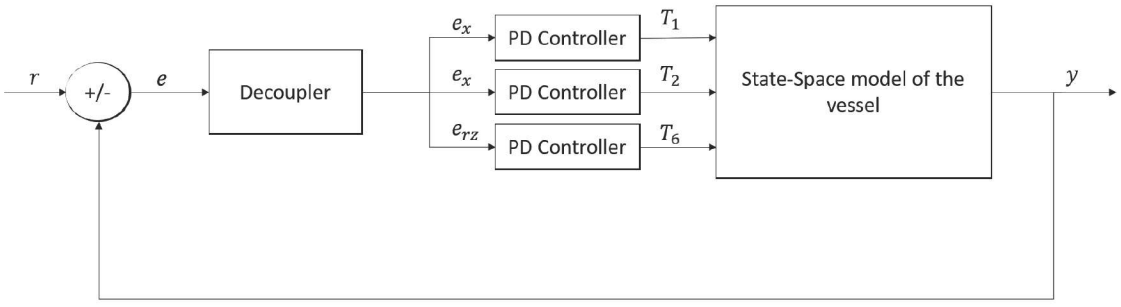

Figure 4.8: PD controller setup for MATLAB tests

Wherein e is the (coupled) position error, $e = r - y$, e_x, e_y and e_{rz} are the uncoupled errors and T_i is the applied thruster force. The control objective for the PD controllers with both control points is to minimize the position error, hence:

$$r - y = 0 \tag{4.19}$$

Note that the errors for the center control point model are calculated at the center, but the errors for the gripper control point model are calculated at the gripper location.

The setup as presented above is tested first using the PD controller gains of the center control point DP system as presented in chapter 3 and with the decoupling module set to the identity matrix. In this setup, a state-space model of the vessel with a center control point is used. The derivation of this state-space model is presented hereafter.

[1] Mathworks example

Dynamic model for testing of the center PD controllers

The dynamic model consists of a state-space representation of the EOM, of which the derivation will be presented in this section. The derivation of the state-space model for the center control point starts with the equations of motion for a DP vessel [7]:

$$\begin{bmatrix} M_{11} & 0 & 0 \\ 0 & M_{22} & 0 \\ 0 & 0 & M_{66} \end{bmatrix}\begin{bmatrix} \ddot{x} \\ \ddot{y} \\ \ddot{\psi} \end{bmatrix} + \begin{bmatrix} B_{11} & 0 & 0 \\ 0 & B_{22} & 0 \\ 0 & 0 & B_{66} \end{bmatrix}\begin{bmatrix} \dot{x} \\ \dot{y} \\ \dot{\psi} \end{bmatrix} + \begin{bmatrix} C_{11} & 0 & 0 \\ 0 & C_{22} & 0 \\ 0 & 0 & C_{66} \end{bmatrix}\begin{bmatrix} x \\ y \\ \psi \end{bmatrix} = \begin{bmatrix} F_1^D + T_1 \\ F_2^D + T_2 \\ F_6^D + T_6 \end{bmatrix} \tag{4.20}$$

Wherein M_{ij} is the total mass, B_{ij} is the total damping, C_{ij} is the total stiffness, F_i^D is the wave drift force and T_i is the applied thruster force. The thruster forces are to be calculated by the PD controller, wherein one part is proportional to the position error and one part is proportional to the velocity. The stiffness

Unlike the state-space model derived for the Kalman Filter in chapter 4.1, the reduction from a second-order differential system to a first-order differential system is not necessary. This is because the MATLAB toolboxes used here handle the equations in this form. Bringing the equations as mentioned in Equation 4.20 to state-space, for both control points gives:

$$\dot{x} = Ax + Bu, \qquad x = \left[x, y, \psi, \dot{x}, \dot{y}, \dot{\psi}\right]^T$$

$$u = \left[F_1^D, F_2^D, F_6^D, T_1, T_2, T_6\right]^T \qquad y = Cx + Du$$

$$\begin{bmatrix} \dot{x} \\ \dot{y} \\ \dot{\psi} \\ \ddot{x} \\ \ddot{y} \\ \ddot{\psi} \end{bmatrix} = \begin{bmatrix} 0 & 0 & 0 & 1 & 0 & 0 \\ 0 & 0 & 0 & 0 & 1 & 0 \\ 0 & 0 & 0 & 0 & 0 & 1 \\ & -[M]_{3x3}^{-1}[C]_{3x3} & & & -[M]_{3x3}^{-1}[B]_{3x3} & \end{bmatrix}\begin{bmatrix} x \\ y \\ \psi \\ \dot{x} \\ \dot{y} \\ \dot{\psi} \end{bmatrix} + \begin{bmatrix} 0 & 0 & 0 & 0 & 0 & 0 \\ 0 & 0 & 0 & 0 & 0 & 0 \\ 0 & 0 & 0 & 0 & 0 & 0 \\ & -[M]_{3x3}^{-1} & & & -[M]_{3x3}^{-1} & \end{bmatrix}\begin{bmatrix} F_1^D \\ F_2^D \\ F_6^D \\ T_1 \\ T_2 \\ T_6 \end{bmatrix} \tag{4.21}$$

Filling in this system of equations for the center control points gives us the state-space model of the vessel:

$$\begin{bmatrix} \dot{x} \\ \dot{y} \\ \dot{\psi} \\ \ddot{x} \\ \ddot{y} \\ \ddot{\psi} \end{bmatrix} = \begin{bmatrix} 0 & 0 & 0 & 1 & 0 & 0 \\ 0 & 0 & 0 & 0 & 1 & 0 \\ 0 & 0 & 0 & 0 & 0 & 1 \\ -\frac{C_{11}}{M_{11}} & 0 & 0 & -\frac{B_{11}}{M_{11}} & 0 & 0 \\ 0 & -\frac{C_{22}}{M_{22}} & 0 & 0 & -\frac{B_{22}}{M_{22}} & 0 \\ 0 & 0 & -\frac{C_{66}}{M_{66}} & 0 & 0 & -\frac{B_{66}}{M_{66}} \end{bmatrix}\begin{bmatrix} x \\ y \\ \psi \\ \dot{x} \\ \dot{y} \\ \dot{\psi} \end{bmatrix} + \begin{bmatrix} 0 & 0 & 0 & 0 & 0 & 0 \\ 0 & 0 & 0 & 0 & 0 & 0 \\ 0 & 0 & 0 & 0 & 0 & 0 \\ -\frac{1}{M_{11}} & 0 & 0 & -\frac{1}{M_{11}} & 0 & 0 \\ 0 & -\frac{1}{M_{22}} & 0 & 0 & -\frac{1}{M_{22}} & 0 \\ 0 & 0 & -\frac{1}{M_{66}} & 0 & 0 & -\frac{1}{M_{66}} \end{bmatrix}\begin{bmatrix} F_1^D \\ F_2^D \\ F_6^D \\ T_1 \\ T_2 \\ T_6 \end{bmatrix} \tag{4.22}$$

For testing purposes, the wave drift forces are assumed zero in this model. Since the stiffness in the horizontal plane is delivered by the PD controllers, C_{11}, C_{22}, and C_{66} are initially set to zero. The damping terms B_{11}, B_{22} and B_{66} are set to the hydrodynamic damping, using the same approach as for the Kalman Filter (see subsection 4.1.1). The remaining damping comes again from the PD controller. The code including the setup as presented in Figure 4.8 with the dynamic model for the center can be found in Appendix B.

Dynamic model for testing of gripper PD controller

The models for the center control point and gripper control point will differ due to their mass, stiffness, and damping matrices. Consequently, this leads to the state-space representation of the equations of motion for the gripper control point to be the same as presented in Equation 4.21, by filling in the coupled terms from the EOM as presented in Equation 4.11 in the previous chapter. The complete matrices including those coupled terms are presented in Appendix A. The mass matrices, hydrodynamic mass matrices, and damping matrices for the gripper location are translated using the method as described in the book of Fossen [17]. The code of the model as presented in Figure 4.8 with the dynamic model at the gripper position can be found in Appendix C.

Decoupler

The decoupler consists of static gains, which give weights to each of the incoming errors, in order to calculate the actual decoupled error. These gains are included in a 3-by-3 matrix, an example of the decoupled error calculation is shown in Equation 4.23 below.

$$\begin{bmatrix} e_x \\ e_y \\ e_{rz} \end{bmatrix}^T = \begin{bmatrix} e(1) & e(2) & e(3) \end{bmatrix} \cdot \begin{bmatrix} D_{11} & D_{12} & D_{13} \\ D_{21} & D_{22} & D_{23} \\ D_{31} & D_{32} & D_{33} \end{bmatrix} \tag{4.23}$$

The decoupled errors, e_x, e_y and e_{rz} will then be sent into the PD controllers, which calculate the demanded forces for the vessel to remain in its position. These forces are fed into the state-space model of the vessel, which relates the forces to the states. The states, in this case, are the displacements in the surge and sway direction, the yaw rotation, and their corresponding velocities or angular velocity.

4.4. System verification

To ensure that the controller presented in Figure 4.8 works adequately, tests were conducted at the center position first, as the outputs for the center control point controller are known. The PD controller and decoupling module were implemented in the external DP model that is connected to the model of the vessel in Orcaflex, in order to perform tests in the time domain. The responses of the implemented controller were compared to the responses of the PD controller model of HES in Orcaflex and the MATLAB model that calculates the responses based on the state-space model as presented in the previous subsection. Summarized, the three models for the verification tests that will be presented hereafter consisted of the following:

- **Model 1:** MATLAB model as defined in Figure 4.8, with state-space model corresponding to the center control point.
- **Model 2:** Original Orcaflex model of the Aegir, including a DP module, provided by HES. The Kalman Filter and thruster allocation were put off for this test. No external (environmental) forces due to wind, waves or current were applied for the test.
- **Model 3:** Model 2 with the new PD controller. The decoupler from Model 1 is implemented here, the decoupling matrix is initially set to the identity matrix.

If all above mentioned three models show equal responses, the design and implementation of the MIMO PD controller were assumed to be valid for this study. The gains for the PD controller in the center of the vessel were provided by HES and defined in Chapter 3.1.1.

4.4.1. Response test

For the first test, the response is checked after applying a certain force. Tests were done for each DOF separately while constraining the remaining DOF in the horizontal plane. The forces applied to the vessel had the same magnitude as the P gains of the controller and were applied at the center of the vessel. Since the units for the P gains are defined as kN/m for the displacements and kN/deg for the rotation, a response of 1 meter is expected for the surge and sway direction and a response of 1 degree in the yaw direction for all models. The forces are applied at the center of the vessel. Since the decoupler is set to the identity matrix here, no influences should be present from the module. Results are plotted for all three models in Figure 4.9.

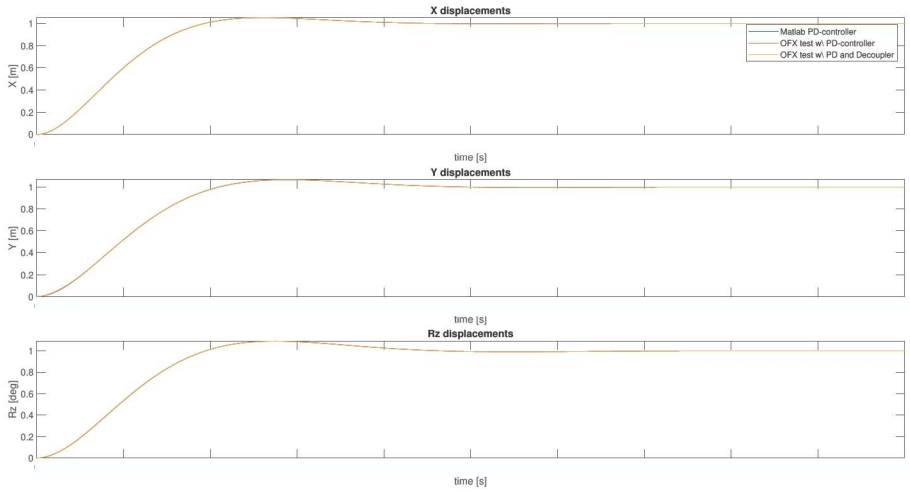

Figure 4.9: PD outputs for center CP model - Response tests

As can be seen in Figure 4.9, all three models have an equal response and converge to the expected value of 1. Therefore, the new testing setup as presented in Figure 4.8 is assumed to be valid for the center control point.

4.4.2. Force response tests

To validate the decoupling matrix and its implementation, tests with various gains in the decoupler were done to check whether the output forces are logical. These tests were done with only Model 3 since all three models gave equal responses and model 3 is the model that had to be implemented for the gripper position Orcaflex model eventually.
The test presented here is done for only the surge direction, changing only D_{11} from the decoupling matrix (see Equation 4.23). Tests were performed with gains of 1, 10, and 0.5 and an applied force in the X-direction, applied in the center of the vessel and equal for all tests. Results are shown in Figure 4.10.

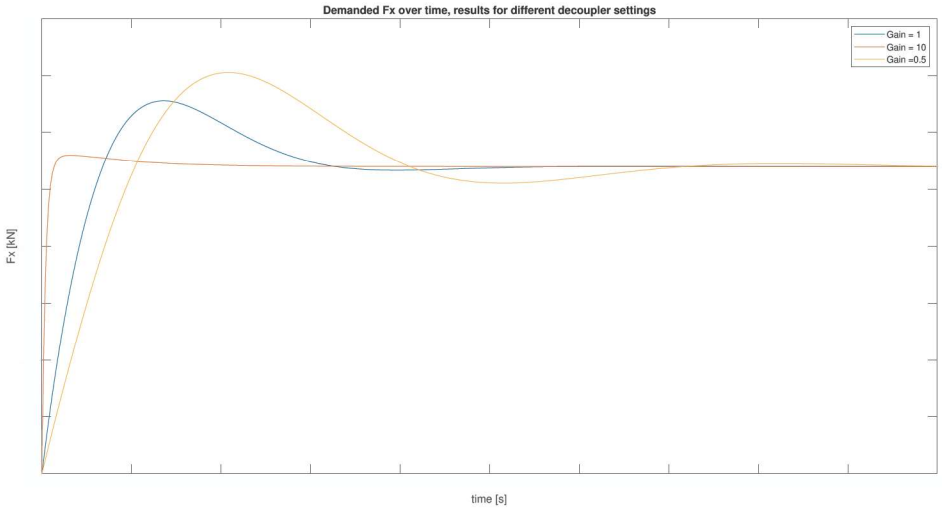

Figure 4.10: PD outputs for center CP model - Force response tests

When considering the PID equation (see Equation 2.10), a higher P-gain should lead to a larger initial error and thus a larger demanded force at the beginning of a simulation. Hence, a lower gain should result in a smaller initial error and thus a smaller demanded force at the beginning of a simulation and a slower response of the PD controller. This expectation is supported by the results in Figure 4.10, which demonstrate that the larger gain results in a larger initial force than the lower gain. Also, higher P gains should lead to faster settling time, which is also the case when considering Figure 4.10.

4.5. Controller integration at the gripper position

As stated earlier, for the eventual analysis a MIMO PD controller including a decoupling module was required at the gripper location. Since the controller is tested and assumed to be working at the center position, it can now be implemented at the gripper position. Again, tests are performed to check whether the controller performs as expected.

4.5.1. Design requirements and tuning results

For the Aegir vessel, the DP response is optimized by HES for the center control point. Hence, one aimed for an equal response for the controller at the gripper location compared to PD controllers for the center control point. Also, one would aim for an almost equal response at the gripper position compared to the center position in order to make a proper comparison between the eventual models. This requires approximately equal settling times and overshoots as for the PD controller for the center position. As can be seen in Figure 3.6, the settling times lie around *** seconds and the overshoots lie around ***%.

The step responses of the PD controller model for the center location in MATLAB were used as a tuning requirement for the PD controller at the gripper location. The controller at the gripper location was tuned automatically using the *looptune* command in MATLAB, with a *maximum relative matching error* of 0.2. Results are shown in Figure 4.11, wherein the red lines indicate the step response for the tuned PD controllers for the gripper control point and the blue dotted lines indicate the step response of the PD controllers at the center location.

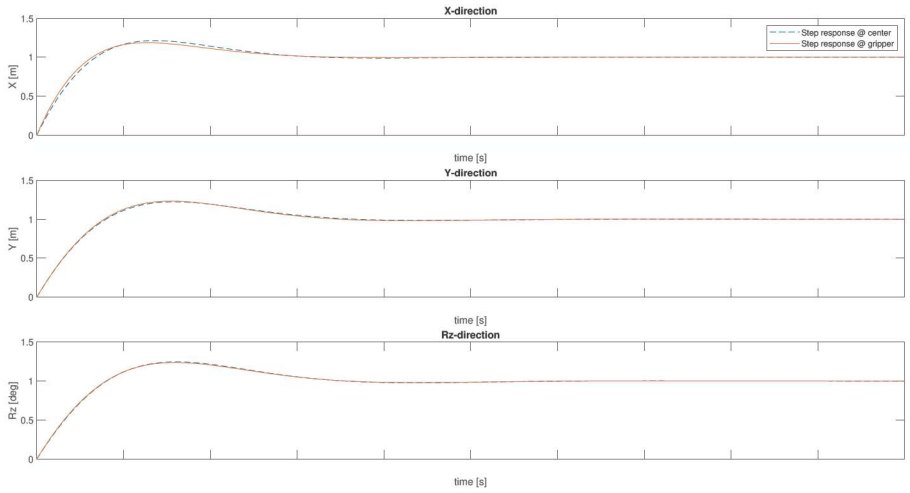

Figure 4.11: Tuning goal for PD controller with gripper CP vs. actual PD controller response at gripper location

The tuning resulted in different control gains at the gripper location for both the PD controller and decoupler. Results are shown in Table 4.2 and 4.3.

Table 4.2: PID gains at gripper location

	X-gain	Y-gain	Rz-gain
P	***	***	***
D	***	***	***

Table 4.3: Decoupling matrix at gripper location

	u1	u2	u3
y1	***	***	***
y2	***	***	***
y3	***	***	***

4.5.2. Decoupling test

To validate the gains of the decoupler (see Table 4.3) and the PD settings (see Table 4.2) for the new system, the step responses are checked. Figure 4.12 shows the response of the state-space model for the gripper location, in the setup as presented in Figure 4.8 and including the new PD gains and Decoupler gains, to a step input of unit amplitude.

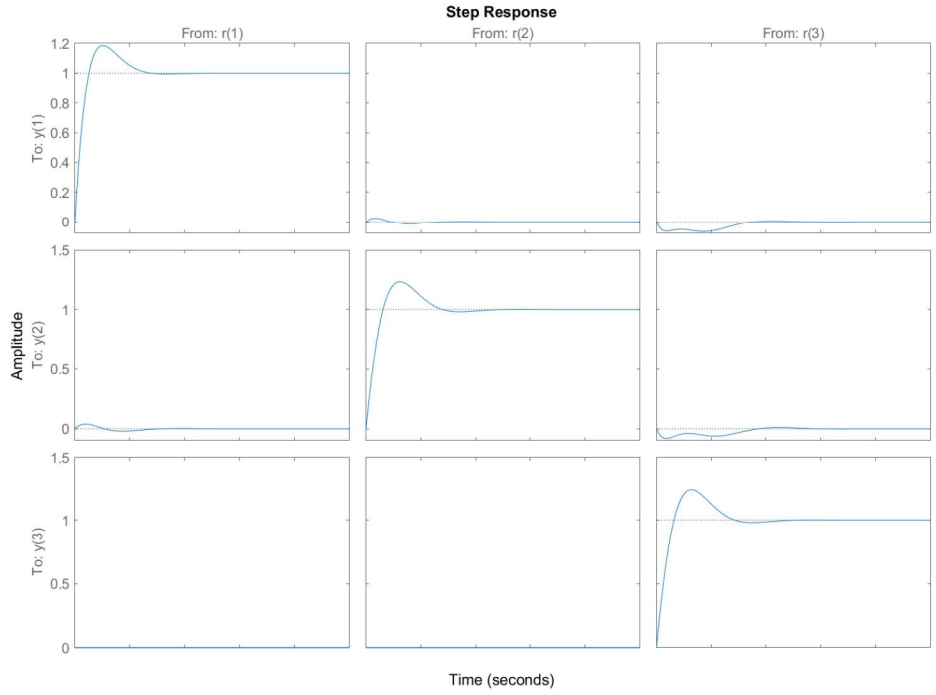

Figure 4.12: Step responses of the new controller

As stated earlier in this section, the control objective for the PD controller at the gripper location is to keep the error equal to zero ($r - y = 0$). The signal that is sent into the system at r in this test, is of constant amplitude 1. If the system wants to satisfy the control objective, y should become 1 too. Additionally, if the decoupling module works as expected, only a significant response should show in the diagonal plots of Figure 4.12. When considering the plots in this figure, one can see that the responses are indeed in line with the expectations.

4.5.3. Response tests

The same response tests were conducted as for the center control point model, applying the force now at the gripper location. The models compared consisted of the following:

- **Model 1** The PD controller in the MATLAB setup, as shown in Figure 4.8, including the newly calculated PD gains and static gains for the decoupling module.
- **Model 2** The new PD controller including the decoupling module implemented in the external DP module of Orcaflex, connected to an Orcaflex model of the vessel. The Kalman Filter and thruster allocation were put off for this test. No external (environmental) forces due to wind, waves, or current were applied for the test.

The applied forces are chosen in such a way, that the outputs resulted in a displacement of 1 meter at the gripper location. The outputs are not as straightforward as for the center position, since the error signal is decoupled before sending it to the PD controller. However, the results of this test tell that the models considered have an equal response. And, that the settling time and overshoot are indeed similar to the PD controller response of the controller in the center position (see Figure 4.9). Results for the gripper location are shown in Figure 4.13.

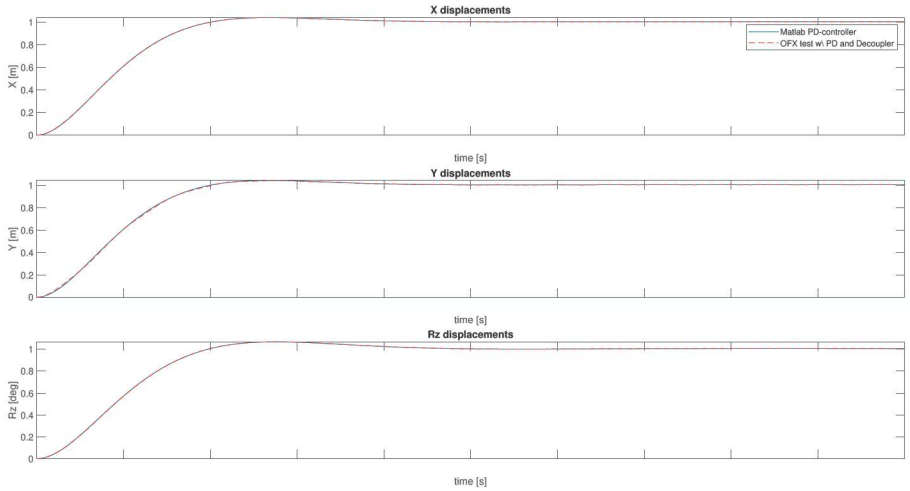

Figure 4.13: PD outputs for gripper CP model - Response tests

4.6. New DP system overview

As the new components of the new proposed DP system are designed and tested, it is now clear what the new DP system looks like. An overview of the new DP system is shown in Figure 4.14 below. The components indicated in green are introduced for the new system. The conventional system was shown in Figure 3.2.

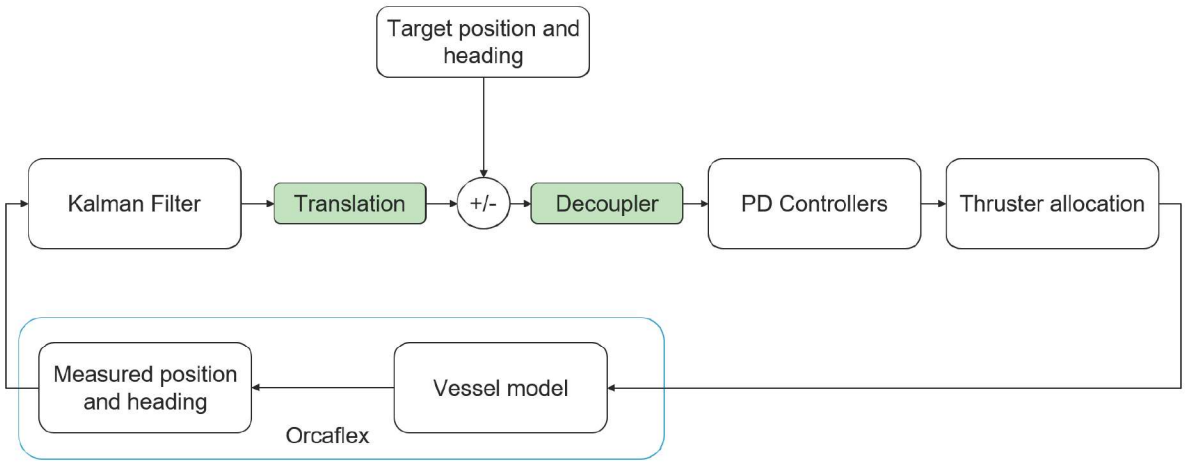

Figure 4.14: External DP module setup for time domain simulations - gripper control point (new) model

As stated in chapter 3, it was found that the new DP system needed a new Kalman Filter, controller and that it needed some modification to the thruster allocation. In the thruster allocation algorithm, the distances per thruster to the control point were defined, as the demanded forces are calculated at the control point. Since the control point changed, these distances needed a change too. Hence, all coordinates were adjusted in the thruster allocation algorithm for the new DP model.

5
Motion response results

After implementing all the newly designed components and settings of the DP system as described in chapter 4 and the thruster allocation with the limits as discussed in subsection 2.1.4 for the gripper control point model, time domain simulations were done to study the dynamic behavior of the vessel on DP. This chapter discusses the motion response results for both the conventional DP system with the center control point and the new DP system with the gripper control point. By doing so, the second and third sub-questions can be answered, which concern the DP footprint and motion responses of the new model in comparison with the old model. The results presented and compared in this chapter are the results of the following two models:

- **Center control point model**: consisting of the conventional DP system used by HES.
- **Gripper control point model**: consisting of the new DP system of which the design is presented in the previous chapters of this report.

All the results presented in this chapter are obtained in the body-bound frame **V** as discussed in section 2.2.

5.1. Base case results

This section presents the results obtained from the time domain simulations for the so-called 'base case' sea state. This base case was already defined in chapter 3, but a summary of the environmental conditions is repeated here for clarity:

Table 5.1: Input data for time domain simulations - Base case

Spectrum		JONSWAP
Hs	[m]	1.5
Wave direction	[deg]	135
Tp	[s]	8

Due to the start-up time of the thruster allocation algorithm and the fact that the Kalman Filter needs some settling time, the first 200 seconds of the simulations are neglected while obtaining the results. In order to make the fairest possible comparison, the exact same wave trains were applied in simulations for both models.

5.1.1. Trajectories at the gripper location

One of the most important results for this study would be the gripper footprint and/or envelope. The footprint consists of the vessel its horizontal trajectory during the simulation and the envelope is a plot of the extreme values of the footprint during this simulation. The footprints and envelopes for both center control point and gripper control point are displayed in Figure 5.1. The results are obtained at the gripper location for both models, hence $[x, y] = [0, 0]$ corresponds to the gripper location.

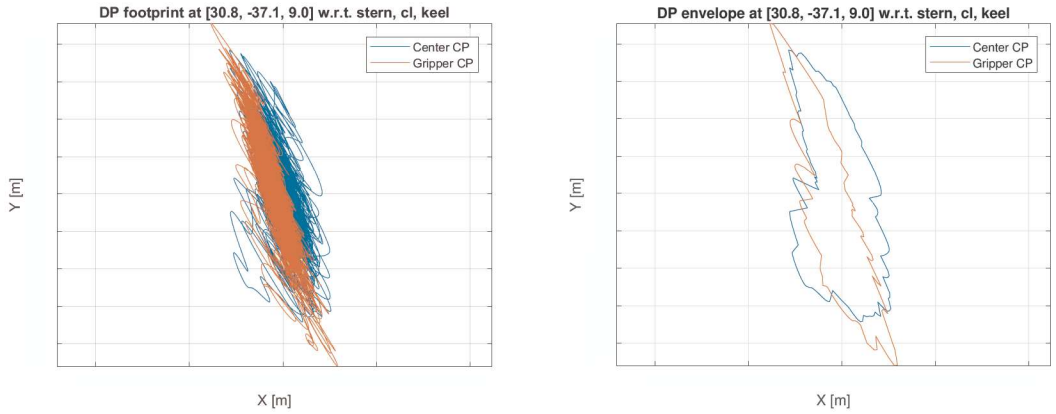

(a) DP Footprints for center CP model and gripper CP model.

(b) DP Envelope plots for center CP model and gripper CP model.

Figure 5.1: Trajectory plots at the alternative location for Hs = 1.5, wavedir. = 135 deg and Tp = 8s

As can be seen in Figure 5.1, the gripper control point model shows a slight improvement in the x-direction. The total horizontal motions and their corresponding statistic values for the motions in the horizontal plane are presented in the section hereafter.

5.1.2. Motions in the horizontal plane

To get more complete view on the vessel its behavior during the simulations, the time traces are plotted for the motions in the horizontal plane. The results are again obtained at the coordinates of the gripper and shown in Figure 5.2.

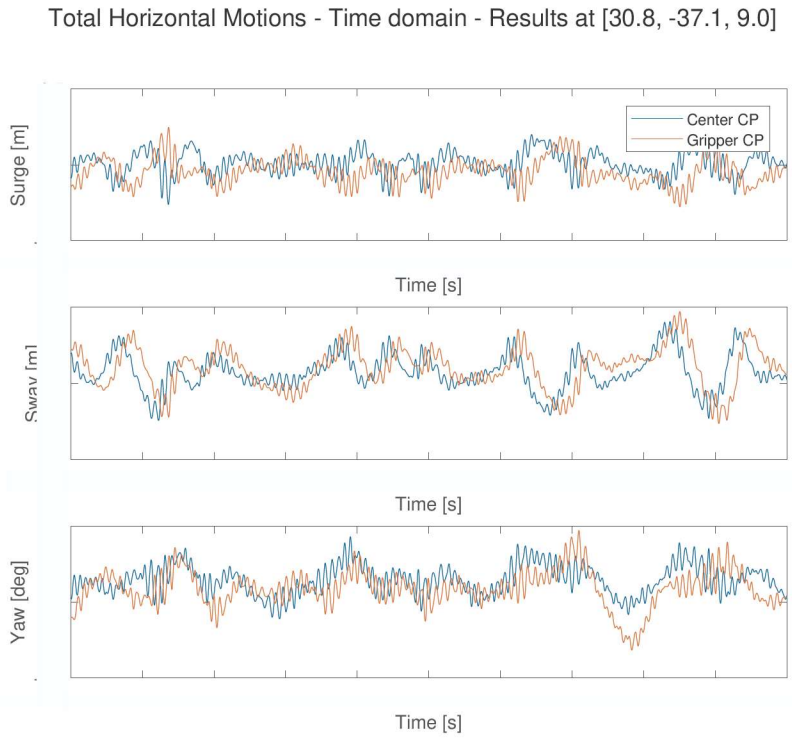

Figure 5.2: Total motions in the horizontal plane during 3h time domain simulation in Hs = 1.5m, wavedir. = 135 deg and Tp = 8s; results obtained at t = ***

When considering Figure 5.2, it can be seen that difference between the two models are marginal. Although results are only presented here for a short timetrace of *** seconds, no clear differences were observed over the whole 3 hour simulation.

To gather further insights in the horizontal motions, the results were plotted in the frequency domain in Figure 5.3.

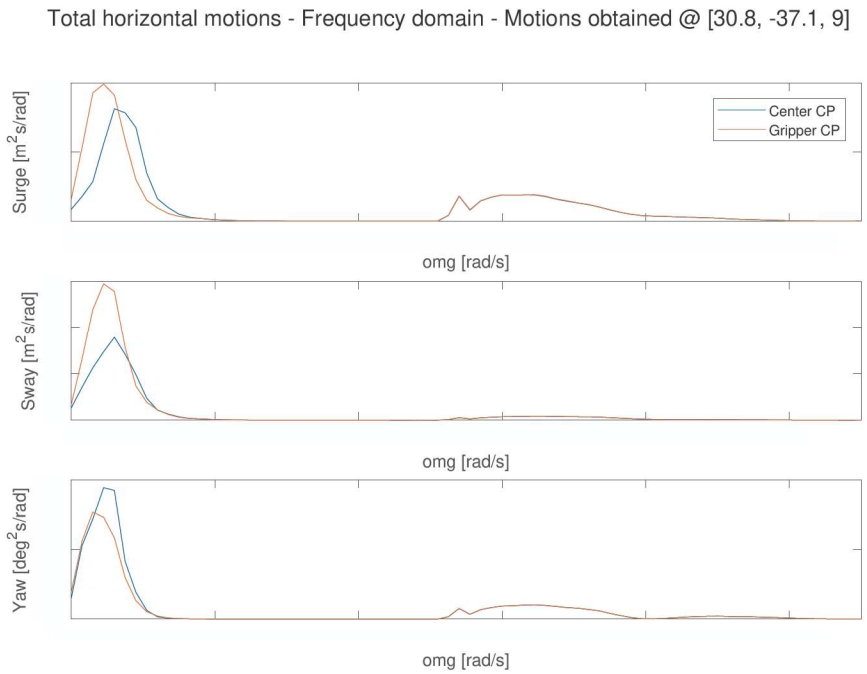

Figure 5.3: Total motions during 3h time domain simulation in Hs = 1.5m, wavedir. = 135 deg and Tp = 8s - Frequency domain plot

The main observations from these plots are that in the lower frequency regions, there is a lower response for the yaw motion for the gripper control point compared to the center control point, but a slightly larger response for the surge and sway motions for the gripper control point model. However, the differences in surge are marginal.

Statistic values for the simulation are displayed in Table 5.2 and Table 5.3. The presented values are obtained for the low frequency motions, since these are the motions that one would improve when trying to improve a DP system. To obtain these low frequency motions, the same bandpass filter algorithm as for the Kalman Filter in section 4.1 was used, using equal cut-off frequency.

Table 5.2: Motion statistics for 3h time domain simulations, with sea state Hs = 1.5m, 135deg, Tp = 8s

	Standard deviation		
	Center CP model	Gripper CP model	Difference
Surge [m]			8%
Sway [m]			22%
Heave [m]			-12%

Since no Integral term was included for the controllers in both models, the mean values are left out. The actual DP system would contain an Integral gain in the PID controller, which is left out in this study. The Integral gain would, if programmed correctly, try to correct for this mean value. The standard deviation, however, is a measure of the dispersion of the dataset, and a lower value would indicate that

the obtained values lie closer to its mean; i.e. fewer motion deviations. When considering the results in Table 5.2, there is a smaller standard deviation observed for the yaw motion and therefore a smaller motion response for yaw for the gripper control point model. Looking at the extreme values in Table 5.3, one observes a decrease in the Yaw motion's maximum value for the gripper control point model, and some decrease in the maximum value for the surge motion. All other extreme values are observed to be bigger for the gripper control point.

Table 5.3: Motion responses extreme values 3h time domain simulations, with sea state of Hs = 1.5m, 135deg, Tp = 8s

	Minimum			Maximum		
	Center CP	Gripper CP	Difference	Center CP	Gripper CP	Difference
Surge [m]			1%			-3%
Sway [m]			46%			3%
Yaw [deg]			196%			-17%

Conclusion

Concluding from the observations mentioned in this section, it can be stated that there is an improvement for the yaw motion for the gripper control point model compared the conventional DP model in the current environmental conditions. Some slight improvement appears for the motion responses in the surge direction in terms of the DP footprint. Note that these conclusions only apply to this sea state and the model in its current form.

5.2. Results for Hs = 1.0m

In order to investigate the performance of both models in more detail, simulations were done for different wave heights within the vessel its operational limits. The results presented here concern the results for the first wave height variation with a significant wave height of 1.0 meters.

Note that the simulations presented in this section are only one-hour simulations, due to the very large simulation time of the models with thruster allocation. Therefore, no statistics are presented for the motions, since an insufficient amount of cycles is passed [7] for the low-frequency motions. Just as for the base case, the applied wave trains are equal for both control point models. In this way, one can get an idea of the difference in responses between both models.

For clarity, the input data for the simulations is repeated here:

Table 5.4: Input data for wave height variation simulations with Hs = 1.0m

Spectrum		JONSWAP
Significant wave height (Hs)	[m]	1.0
Wave direction	[deg]	135
Peak period (Tp)	[s]	8

Just as for the base case, the first 200 seconds of the simulation were neglected due to the start-up time of the thruster allocation algorithm and settling time of the Kalman Filter.

5.2.1. Trajectories at the gripper location

For the significant wave height of Hs = 1.0m, differences between the footprints are marginal and no improvement in the x-direction was observed here for the gripper control point model. The trajectory in the y-direction is observed to be even larger for the gripper control point model. The trajectories are shown in Figure 5.4.

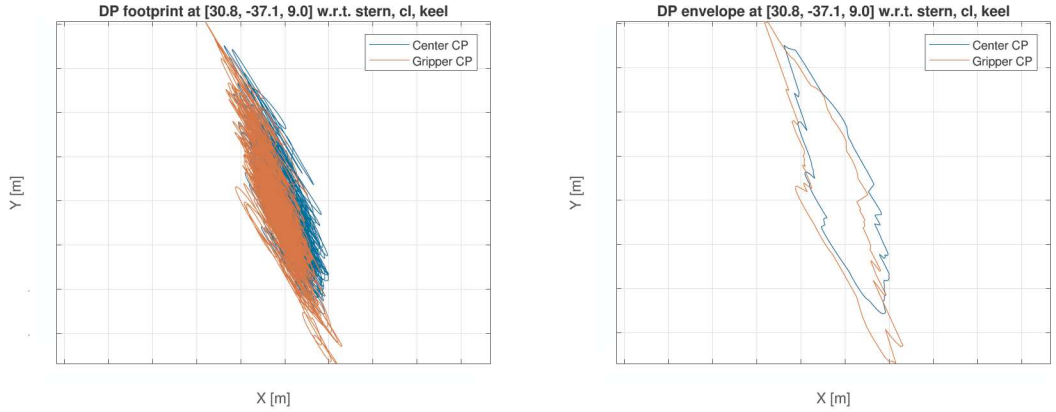

(a) DP Footprints for center CP model and gripper CP model.

(b) DP Envelope plots for center CP model and gripper CP model.

Figure 5.4: Trajectory plots at the gripper location, during 1h time domain simulations, with sea state Hs = 1.0m, 135deg, Tp = 8s.

5.2.2. Total horizontal motions

The results for the total horizontal motions for this one hour simulation are plotted in the time domain in Figure 5.5 and the results in the frequency domain are shown in Figure 5.6. When considering Figure 5.5, no significant differences between both models are observed. However, when observing these time traces it is observed that more first order responses are present for this simulation.

Looking at Figure 5.6, it is observed that there is again a significant improvement for the yaw responses in the gripper control point model, compared to the center control point model. For sway, the responses are higher for the gripper control point model, which was equally observed for the base case simulation in chapter 5. Differences in surge are marginal.

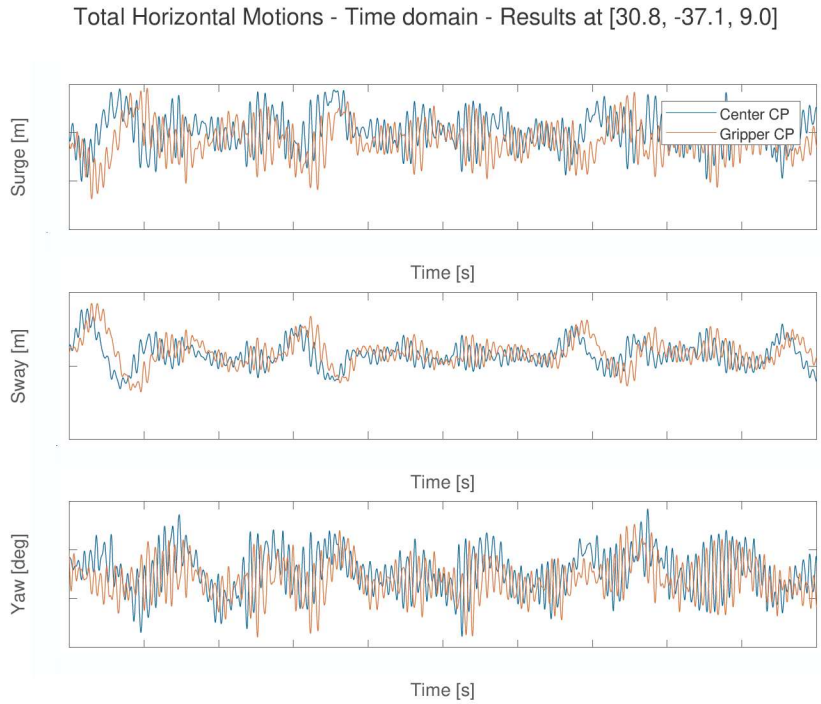

Figure 5.5: Total horizontal motions in the horizontal plane for Hs = 1.0m, wavedir. = 135 deg and Tp = 8s; results obtained at t = ***

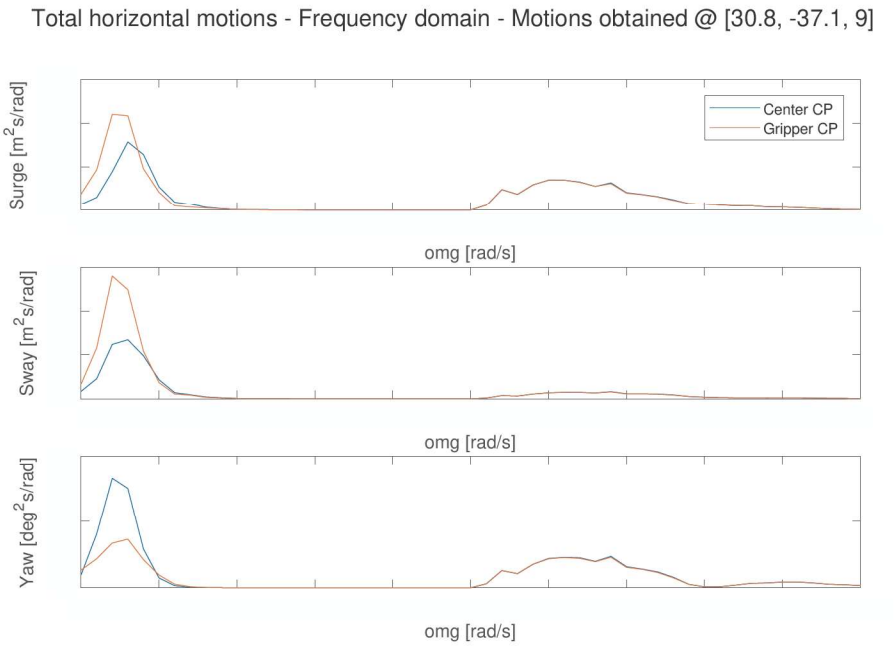

Figure 5.6: Total motions in the horizontal plane for Hs = 1.0m, wavedir. = 135 deg and Tp = 8s - Frequency domain plots

5.2.3. Conclusion

In general, the differences between both models were marginal in terms of the DP footprint for the simulations of Hs = 1.0m. The sway motion appeared to be bigger for the gripper control point in this sea state. Just as for the base case in the previous chapter, the yaw motion responses are smaller for the gripper control point model for this significant wave height, compared to the center control point.

5.3. Results for Hs = 2.0m

The second wave height variation consisted of equal conditions and an identical approach was conducted as for the first variation. Note again, that the simulations for Hs = 2.0m are only one-hour simulations. The input data for the simulations are repeated here for clarity:

Table 5.5: Input data for wave height variation simulations with Hs = 2.0m

Spectrum		JONSWAP
Significant wave height (Hs)	[m]	2.0
Wave direction	[deg]	135
Peak period (Tp)	[s]	8

5.3.1. Trajectories at the alternative location

The DP footprint and the DP envelope are plotted in Figure 5.7 below. As can be seen, equal results can be observed as for the base case (see Figure 5.1 in the previous section). The differences in responses are marginal, although there is a small improvement in the x-direction observed for the gripper control point model. Something remarkable that happens for the center control point model, are the outliers that are observed in the footprint plot between $x =$ *** and $y =$ *** These outliers were observed for both models at different sea states and the cause of this will be discussed more in detail in the Discussion in chapter 7.

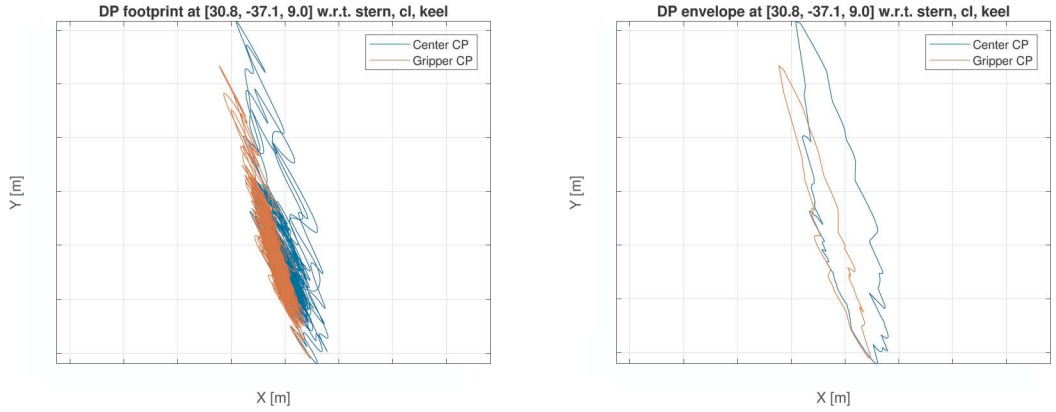

(a) DP Footprints for center CP model and gripper CP model.

(b) DP Envelope plots for center CP model and gripper CP model.

Figure 5.7: Trajectory plots at the gripper location, during 1h time domain simulations, with sea state Hs = 2.0m, 135deg, Tp = 8s.

5.3.2. Total horizontal motions

Just as for the other sea states, the results for the total second-order horizontal motions are plotted. The results are presented in Figure 5.8 in the time domain, between $t =$ *** and frequency domain plots are presented in Figure 5.9. Quite similar results are obtained for this sea state compared to the other sea states as mentioned before; no clear differences are observed when looking at the time domain plots. Only it seems that the extreme values for the yaw responses are lower at this given time window.

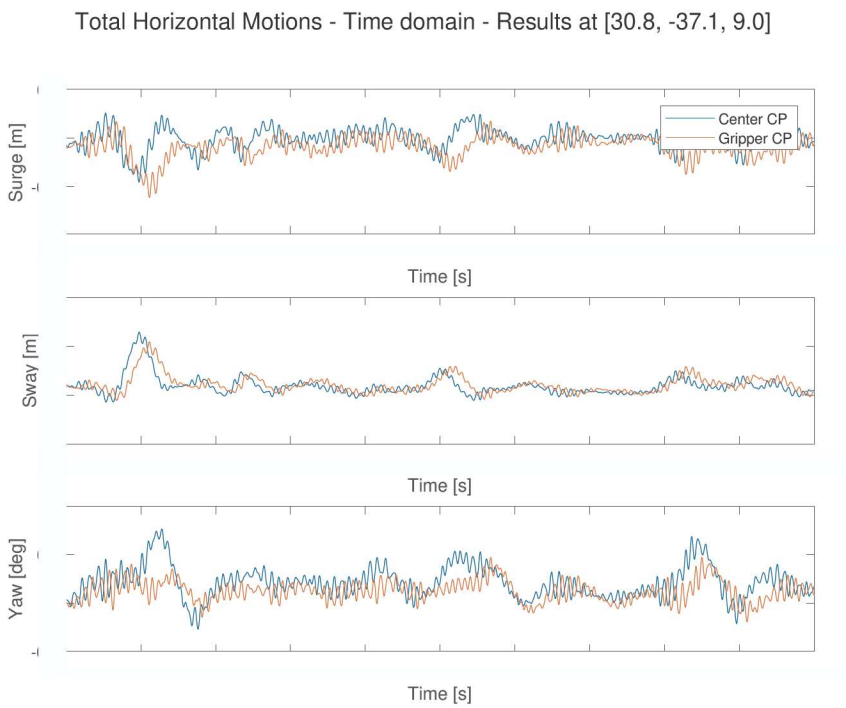

Figure 5.8: Total horizontal motions in the horizontal plane for Hs = 2.0m, wavedir. = 135 deg and Tp = 8s; results obtained at t = [2000 3000]

When considering the results in the frequency domain in Figure 5.9, the surge responses in the lower frequency regions are observed to be lower for the gripper control point model compared to the center control point model. For the yaw motion, equal observations are made as for other sea states: it is smaller for the gripper control point in the lower frequency region.

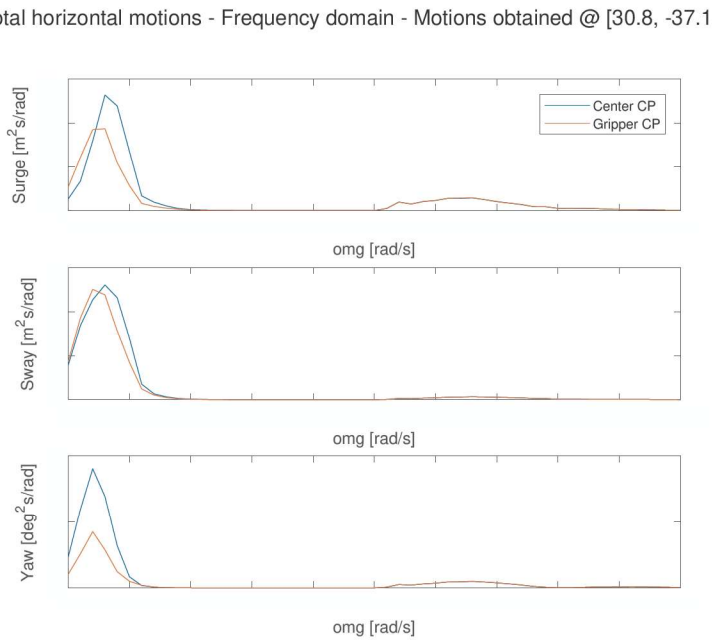

Figure 5.9: Total motions in the horizontal plane for Hs = 2.0m, wavedir. = 135 deg and Tp = 8s - Frequency domain plots

5.3.3. Conclusion

For the simulations of Hs = 2.0m, the footprint improved for the gripper control point model in the x direction compared to the center control point model. However, a big outlier was observed for the center model. These outliers were observed during several simulations and will be discussed more in detail in the Discussion in chapter 7. When considering the total horizontal motions, a small improvement in the surge motion is observed for the gripper control point model, and the yaw response improved again for the gripper control point model.

6
Thruster behavior and energy consumption

In order to find an answer to the last research question that concerns the demanded power of the thrusters and their behavior, the results related to the thrusters are presented in this chapter. First, the applied DP forces will be discussed, together with the ramp-up speeds and azimuth rates per thruster. After that, the power and energy consumption are discussed.

6.1. DP Forces for the base case

Important results that need to be considered to check the behavior of the thrusters are the applied forces by the thrusters. This section presents the applied DP forces, as well as plots showing the demanded vs. obtained forces. The results presented in this section are the results for the 'base case' sea state.

6.1.1. Applied DP forces

The first results presented here, are the total applied forces in the x-direction, y-direction, and the applied moment around the z-axis by all thrusters. Results are presented in the time domain in and in the frequency domain hereafter in Figure 6.1 and Figure 6.2 respectively. The forces are plotted for the point of application for both models, i.e. their control points.

Figure 6.1: DP Forces during 3h time domain simulation in Hs = 1.5m, wavedir. = 135 deg and Tp = 8s; results obtained at t = [2000 3000]

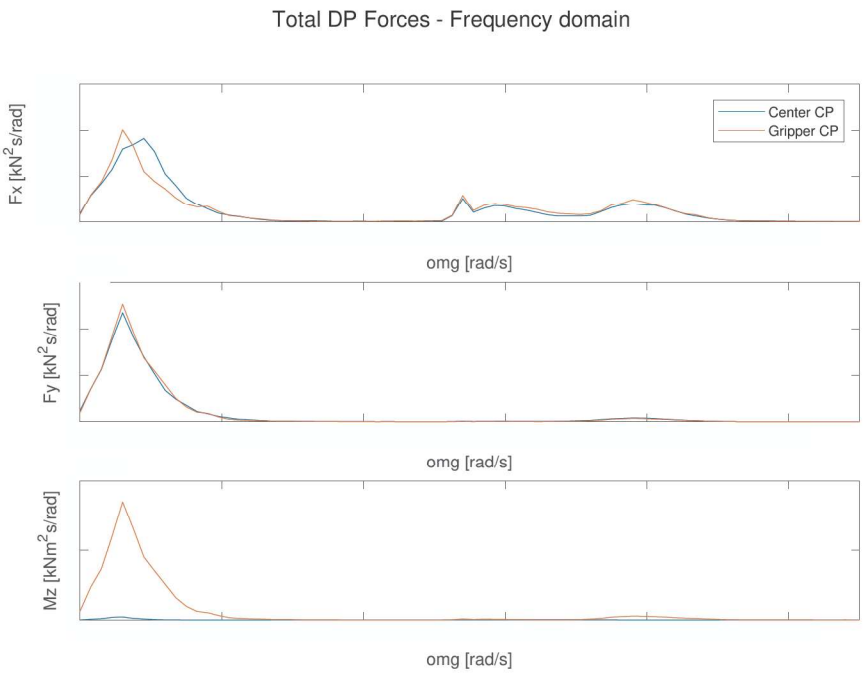

Figure 6.2: DP forces during 3h time domain simulation in Hs = 1.5m, wavedir. = 135 deg and Tp = 8s - Frequency domain plots

The main observations obtained from the plots in Figure 6.1 and Figure 6.2 are that the applied forces in the x-direction and y-direction have the same order of magnitude for both models. The applied yaw moment, or moment around the z-axis, has increased significantly for the gripper control point model compared to the center control point model. The statistics of the applied forces are presented in Table 6.1 and Table 6.2. Considering the statistics and extreme values for the forces, equal observations can be obtained as for the plots.

Table 6.1: Force statistics for 3h time domain simulations, with sea state Hs = 1.5m, 135deg, Tp = 8s

	Standard deviation		
	Center CP	Gripper CP	Difference
Fx [kN]			-1%
Fy [kN]			1%
Mrz [kNm]			484%

Table 6.2: Force extreme values for 3h time domain simulations, with sea state Hs = 1.5m, 135deg, Tp = 8s

	Minimum			**Maximum**		
	Center CP	Gripper CP	Difference	Center CP	Gripper CP	Difference
Fx [kN]			53%			-6%
Fy [kN]			-3%			-13%
Mrz [kNm]			522%			18%

6.1.2. Demanded vs. obtained forces

Plots were made for the demanded and obtained forces. The 'demanded' forces refer to the actual forces calculated by the PD controllers to keep the vessel at its position. The 'obtained' forces are the total forces as delivered by the thrusters. Results are shown in Figure 6.3 and Figure 6.4 in the time domain and frequency domain respectively. When taking a close look at Figure 6.3, it can be stated that for the gripper control point model, there is a slightly higher error rate observed between obtaining the demanded forces, for example at $t =$ *** The RMSE were calculated for the differences between the demanded and obtained forces over the simulation and are displayed in Table 6.3. As can be seen in this table, the RMSE is indeed slightly higher for Fx and Fy and significantly higher for Mz. Also, the maximum errors were calculated between the demanded and obtained forces and displayed in Table 6.4. As can be seen in this table, the maximum errors are also higher for the gripper control point model in all directions.

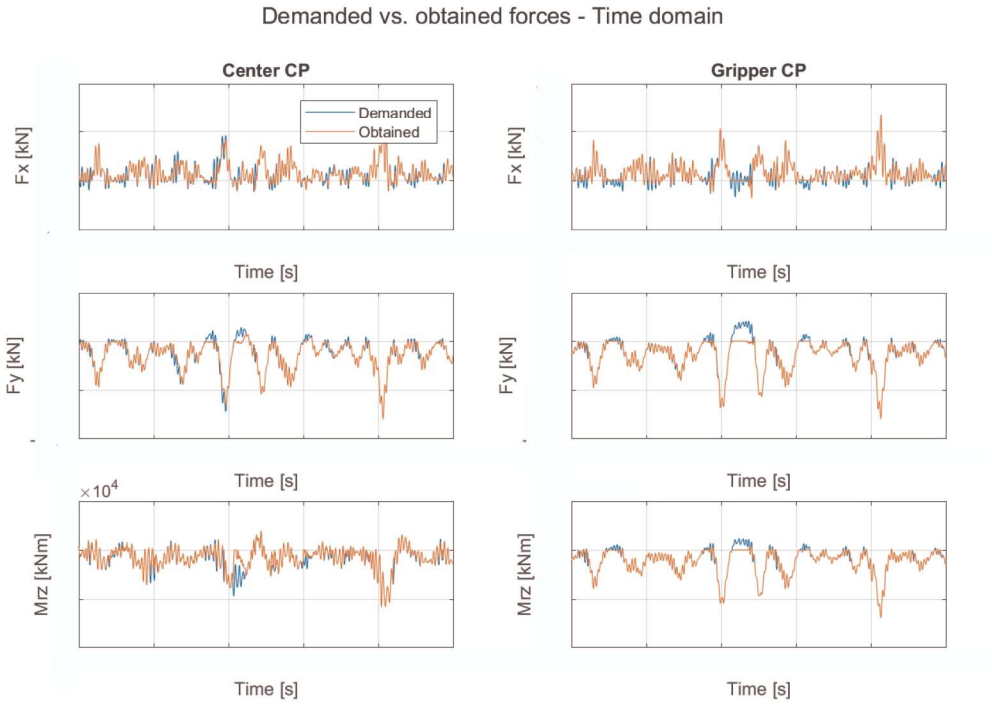

Figure 6.3: Demanded vs. obtained forces during 3h time domain simulation in Hs = 1.5m, wavedir. = 135 deg and Tp = 8s; results obtained at t = [6000 7000]

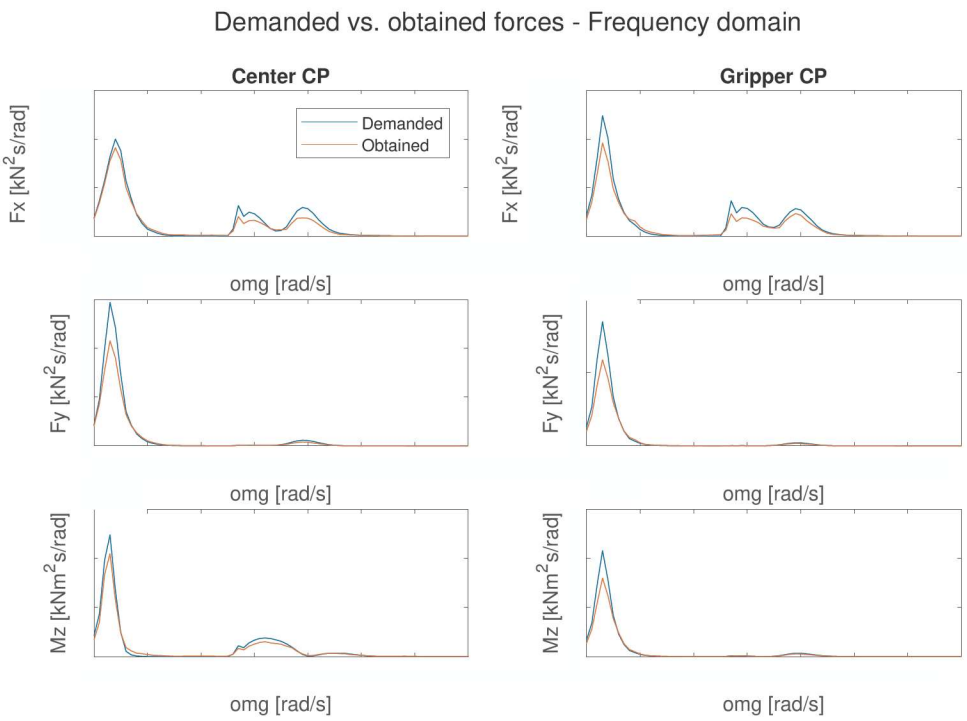

Figure 6.4: Demanded vs. obtained forces during 3h time domain simulation in Hs = 1.5m, wavedir. = 135 deg and Tp = 8s - Frequency domain plots

Table 6.3: RMSE for demanded vs. obtained forces during 3h time domain simulation in Hs = 1.5m, wavedir. = 135 deg and Tp = 8s

	Root Mean Square Error	
	Center CP model	Gripper CP model
Fx [kN]	12.59	14.00
Fy [kN]	39.95	43.53
Mz [kNm]	748.91	3207.44

Table 6.4: Maximum errors between demanded vs. obtained forces during 3h time domain simulation in Hs = 1.5m, wavedir. = 135 deg and Tp = 8s

	Maximum Error	
	Center CP	Gripper CP
Fx [kN]	139.74	142.41
Fy [kN]	398.05	425.57
Mz [kNm]	4911.09	36345.97

6.1.3. Conclusion

It was observed that the applied DP forces in the x-direction and y-direction are of equal magnitude for both models. However, the applied moment around the z-axis is significantly higher for the gripper control point model. Due to equal total power (see section 6.3 hereafter), the higher applied moment is probably only due to an increase in the lever-arm of the applied forces. No problems were observed in obtaining the demanded forces between both models, however, the gripper control point model has higher RMSE values and maximum erros for all DP forces compared to the center control point model.

6.2. Thruster behavior for the base case

Since the point of application of the total applied force changed, some modifications were done to the thruster allocation algorithm (see section 4.6). The results presented here are to check whether the thrusters themselves stay within the specified limits and to see if their behavior changes when the allocation needs to do the calculations with respect to the gripper location.

6.2.1. Ramp-up speeds

To start, results concerning the ramp-up speeds per thruster are shown in Figure 6.5. As stated in Table 3.6 in chapter 3, the limits for the ramp-up speeds for the thrusters are defined as:

- Maximum of *** kN/s for thrusters 1 to 4,
- maximum of *** kN/s for thruster 5 and 6.

A comparison between the ramp-up speeds of both models is displayed in Figure 6.5. The results shown are only presented here for a specified time of $t = [6300\ 6600]$ for clarity, but the complete time trace was checked. From the results, it can be stated that for both simulations, none of the thrusters exceed the required limits for the ramp-up speed. Hence, the code was assumed to be implemented correctly. No other clear differences were obtained from the ramp-up speed plots.

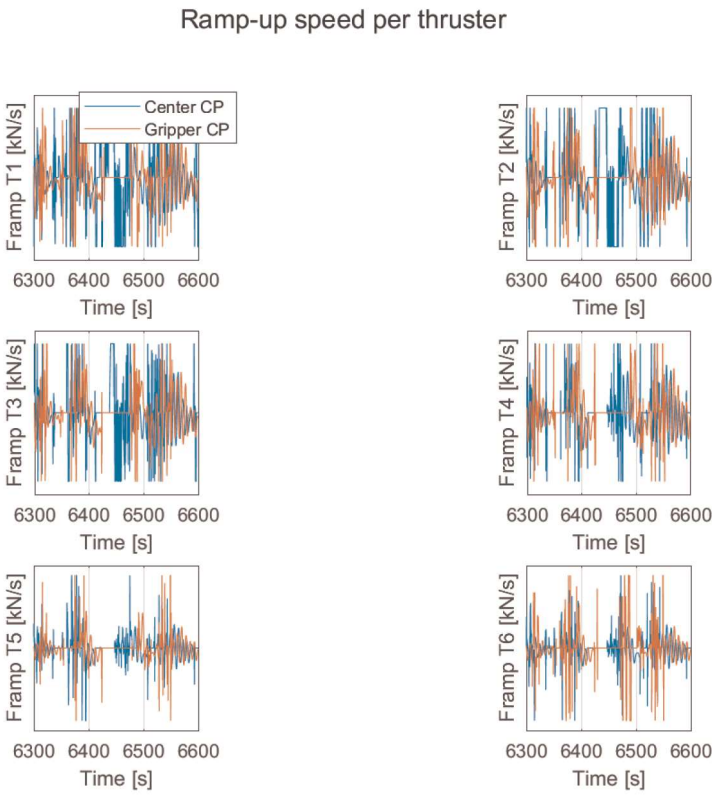

Figure 6.5: Ramp up speeds of thrusters during 3h time domain simulations, with sea state Hs = 1.5m, 135deg, Tp = 8s - Results obtained at t = [6300 6600]

6.2.2. Azimuth and azimuth speed

The azimuth angles of the thrusters are plotted in Figure 6.6. The azimuth speeds per thruster are displayed in Figure 6.7. When considering Figure 6.6, no clear differences can be distinguished between the thrusters of both models. The big shifts appear due to the fact that the algorithm only allows the results to be between $[0\ 360]$ degrees.

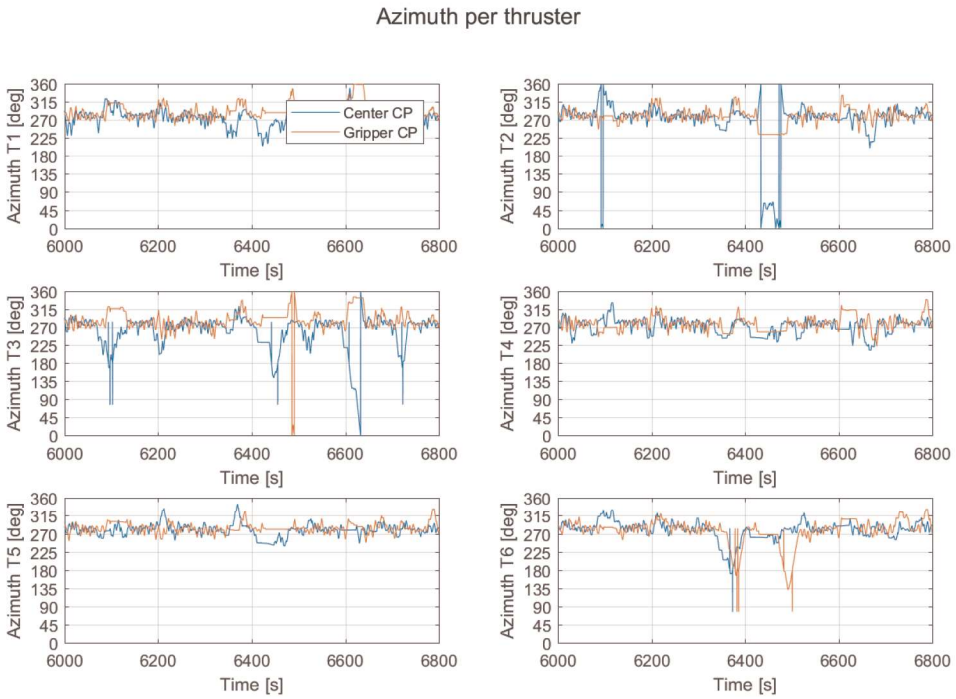

Figure 6.6: Azimuth of thrusters during 3h time domain simulation in Hs = 1.5m, wavedir. = 135 deg and Tp = 8s; results obtained at t = [6000 6800]

The azimuth speed limits were checked for each thruster too and were defined in Table 3.6 in chapter 3. For clarity, the limits are repeated here:

- For thrusters 1 to 4, a maximum azimuth rate of *** deg/s,
- for thrusters 5 and 6, a maximum azimuth rate of *** deg/s.

Again, results are presented for the specified time of $t = [6300\ 6600]$, but results were checked for the complete analysis. As can be seen in Figure 6.7, all thrusters stay within the specified limits in both models.

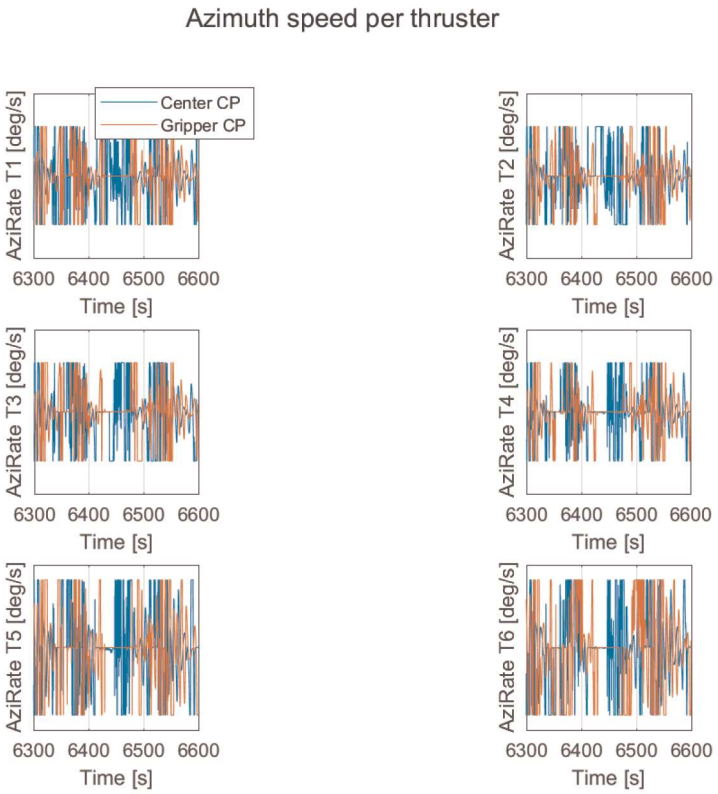

Figure 6.7: Azirate of thrusters during 3h time domain simulations, with sea state Hs = 1.5m, 135deg, Tp = 8s - Results obtained at t = [6300 6600]

6.2.3. Conclusion

It was observed that the thrusters do not have major behavior changes in terms of azimuth, azimuth rates, and ramp-up speeds. Also, the thrusters stay within the specified limits for both models. Therefore, it was assumed that the code was implemented correctly. Whether there is a difference in the distribution and outputs of power is discussed in the next section.

6.3. Energy consumption for the base case

The thruster allocation algorithm from HES gives an output of the delivered thrust over time for each thruster individually. These delivered thrusts were converted to power, by using the propeller diagrams (for DP-speed state) for the specific types of thrusters the Aegir is equipped with. The propeller diagrams relate the delivered thrust by the propeller to the input power. Which is not the power delivered by the thrusters themselves, but the power used to propulse them.

6.3.1. Energy consumption per thruster

Results per thruster over time for both models are plotted in Figure 6.8 for $t =$ *** . As can be seen in Figure 6.8, the differences in input power per thruster are marginal. Something remarkable observed here is that there seems to be some sort of lag between both signals, which is also observed for the DP forces in section 6.1. To gain more insights into the thruster behaviors, the average power and the energy consumed per thruster are calculated for both models. The consumed energy is obtained by calculating the area under the curves for the whole simulation in Figure 6.8, neglecting the startup time of 200s, and dividing it by 3600 seconds to obtain kWh. The results are shown in Table 6.5. Something that can be observed from Table 6.5 is that the differences in thruster 4, 5, and 6 are marginal between both models. However, the average input powers and the total energy consumptions for thrusters 1 to 3 are lower in the gripper control point model.

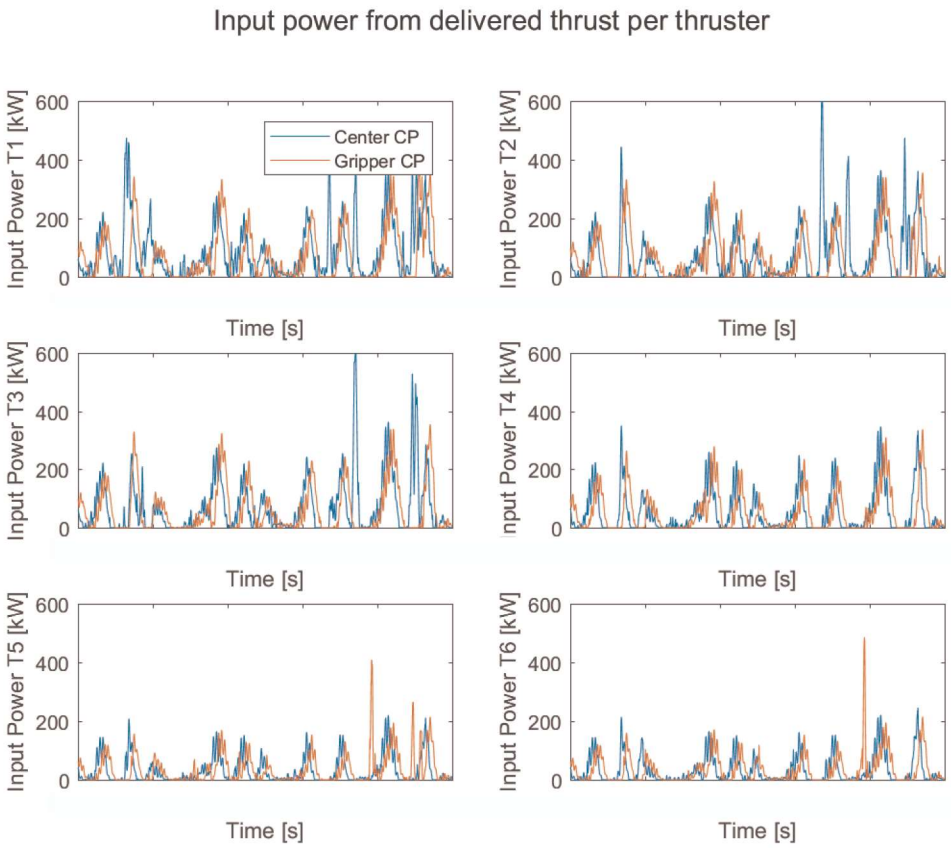

Figure 6.8: Input power per thruster during 3h time domain simulation in Hs = 1.5m, wavedir. = 135 deg and Tp = 8s; results obtained at t = ***

Table 6.5: Mean input power and energy consumption per thruster for Hs = 1.5m, 135 deg., Tp = 8s.

		Thruster 1	Thruster 2	Thruster 3	Thruster 4	Thruster 5	Thruster 6
Center Control Point							
	Mean input power [kW]	73.9	58.0	71.9	39.3	23.8	24.9
	Energy consumption [kWh]	217.64	170.70	211.64	115.60	70.13	73.32
Gripper Control Point							
	Mean input power [kW]	49.7	49.8	47.1	40.5	24.8	25.7
	Energy consumption [kWh]	146.45	146.64	138.76	119.25	72.88	75.72

6.3.2. Total energy consumption

To get an idea about the energy consumption of the vessel operating on DP, the total input powers were calculated as the sum of the input power of the thruster and compared for both models. The results are plotted over time in Figure 6.9. However, no significant differences are seen between both models. At first glance, the input power between both models seems equal.

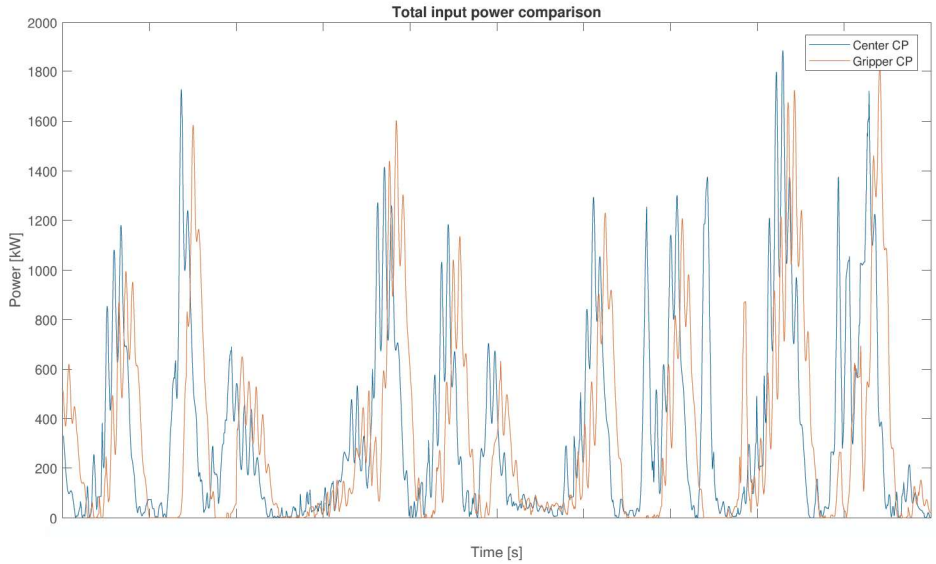

Figure 6.9: Total sum of input powers during 3h time domain simulations, with sea state Hs = 1.5m, 135deg, Tp = 8s - Results obtained at t = [2000 3000]

To substantiate this, the total energy consumed during the simulation was calculated. For the calculation of the energy consumption, the area under the curves of Figure 6.9 is calculated and divided by 3600 seconds to get to kWh. Results are shown in Table 6.6. And as can be seen, less energy is consumed for the gripper control point model.

Table 6.6: Total mean input power and energy consumption for Hs = 1.5, 135 deg, Tp = 8s.

	Center CP model	Gripper CP model
Average power [kW]	292	238
Total energy consumption [kWh]	859	700

6.3.3. Conclusion

For the base case sea state, a difference in the distribution of power is observed for thrusters 1 to 3. Thrusters 1 to 3 require less power in the gripper control point model, compared to the center control point model. Overall, the gripper control point model consumed 159 kWh less energy compared to the center control point model, which is 19 % less.

6.4. Results for Hs = 1.0m

As it was already proven that the thrusters stay within their limits during the simulations and since equal behaviors were found in the plots for the ramp-up speeds, azimuth speeds, and azimuth, only the DP forces and energy consumption will be discussed for the wave height variations. For the complete results of this sea state is referred to Appendix D.

6.4.1. DP Forces

The DP forces for the one-hour simulation in Hs = 1.0m are plotted in the time domain in Figure 6.10. Equal observations can be made as for the base case in chapter 5; the forces in the X and Y direction are of equal magnitude, but the applied yaw moment is significantly higher for the gripper control point model. Also, the same sort of phase shift/lag is observed here between models as observed for the base case. The demanded vs. obtained forces are plotted in the frequency domain in Figure 6.11.

Figure 6.10: DP Forces during 1h time domain simulation in Hs = 1.0m, wavedir. = 135 deg and Tp = 8s; results obtained at t = [2000 3000]

Looking at Figure 6.11, the errors between the demanded and the obtained forces are significantly larger when comparing them to the base case simulations in chapter 5. The orders of magnitude for forces in the x-direction and y-direction are again equal between both models, but the applied moment around the z-axis is again much higher in the gripper control point model. The RMSE is presented in Table 6.7 and the RMSE values are again higher for the gripper control point model, compared to the center control point model. The maximum errors are presented in Table 6.8. As can be seen, the maximum errors are higher for forces in the y-direction and the moments around the z-axis for the gripper control point model. However, the maximum error for the forces applied in the x-direction appears to be lower for the gripper control point model.

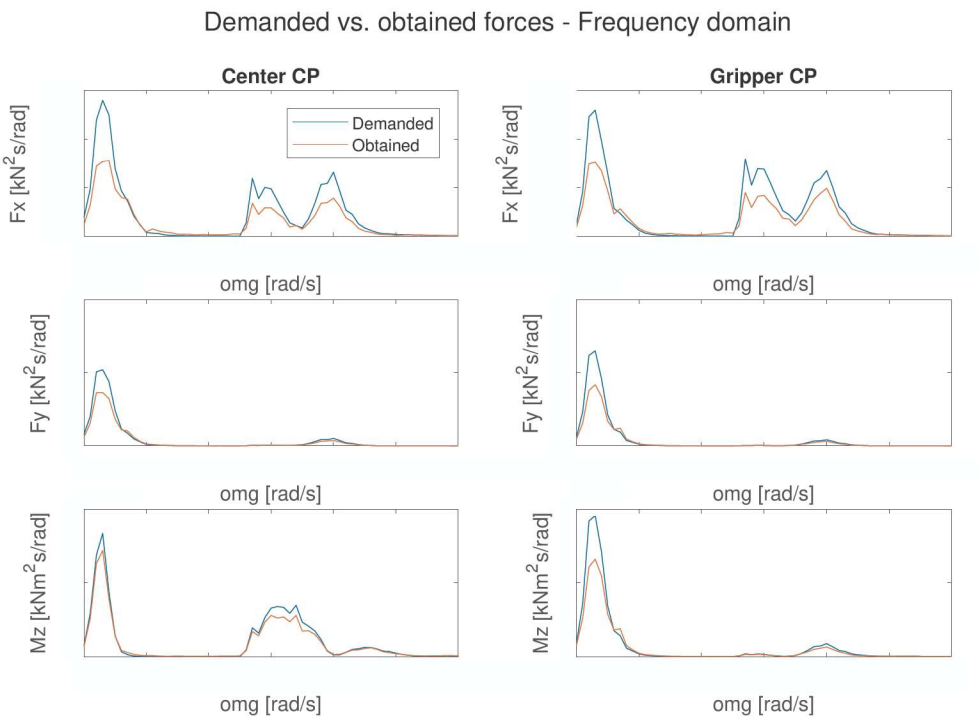

Figure 6.11: Demanded vs. obtained forces during 1h time domain simulation in Hs = 1.0m, wavedir. = 135 deg and Tp = 8s - Frequency domain plots

Table 6.7: RMSE for demanded vs. obtained forces during 1h time domain simulation in Hs = 1.0m, wavedir. = 135 deg and Tp = 8s

	Root Mean Square Error	
	Center CP model	Gripper CP model
Fx [kN]	9.06	9.22
Fy [kN]	19.19	21.97
Mz [kNm]	313.09	1655.72

Table 6.8: Maximum errors between demanded vs. obtained forces during 1h time domain simulation in Hs = 1.0m, wavedir. = 135 deg and Tp = 8s

	Maximum Error	
	Center CP	Gripper CP
Fx [kN]	86.62	58.93
Fy [kN]	146.73	155.29
Mz [kNm]	1905.18	13010.54

6.4.2. Energy consumption

The results of the one hour simulation concerning the power inputs per thruster are shown in Figure 6.12, the average input power and energy consumption are shown in Table 6.9. An equal approach is used here as for the base case simulations in chapter 5.
When considering Figure 6.12 and Table 6.9, the distribution of power is different between both models. Thruster 1 to 3 seem to deliver more power in this sea state for the gripper control point model compared to the center control point model. Thrusters 4, 5 and 6 however, seem to deliver significantly less power in the gripper control point model compared to the center control point model. The exact opposite is observed for the base case in chapter 5.

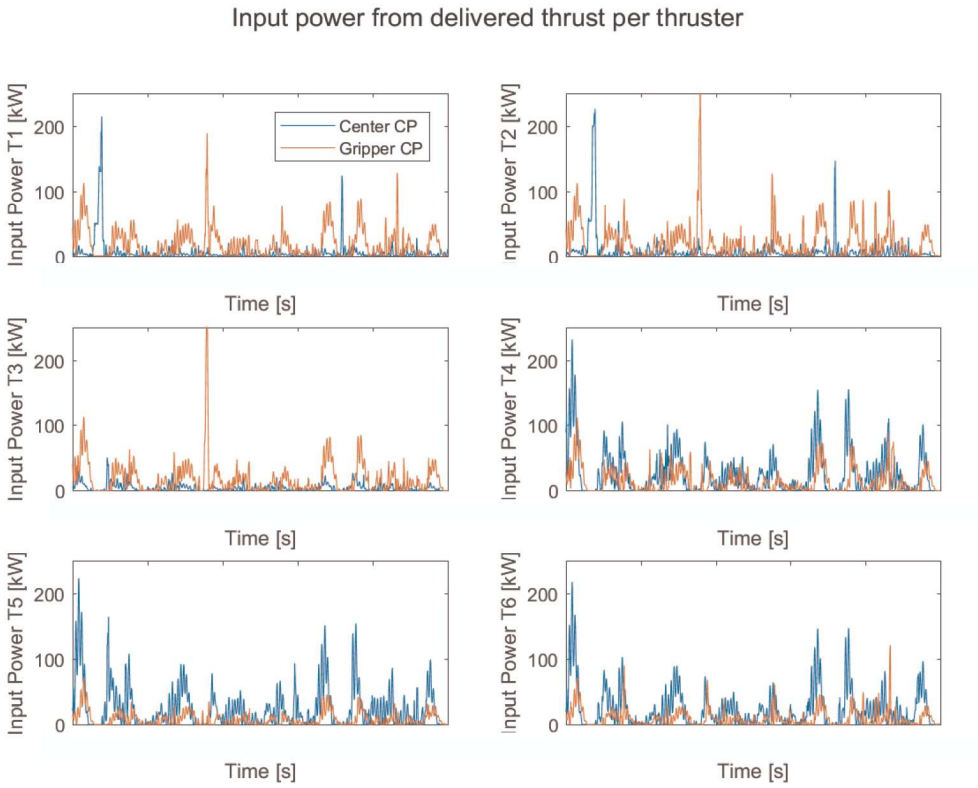

Figure 6.12: Input power per thruster during 1h time domain simulation in Hs = 1.0m, wavedir. = 135 deg and Tp = 8s; results obtained at t = [2000 3000]

Table 6.9: Mean input power and energy consumption per thruster for Hs = 1.0m, wave dir. 135 deg, Tp = 8s

	Thruster 1	Thruster 2	Thruster 3	Thruster 4	Thruster 5	Thruster 6
Center Control Point						
Mean input power [kW]	11.5	13.1	6.2	23.5	22.5	21.6
Energy Consumption [kWh]	10.9	12.4	5.9	22.2	21.3	20.4
Gripper Control Point						
Mean input power [kW]	15.9	16.4	15.6	12.9	7.4	8.2
Energy Consumption [kWh]	15.0	15.5	14.7	12.2	7.0	7.8

Results concerning the total power and energy consumption are displayed in Table 6.10. Again, equal observations are made for the base case of Hs = 1.5m. As can be seen in this table, the average power and energy consumed during the 1-hour simulation are again lower for the gripper control point model. Note that for the calculations here, the startup time of 200s is again neglected. Therefore, mean input power doesn't equal energy consumption.

Table 6.10: Total mean input power and energy consumption for Hs = 1.0m, 135 deg, Tp = 8s.

	Center CP model	Gripper CP model
Average Power [kW]	98.5	76.4
Energy consumption [kWh]	93.0	72.1

6.4.3. Conclusion

When considering the forces, for this significant wave height the error between demanded and obtained forces was observed to be bigger in both models, when comparing these results to the other sea states. Differences in RMSE are marginal between the models for Fx and Fy but are both significantly higher for Mz. The maximum error between the demanded and obtained forces is found to be lower for Fx, equal for Fy, and higher for Mz in the gripper model. When comparing the applied forces for Hs = 1.0m, it can be stated that the differences in applied forces in the x-direction and y-direction are marginal between both models, but the applied moment around the z-axis is again higher for the gripper control point. The total energy consumed for Hs = 1.0m, was again lower for the gripper control point model.

6.5. Results for Hs = 2.0m

Equal results are presented here as for the simulations of the significant wave height of 1 meter. For the complete results of this sea state with a significant wave height of 2.0 meters is referred to Appendix E.

6.5.1. DP Forces

The demanded vs. obtained forces for this sea state are plotted in Figure 6.13. Observed is that obtaining the demanded forces is no problem for this sea state in both models. A remarkable result for this sea state is that the error between the demanded and obtained forces is smaller for the gripper control point model, compared to the center control point. Besides this, the order of magnitude of the forces in the x and y direction are of equal magnitude, although the demanded forces in these directions are somewhat smaller for the gripper control point. The yaw moment is again larger for the gripper control point. The RMSE are presented in Table 6.11. A remarkable result here is that the RMSE values for the forces in the x and y direction have a smaller RMSE for the gripper control point model. Although, the maximum errors as presented in Table 6.12 are found to be equal for the forces in the x-direction, but lower in the y-direction for the gripper control point model. The maximum error for Mz is again significantly higher in the gripper control point model.

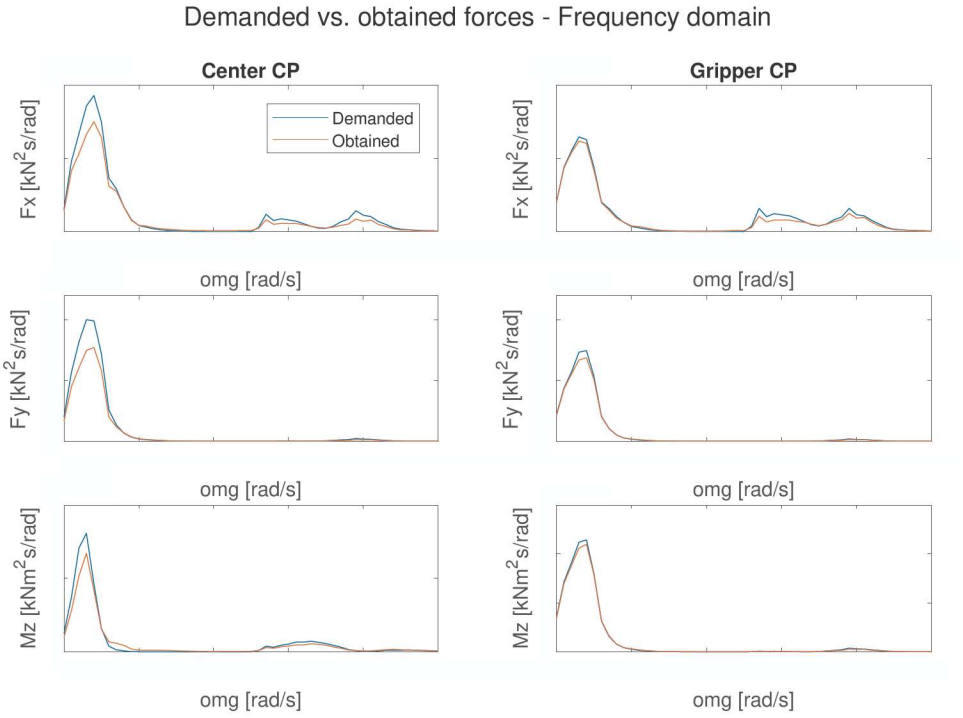

Figure 6.13: Demanded vs. obtained forces during 1h time domain simulation in Hs = 2.0m, wavedir. = 135 deg and Tp = 8s - Frequency domain plots

Table 6.11: RMSE for demanded vs. obtained forces during 1h time domain simulation in Hs = 2.0m, wavedir. = 135 deg and Tp = 8s

	Root Mean Square Error	
	Center CP model	Gripper CP model
Fx [kN]	17.71	13.97
Fy [kN]	69.05	29.66
Mz [kNm]	1304.66	2296.75

Table 6.12: Maximum errors between demanded vs. obtained forces during 3h time domain simulation in Hs = 2.0m, wavedir. = 135 deg and Tp = 8s

	Maximum Error	
	Center CP	Gripper CP
Fx [kN]	129.39	128.45
Fy [kN]	293.49	227.93
Mz [kNm]	6026.09	18021.06

6.5.2. Energy consumption

Results concerning the energy consumption for this sea state are presented in Figure 6.14. Equal results for the base case (see Table 6.5) are obtained when considering the input powers per thruster in Table 6.13. Thrusters 1,2,3 and 6 seem to use slightly less energy and the average powers are lower. When considering the total energy consumption and average input powers for this sea state (see Table 6.14), again the gripper control point model uses less energy for the given simulation time. However, the differences observed here are smaller than observed for the base case of Hs = 1.5m. Note again that for the calculations here, the first 200s of the simulation are neglected.

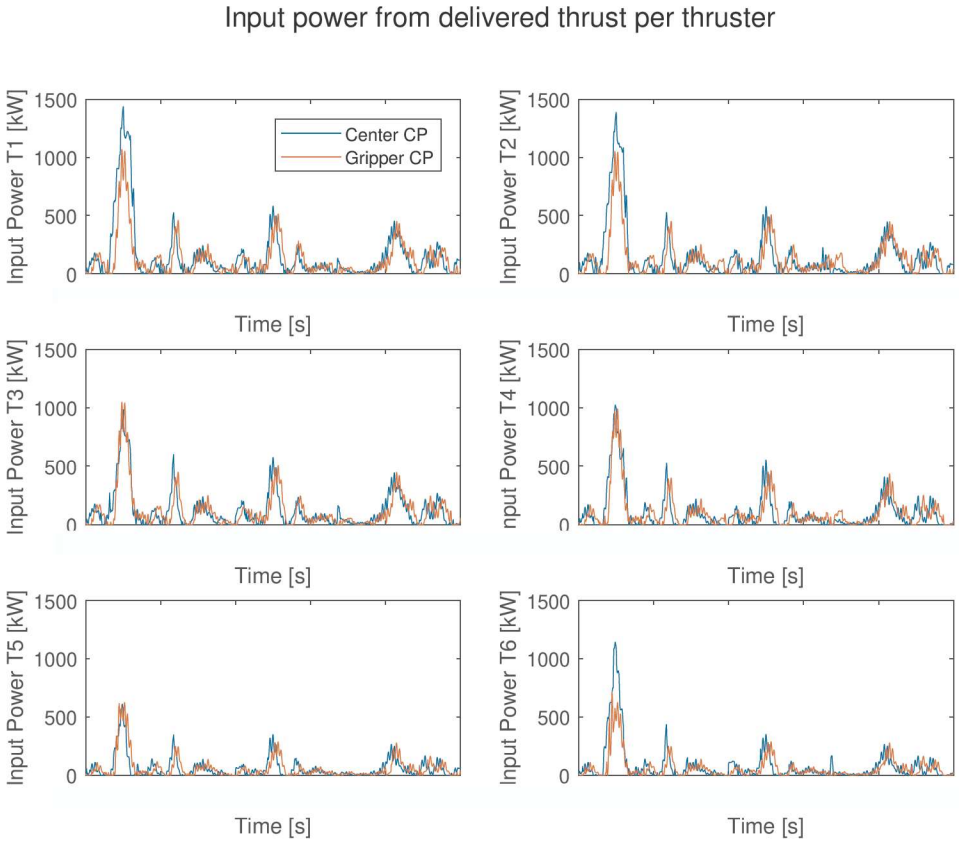

Figure 6.14: Input power per thruster during 1h time domain simulation in Hs = 2.0m, wavedir. = 135 deg and Tp = 8s; results obtained at t = [2000 3000]

Table 6.13: Mean input power and energy consumption per thruster for Hs = 2.0m, wave dir. 135 deg, Tp = 8s

		Thruster 1	Thruster 2	Thruster 3	Thruster 4	Thruster 5	Thruster 6
Center Control Point							
	Mean input power [kW]	128.4	121.6	117.0	94.9	56.6	67.9
	Energy Consumption [kWh]	121.2	114.8	110.4	89.5	53.4	64.1
Gripper Control Point							
	Mean input power [kW]	113.5	113.6	110.3	92.7	54.1	56.0
	Energy Consumption [kWh]	107.1	107.2	104.2	87.5	51.0	52.8

Table 6.14: Total mean input power and energy consumption for Hs = 2.0m, 135 deg, Tp = 8s.

	Center CP model	Gripper CP model
Average input power [kW]	586.4	540.1
Energy consumption [kWh]	553.5	509.8

6.5.3. Conclusion

No problems were observed concerning the demanded and obtained forces and similar observations were made for the forces as for the base case. However, the error between the demanded and obtained forces was smaller for Fx and Fy for the gripper control point. The maximum error between the demanded and obtained forces was found to be lower in the y-direction, and equal in the x-direction for the gripper control point. Again, the maximum error between the demanded and obtained forces for Mz is significantly higher for the gripper control point. For the energy consumption, the gripper control point had a smaller mean input power compared to the center control point, and less energy was consumed for the simulation.

7
Discussion

For this thesis, it was intended to design a new DP system model with a control point at the gripper location of the vessel, in order to minimize the DP footprint at the gripper location. The first part of the thesis consisted of a presentation of the design choices, testing results, and implementation of the new proposed DP system. The second part consisted of a comparison of time-domain results between the conventional DP model with the center control point and the new DP model with the gripper control point. This chapter presents a discussion of the design choices and time-domain results.

7.1. New DP system model design

In this thesis, the Kalman Filter for the new DP model with the gripper control point estimates the states at the center of the vessel, and these states are translated to the gripper location. However, in the first instance, the motion estimates for the new method were first tried to be estimated at the gripper control point itself instead of in the gripper control point relative to the center control point as it is now. State-space equations with coupled equations of motion were applied and the (hydrodynamic) parameters were translated from the center control point to the gripper control point (using the method as described in Fossen [17]). However, this system turned out to be untunable and was giving unstable results. The reason for this remained unclear. Hence, the approach of relative position estimates was chosen. To gain accuracy, the gripper control point model would actually need another Kalman Filter at the gripper control point for the current setup, besides the Kalman Filter in the center. In that way, the estimates in the gripper control point will also be dependent on the velocity estimates at that point, and the noise in this location is taken into account.

As mentioned in the report, no Integral-terms were included for the PD controllers. By including these, the mean wave drift forces can be compensated and the response of the PD controller on the oscillating parts of the wave drift forces can be observed more accurately.

7.2. Time-domain results

In all sea states, an improvement in the yaw motions was observed for the gripper control point model. This improvement is assumed to be due to the increased lever arm to some of the thrusters for the gripper control point compared to the center control point, which would lead to a higher applied moment around the z-axis at the gripper control point.

For this study, the crane was assumed to be rigid and no influences from the motion-compensated gripper were included, which are used by the actual vessel during offshore operations. However, during offshore operations forces will be distributed from the crane and gripper to the vessel.

In the results for Hs = 1.0m, the error between the demanded and obtained forces appeared to be bigger than for the other tested sea states. Therefore, it seems that the current system responds better in sea states with larger Hs, where second-order loads are more dominant and the system's ability to filter in these sea states with larger Hs is appears to be better.

During some simulations, big outliers were observed for certain wave trains and/or sea states. These outliers seemed to appear in both control point models. An example is given in Figure 7.1 for a simulation with the gripper control point under the base case sea state, but with a different wave train applied.

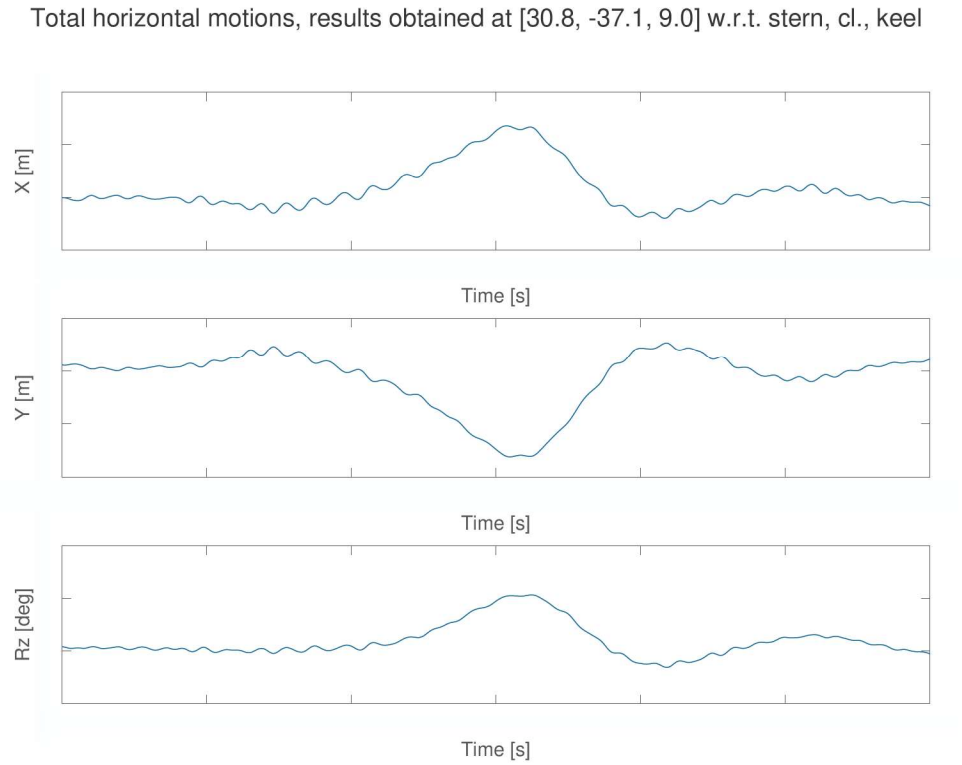

Figure 7.1: Example of an outlier in simulation results; results obtained from simulation with gripper CP in sea state of Hs = 1.5, 135deg, Tp = 8s.

As can be seen in Figure 7.1, large responses are observed in all degrees of freedom at $t = [3300\ 3450]$. The cause of these outliers is due to the fact that the demanded forces aren't obtained, as shown in Figure 7.2.

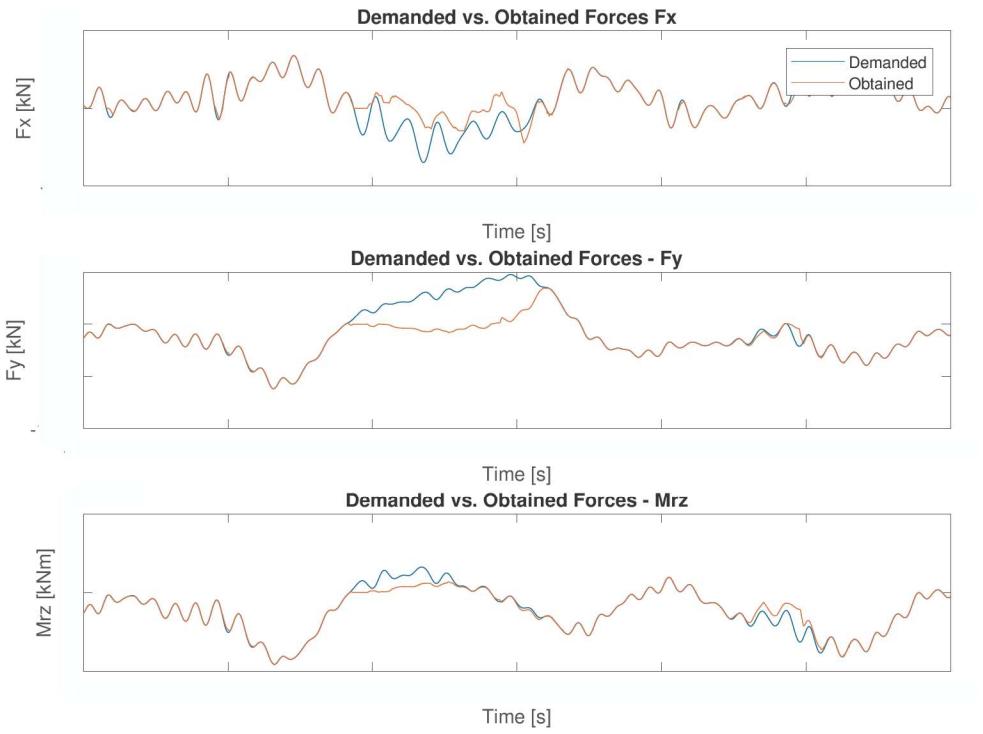

Figure 7.2: Demanded vs. obtained forces; results obtained from simulation with gripper CP in sea state of Hs = 1.5, 135deg, Tp = 8s.

When considering Figure 7.2, it can be seen that the demanded forces aren't delivered in all degrees of freedom at t = *** As the system has proven to be able to deliver higher demanded forces, for example for Hs = 2.0m as presented in chapter 6, it is assumed that the cause of this is not due to higher demanded forces of the system. When checking the thruster outputs at this given point in time, the error between the demanded and obtained forces is suspected due to a malfunction of the thruster allocation algorithm. The algorithm seems to give some of the thrusters a total black-out sometimes and distribute the thrust in an unbalanced way to the thrusters. The azimuth rates and delivered forces for this simulation are shown in Figure 7.3 and Figure 7.4. As can be seen in those figures, there is little to no response at all from the thruster during the timespan of the observed outliers.

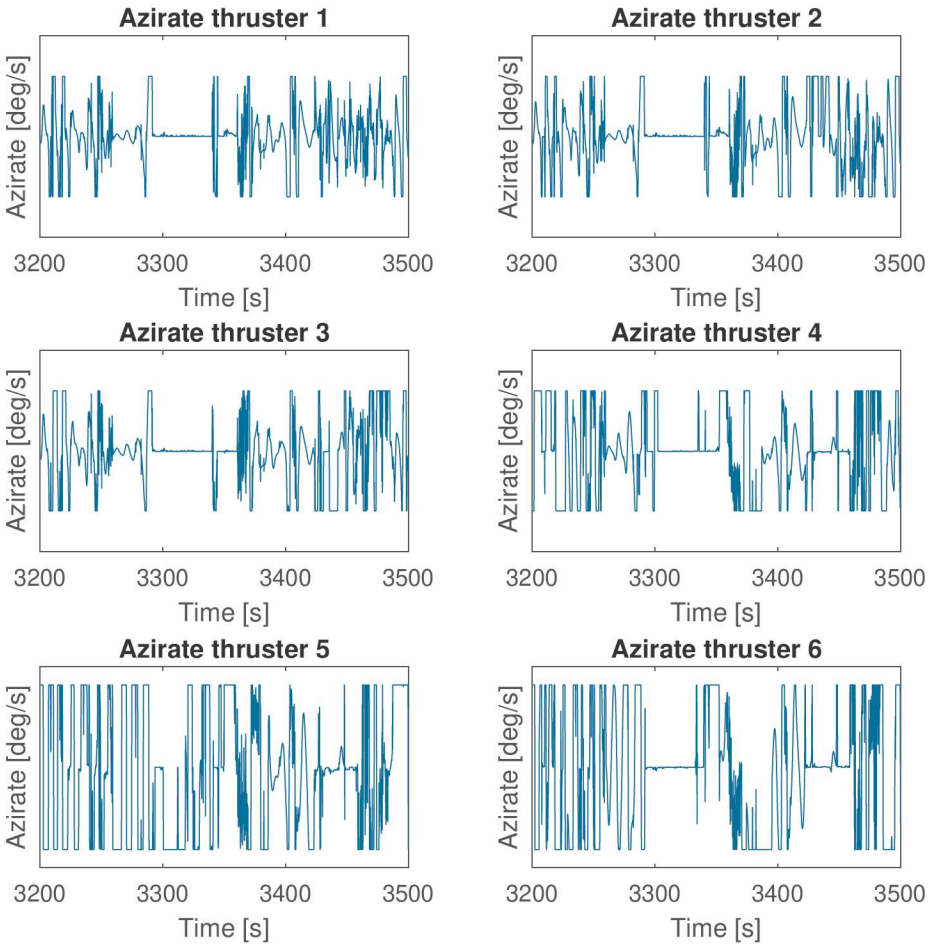

Figure 7.3: Azirates per thruster at time of observed outliers; results obtained from simulation with gripper CP in sea state of Hs = 1.5, 135deg, Tp = 8s.

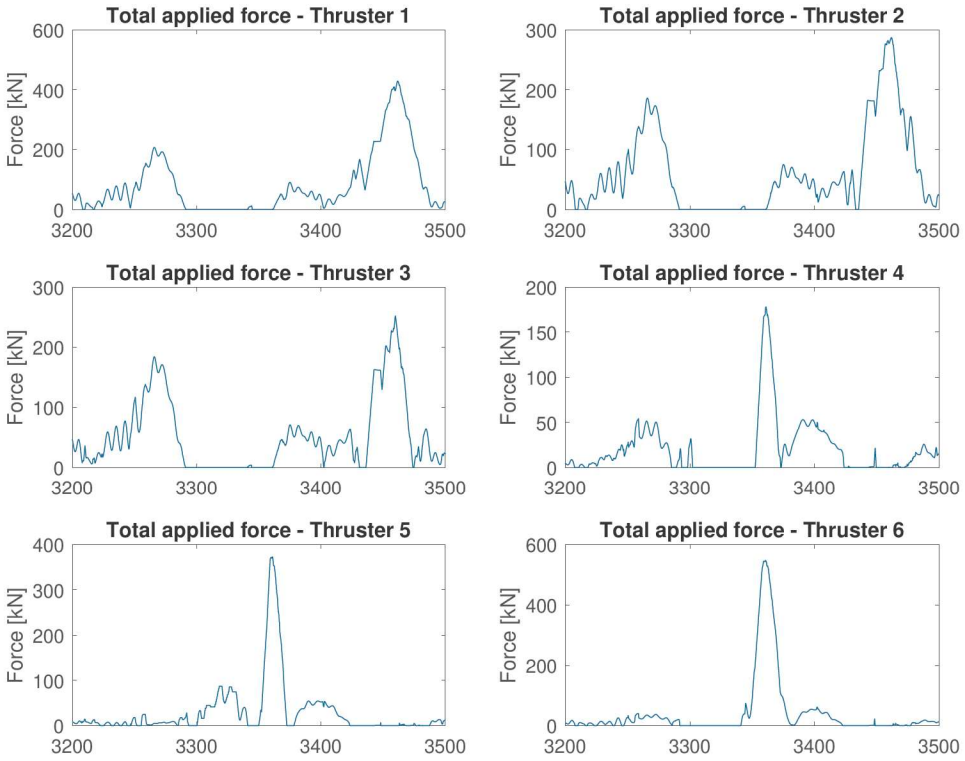

Figure 7.4: Total applied forces per thruster at time of observed outliers; results obtained from simulation with gripper CP in sea state of Hs = 1.5, 135deg, Tp = 8s.

Similar errors were observed for different angles of the incoming waves, which sometimes even led to a total drift off of the vessel. Due to this, it was not possible to test the current system with other incoming wave directions including the thruster allocation. Without thruster allocation, no proper conclusion can be drawn on the performance of the DP system including its limiting factors.

8

Conclusion and recommendations

8.1. Conclusion

The main question of this thesis concerned finding out what the effects of changing a DP Vessel its control point from its conventional location at the center, to a location far away from the center, would be on the DP performance. Wherein DP performance was defined to be dependent on the DP footprint, the total motion responses, and the energy consumption. In order to do this, a new DP system was designed and presented in this thesis. Time domain simulations were performed with the newly designed DP model and the conventional DP model and the results were compared.

The first sub-question concerned the design of the new DP system. It was found that due to the higher motion coupling at the gripper location, the equations of motion change at this point, and therefore changes in the Kalman Filter were needed and a new PD controller was designed and implemented in the existing DP model. To get the state estimations at the gripper position, the state estimations are estimated at the center and then translated to the gripper location in the new DP model. As the estimated states consist of coupled motions, a Decoupling module was added prior to the PD controllers in order to decouple the errors that are sent into the PD controllers. The tuning of the new PD controller was done in such a way, that it responds as equally as possible to the existing PD controller. 1-on-1 comparisons were made with the step responses of both models, to match the outputs of the new controller as much as possible with the conventional controller. The reference point of the thruster allocation algorithm was also modified in order to let the thrusters account for the gripper control point.

The second sub-question was about what the motion responses are for the vessel with the conventional DP system versus the vessel with the newly proposed method in this study. 3-hour simulations were performed for the vessel in bow quartering waves (135 deg) with a significant wave height of 1.5 meters and a peak period of 8 seconds. The low-frequency motion responses of this simulation are presented in Table 5.2 and Table 5.3. From the results in these tables, it became clear that the motion responses in sway got bigger for the gripper control point compared to the center control point. The responses for surge showed marginal differences between both methods. For the yaw motion, a lower response was found for the gripper control point model compared to the center control point model.

To gather insights into the influence of different wave heights, simulations were performed with the same wave direction of 135 degrees and peak period of 8 seconds, but with significant wave heights of 1.0m and 2.0m. Note that these simulations were only done for 1 hour, due to the very large simulation time. When considering the wave height variation results, similar differences in motion responses were observed for the base case with a significant wave height of 1.5 meters: a lower response for the yaw motion in the gripper control point compared to the center control point for both Hs = 1.0m and Hs = 2.0m. The differences in the surge direction between the gripper control point and center control point are marginal for both Hs. In Hs = 1.0m a bigger response for the sway motion from the gripper control point model is observed, just as for the base case. However, for Hs = 2.0m, differences in sway motion are marginal.

The third sub-question was how the DP footprint is affected at the location of interest with the new proposed control point. Results were again obtained from the time domain simulations and DP footprints were plotted at the gripper location for both DP models in different wave heights. According to the DP footprint in the case of a significant wave height of 1.5 meters, a slight improvement in the x-direction was observed for the gripper control point model. When considering the results of the one-

hour simulations for the significant wave heights of 1.0m and 2.0m, the differences were marginal for Hs = 1.0m, but for Hs = 2.0m a lower response in the x-direction was observed.

The fourth and last sub-question concerned the influence of changing the control point on the demanded power of the DP system. From the DP module provided by HES, the delivered thrust per thruster could be obtained. With the help of the propeller diagrams of the actually installed thrusters aboard the Aegir vessel, these delivered thrusts were converted to power inputs. According to the simulations done in this study, the total average power and the total energy consumption during simulations were lower for the gripper control point model, compared to the center control point model. This applies to all significant wave heights. Another observation was that the distributions of power over the thrusters differ between both models.

From the results presented in this study, it is concluded that the system itself has potential, but no hard conclusions can be drawn for the system in its current form. Problems were observed with the current thruster allocation algorithm from HES, which need to be explored in more detail and resolved. From the sea states assessed in this thesis, with the system as presented in this report, it can be stated that changing the control point seems to decrease energy consumption and leads to a slight improvement in the yaw motion response at the location of interest. In summary, based on the tests performed, responses of interest were quite comparable between the two models and therefore it cannot be concluded whether controlling around the alternative point provides an advantage or not.

8.2. Recommendations

The most important next step is to consider the responses of the system on more sea states. In this study, only waves with a direction of 135 degrees, without any spreading are included in the dynamic simulations. In further research, wind, current, and other wave directions should be considered in order to find out the effects on the DP performance in other (bow quartering) wave directions too. From the results of this thesis, it became clear that the thrusters did not seem to have problems with obtaining the demanded forces in the sea states tested. Therefore, the performance can eventually be assessed without the thruster allocation.

The second most important next step is to improve the current approach for estimating the states at the gripper position. A Kalman Filter that includes the velocity and noise covariances at the gripper location, could lead to better estimates and less noise in the overall system.

Another important step to improve the system as presented in this thesis, is to look into the thruster allocation algorithm and find a stable working version for both control point models. With a more stable thruster allocation algorithm, more accurate dynamic simulations can be made, also for other sea states.

In this thesis, only the influences on the system due to waves are assessed. The influence on the low-frequency motions of the system turned out to be marginal in this study. Therefore, it is recommended to look into how the system responds to more sudden excitations. Examples of such excitations are forces induced by the gripper and sudden wind gusts/squalls or currents.

As mentioned in the discussion, no integral term was included for the PD controllers in this study. When one decides to continue with the MIMO P(I)D system, the integral term should be included to cope with the mean wave drift forces and eventual current and wind forces. It is recommended to also look into other forms of controllers, that are more suitable with coupled behaviors.

A

Complete matrices for coupled state-space model

The state-space model inputs for the gripper position as presented in section 4.3, that was use for tests of the PD controller in MATLAB are presented in this appendix.

A.1. Mass and stiffness inverse

$$-[M]_{3x3}^{-1}[C]_{3x3} = \begin{bmatrix} -\frac{C_{11}M_{26}^2+C_{16}M_{16}M_{22}-C_{11}M_{22}M_{66}}{M_{22}M_{16}^2+M_{11}M_{26}^2-M_{11}M_{22}M_{66}} & \frac{M_{16}(C_{22}M_{26}-C_{26}M_{22})}{M_{22}M_{16}^2+M_{11}M_{26}^2-M_{11}M_{22}M_{66}} & -\frac{C_{16}M_{26}^2-C_{16}M_{22}M_{66}+C_{66}M_{16}M_{22}}{M_{22}M_{16}^2+M_{11}M_{26}^2-M_{11}M_{22}M_{66}} \\ \frac{M_{26}(C_{11}M_{16}-C_{16}M_{11})}{M_{22}M_{16}^2-M_{11}M_{26}^2-M_{11}M_{22}M_{66}} & -\frac{C_{22}M_{16}^2+C_{26}M_{11}M_{26}-C_{22}M_{11}M_{66}}{M_{22}M_{16}^2+M_{11}M_{26}^2-M_{11}M_{22}M_{66}} & -\frac{C_{26}M_{16}^2-C_{16}M_{26}M_{16}-C_{26}M_{11}M_{66}+C_{66}M_{11}M_{26}}{M_{22}M_{16}^2+M_{11}M_{26}^2-M_{11}M_{22}M_{66}} \\ -\frac{C_{11}M_{16}M_{22}-C_{16}M_{11}M_{22}}{M_{22}M_{16}^2+M_{11}M_{26}^2-M_{11}M_{22}M_{26}} & -\frac{C_{22}M_{11}M_{26}-C_{26}M_{11}M_{22}}{M_{22}M_{16}^2+M_{11}M_{26}^2-M_{11}M_{22}M_{26}} & -\frac{C_{16}M_{16}M_{22}+C_{26}M_{11}M_{26}-C_{66}M_{11}M_{22}}{M_{22}M_{16}^2+M_{11}M_{26}^2-M_{11}M_{22}M_{26}} \end{bmatrix}$$

A.2. Mass and damping inverse

$$-[M]_{3x3}^{-1}[B]_{3x3} = \begin{bmatrix} -\frac{B_{11}M_{26}^2+B_{16}M_{16}M_{22}-B_{11}M_{22}M_{66}}{M_{22}M_{16}^2+M_{11}M_{26}^2-M_{11}M_{22}M_{66}} & \frac{M_{16}(B_{22}M_{26}-B_{26}M_{22})}{M_{22}M_{16}^2+M_{11}M_{26}^2-M_{11}M_{22}M_{66}} & -\frac{B_{16}M_{26}^2-B_{16}M_{22}M_{66}+B_{66}M_{16}M_{22}}{M_{22}M_{16}^2+M_{11}M_{26}^2-M_{11}M_{22}M_{66}} \\ \frac{M_{26}(B_{11}M_{16}-B_{16}M_{11})}{M_{22}M_{16}^2-M_{11}M_{26}^2-M_{11}M_{22}M_{66}} & -\frac{B_{22}M_{16}^2+B_{26}M_{11}M_{26}-B_{22}M_{11}M_{66}}{M_{22}M_{16}^2+M_{11}M_{26}^2-M_{11}M_{22}M_{66}} & -\frac{B_{26}M_{16}^2-B_{16}M_{26}M_{16}-B_{26}M_{11}M_{66}+B_{66}M_{11}M_{26}}{M_{22}M_{16}^2+M_{11}M_{26}^2-M_{11}M_{22}M_{66}} \\ -\frac{B_{11}M_{16}M_{22}-B_{16}M_{11}M_{22}}{M_{22}M_{16}^2+M_{11}M_{26}^2-M_{11}M_{22}M_{26}} & -\frac{B_{22}M_{11}M_{26}-B_{26}M_{11}M_{22}}{M_{22}M_{16}^2+M_{11}M_{26}^2-M_{11}M_{22}M_{26}} & -\frac{B_{16}M_{16}M_{22}+B_{26}M_{11}M_{26}-B_{66}M_{11}M_{22}}{M_{22}M_{16}^2+M_{11}M_{26}^2-M_{11}M_{22}M_{26}} \end{bmatrix}$$

A.3. Mass inverse

$$-[M]_{3x3}^{-1} = \begin{bmatrix} \frac{M_{26}^2-M_{22}M_{66}}{M_{22}M_{16}^2+M_{11}M_{26}^2-M_{11}M_{22}M_{66}} & -\frac{M_{16}M_{26}}{M_{22}M_{16}^2+M_{11}M_{26}^2-M_{11}M_{22}M_{66}} & \frac{M_{16}M_{22}}{M_{22}M_{16}^2+M_{11}M_{26}^2-M_{11}M_{22}M_{66}} \\ -\frac{M_{16}M_{26}}{M_{22}M_{16}^2+M_{11}M_{26}^2-M_{11}M_{22}M_{66}} & \frac{M_{16}^2-M_{11}M_{66}}{M_{22}M_{16}^2+M_{11}M_{26}^2-M_{11}M_{22}M_{66}} & \frac{M_{11}M_{26}}{M_{22}M_{16}^2+M_{11}M_{26}^2-M_{11}M_{22}M_{66}} \\ \frac{M_{11}M_{26}}{M_{22}M_{16}^2+M_{16}M_{22}^2-M_{11}M_{22}M_{66}} & \frac{M_{11}M_{26}}{M_{22}M_{16}^2+M_{11}M_{26}^2-M_{11}M_{22}M_{66}} & -\frac{M_{11}M_{22}}{M_{22}M_{16}^2+M_{11}M_{26}^2-M_{11}M_{22}M_{66}} \end{bmatrix}$$

B

MATLAB code for PD controller testing with center control point

```
clear all
clc
close all

% Defininig the symbols
syms K B M M_11 M_22 M_66 M_16 M_26 K_11 K_22 K_66 K_16 K_26 B_11...
B_22 B_66 B_16 B_26 F_thx F_thy M_th F_hydx F_hydy xt xt_dot xt_ddot yt
    yt_dot yt_ddot...
psi psi_dot psi_ddot M_hyd F_thrust

% Substituting the stiffness, damping and mass matrices with their
    numerical values
K       = subs(K,K,[K_11 0 0;0 K_22 0; 0 0 K_66]);
B       = subs(B,B,[B_11 0 0;0 B_22 0; 0 0 B_66]);
M       = subs(M,M,[M_11 0 0;0 M_22 0; 0 0 M_66]);


%% Defining the external forces and moments on the vessel
F_trust = [F_thx; F_thy; M_th];
F_hyd   = [F_hydx; F_hydy; M_hyd];


%% Defining the mathematical model of the vessel
q       = [xt;yt;psi];                                  % Position vector
q_dot   = [xt_dot; yt_dot; psi_dot];                    % Velocity vector
q_ddot = M\(-K*q - B*q_dot + F_hyd + F_thrust);         % EQM

%% Defining the state space system
x_dot = [q_dot;q_ddot];                         % State derivative vector
x     = [q; q_dot];                             % State vector
u     = [0;0;0;F_thx;F_thy;M_th];% Input vector
y     = x;                                      % Output vector

% Assigning names to the states, inputs and outputs
x_names = {'xt','yt','psit','xt_dot','yt_dot','psit_dot'};
u_names = {'F_thx', 'F_thy', 'M_th','F_hydx','F_hydy','M_hyd'};
y_names = {'x_t','y_t','psi_t','x_t_dot','y_t_dot','psi_t_dot'};
x_units = {'m','m','m','m/s','m/s','rad/s'};
u_units = {'kN','kN','kNm','kN','kN','kNm'};
y_units = {'m','m','m','m/s','m/s','rad/s'};

%% Get symbolic state-space matrices
StateSpace.A = [zeros(3) eye(3); M\-K M\-B];
```

```
StateSpace.B = [zeros(3,6); inv(M) inv(M)];
StateSpace.C = eye(6);
StateSpace.D = zeros(6);

StateSpace.A
StateSpace.B
StateSpace.C
StateSpace.D

% Load numerical values for mass
load AegirMassCenterPos.mat

% Set DP stiffness (set to zero if PID controller is used)
K_11 = 0;
K_22 = 0;
K_66 = 0;

% Set hyd. damping
B_11 = ***;
B_22 = ***;
B_66 = ***;

% Substituting the remaining symbols with their numerical values
StateSpace.A = subs(StateSpace.A, {'M_11','M_22','M_66','M_16','M_26','
    K_11'...
,'K_22','K_66','K_16','K_26','B_11','B_22','B_66','B_16','B_26'},{M_11,
    M_22,...
M_66,M_16,M_26,K_11,K_22,K_66,K_16,K_26,B_11,B_22,B_66,B_16,B_26});


StateSpace.B = subs(StateSpace.B, {'M_11','M_22','M_66','M_16','M_26','
    K_11'...
,'K_22','K_66','K_16','K_26','B_11','B_22','B_66','B_16','B_26'},{M_11,
    M_22,...
M_66,M_16,M_26,K_11,K_22,K_66,K_16,K_26,B_11,B_22,B_66,B_16,B_26});


%% State Space Matrices
SS_Matrices.A = eval(StateSpace.A);
SS_Matrices.B = eval(StateSpace.B);
SS_Matrices.C = StateSpace.C;
SS_Matrices.D = StateSpace.D;

SS_Matrices.A
SS_Matrices.B
SS_Matrices.C
SS_Matrices.D

SysSS_Name = ['Dynamic model'];
SysSS = ss(SS_Matrices.A,SS_Matrices.B,SS_Matrices.C,SS_Matrices.D,'
    StateName',x_names,'InputName',u_names,'OutputName',y_names,'Name',
    SysSS_Name,'StateUnit',x_units,'InputUnit',u_units,'OutputUnit',y_units
    );
%% Define system again
G = SysSS;
G.InputName = u_names;
```

```
G.OutputName = 'y';

%% Represent components of the controller
D = tunableGain('Decoupler',eye(3));
D.InputName  = 'e';
D.OutputName = {'e_x','e_y','e_rz'};
% D.Gain.Free  = [0 0 0;0 0 0;0 0 0];

PID_X = tunablePID('PID_X','pid');
PID_X.InputName = 'e_x';
PID_X.OutputName = 'F_thx';
PID_X.Kp.Value = ***;
PID_X.Ki.Value = 0;
PID_X.Kd.Value = ***;
PID_X.Tf.Value = 0.0001;
PID_X.Tf.Free = false;
PID_X.Kp.Free = false;
PID_X.Ki.Free = false;
PID_X.Kd.Free = false;

PID_Y = tunablePID('PID_Y','pid');
PID_Y.InputName = 'e_y';
PID_Y.OutputName = 'F_thy';
PID_Y.Kp.Value = ***;
PID_Y.Ki.Value = 0;
PID_Y.Kd.Value = ***;
PID_Y.Tf.Value = 0.0001;
PID_Y.Tf.Free = false;
PID_Y.Kp.Free = false;
PID_Y.Ki.Free = false;
PID_Y.Kd.Free = false;

PID_rz = tunablePID('PID_rz', 'pid');
PID_rz.InputName = 'e_rz';
PID_rz.OutputName = 'M_th';
PID_rz.Kp.Value = ***;
PID_rz.Ki.Value = 0;
PID_rz.Kd.Value = ***;
PID_rz.Tf.Value = 0.0001;
PID_rz.Tf.Free = false;
PID_rz.Kp.Free = false;
PID_rz.Ki.Free = false;
PID_rz.Kd.Free = false;

sum1 = sumblk('e = r - y',3);

%% Connect controller components
C0 = connect(PID_X,PID_Y,PID_rz,D,sum1,{'r','y'},{'F_thx','F_thy','M_th'})
    ;

%% Tune the control system
wc = [0.01,0.2];
[G,C,gam,Info] = looptune(G,C0,wc);

%% Display tuned control parameters
showTunable(C)
```

```
T = connect(G,C,'r','y',{'F_thx','F_thy','M_th'});
t = linspace(1e-6,500,5001);

% system stability info
figure;
loopview(G,C,Info)
% Check coupling
figure;
step(T)

%% analysispoints

Txy = getIOTransfer(T,'F_thx','y');
Tyy = getIOTransfer(T,'F_thy','y');
Trzy = getIOTransfer(T,'M_th','y');

T0 = T;
% Save step response for center model to use for tuning the gripper model
save center_response.mat T0 t

% Testing PD controller with forces
opt  = stepDataOptions('StepAmplitude',***);
X_PD = step(Txy,t,opt);

opt  = stepDataOptions('StepAmplitude',***);
Y_PD = step(Tyy,t,opt);

opt  = stepDataOptions('StepAmplitude',***);
RZ_PD = step(Trzy,t,opt);

figure
subplot(3,1,1)
plot(t,X_PD(:,1))
xlim([0 200])
ylim([0 1.2])
ylabel('X [m]')
xlabel('time [s]')
title('X displacements')

subplot(3,1,2)
plot(t,Y_PD(:,2))
xlim([0 200])
ylim([0 1.2])
ylabel('Y [m]')
xlabel('time [s]')
title('Y displacements')

subplot(3,1,3)
plot(t,RZ_PD(:,3))
xlim([0 200])
ylim([0 1.2])
ylabel('Rz [-]')
xlabel('time [s]')
title('Rz displacements')
```

C

MATLAB code for PD controller testing with gripper control point

```
clear all
clc
close all
% Defininig the symbols
syms K B M M_11 M_22 M_66 M_16 M_26 K_11 K_22 K_66 K_16 K_26 B_11...
B_22 B_66 B_16 B_26 F_thx F_thy M_th F_hydx F_hydy xt xt_dot xt_ddot yt
    yt_dot yt_ddot...
psi psi_dot psi_ddot M_hyd F_thrust

% Substituting the stiffness, damping and mass matrices with their
    numerical values
K = subs(K,K,[K_11 0 K_16;0 K_22 K_26; K_16 K_26 K_66]);
B = subs(B,B,[B_11 0 B_16;0 B_22 B_26; B_16 B_26 B_66]);
M = subs(M,M,[M_11 0 M_16;0 M_22 M_26; M_16 M_26 M_66]);


%% Defining the external forces and moments on the vessel
F_trust = [F_thx; F_thy; M_th];
F_hyd = [F_hydx; F_hydy; M_hyd];


%% Defining the mathematical model of the vessel
q = [xt;yt;psi];                                  % Position vector
q_dot = [xt_dot; yt_dot; psi_dot];                % Velocity vector
q_ddot = M\(-K*q - B*q_dot + F_hyd + F_thrust); % EQM


%% Defining the state space system
x_dot = [q_dot;q_ddot];                          % State derivative vector
x = [q; q_dot];                                  % State vector
u = [F_hydx;F_hydy;M_hyd;F_thx;F_thy;M_th];      % Input vector
y = x;                                           % Output vector

% Assigning names to the states, inputs and outputs
x_names = {'xt','yt','psit','xt_dot','yt_dot','psit_dot'};
u_names = {'F_hydx','F_hydy','M_hyd','F_thx', 'F_thy', 'M_th'};
y_names = {'x_t','y_t','psi_t','x_t_dot','y_t_dot','psi_t_dot'};

%% Get symbolic state-space matrices
StateSpace.A = [zeros(3) eye(3); M\-K M\-B];
StateSpace.B = [zeros(3,6); inv(M) inv(M)];
StateSpace.C = eye(6);
StateSpace.D = zeros(6);
```

```
StateSpace.A
StateSpace.B
StateSpace.C
StateSpace.D

% Load numerical values
load AegirMassGripper.mat

% Set hyd stiffness, set to zero if PID is used
K_11 = 0;
K_22 = 0;
K_66 = 0;
K_16 = 0;
K_26 = 0;

% Set hyd damping
B_11 = ***;
B_22 = ***;
B_66 = ***;
B_16 = ***;
B_26 = ***;

% Substituting the remaining symbols with their numerical values
StateSpace.A = subs(StateSpace.A, {'M_11','M_22','M_66','M_16','M_26','
    K_11'...
,'K_22','K_66','K_16','K_26','B_11','B_22','B_66','B_16','B_26'},{M_11,
    M_22,...
M_66,M_16,M_26,K_11,K_22,K_66,K_16,K_26,B_11,B_22,B_66,B_16,B_26});

StateSpace.B = subs(StateSpace.B, {'M_11','M_22','M_66','M_16','M_26','
    K_11'...
,'K_22','K_66','K_16','K_26','B_11','B_22','B_66','B_16','B_26'},{M_11,
    M_22,...
M_66,M_16,M_26,K_11,K_22,K_66,K_16,K_26,B_11,B_22,B_66,B_16,B_26});


%% State Space Matrices
SS_Matrices.A = eval(StateSpace.A);
SS_Matrices.B = eval(StateSpace.B);
SS_Matrices.C = StateSpace.C;
SS_Matrices.D = StateSpace.D;

SS_Matrices.A
SS_Matrices.B
SS_Matrices.C
SS_Matrices.D

SysSS_Name = ['Dynamic model'];
SysSS = ss(SS_Matrices.A,SS_Matrices.B,SS_Matrices.C,SS_Matrices.D,'
    StateName',x_names,'InputName',u_names,'OutputName',y_names,'Name',
    SysSS_Name);

%% Define system again
G = SysSS;
G.InputName = u_names;
```

```
G.OutputName = 'y';

%% Represent components of the controller
D = tunableGain('Decoupler',eye(3));
D.InputName = 'e';
D.OutputName = {'e_x','e_y','e_rz'};
% D.Gain.Free  = [0 0 0;0 0 0;0 0 0];

PID_X = tunablePID('PID_X','pid');
PID_X.InputName = 'e_x';
PID_X.OutputName = 'F_thx';
PID_X.Kp.Value = ***;
PID_X.Ki.Value = 0;
PID_X.Kd.Value = ***;
PID_X.Tf.Value = 0.0001;
PID_X.Tf.Free = false;
PID_X.Kp.Free = true;
PID_X.Ki.Free = false;
PID_X.Kd.Free = true;
PID_X.Kp.Maximum = ***;



PID_Y = tunablePID('PID_Y','pid');
PID_Y.InputName = 'e_y';
PID_Y.OutputName = 'F_thy';
PID_Y.Kp.Value = ***;
PID_Y.Ki.Value = 0;
PID_Y.Kd.Value = ***;
PID_Y.Tf.Value = 0.0001;
PID_Y.Tf.Free = false;
PID_Y.Kp.Free = true;
PID_Y.Ki.Free = false;
PID_Y.Kd.Free = true;
PID_Y.Kp.Maximum = ***;



PID_rz = tunablePID('PID_rz', 'pid');
PID_rz.InputName = 'e_rz';
PID_rz.OutputName = 'M_th';
PID_rz.Kp.Value = ***;
PID_rz.Ki.Value = 0;
PID_rz.Kd.Value = ***;
PID_rz.Tf.Value = 0.0001;
PID_rz.Tf.Free = false;
PID_rz.Kp.Free = true;
PID_rz.Ki.Free = false;
PID_rz.Kd.Free = true;
PID_rz.Kp.Maximum = ***;


sum1 = sumblk('e = r - y',3);

%% Connect controller components
C0 = connect(PID_X,PID_Y,PID_rz,D,sum1,{'r','y'},{'F_thx','F_thy','M_th'})
```

```
    ;

%% load center responses to set tuning requirements
load center_response.mat

Req1 = TuningGoal.Transient('r','y',T0,'step');
Req1.RelGap = 0.2;

%% Tune the control system
wc = [0.01,0.2];

[G,C,gam,Info] = looptune(G,C0,Req1);

figure('Position',[100,100,520,1000])
loopview(G,C,Info)

%% Display tuned control parameters
showTunable(C)

T = connect(G,C,'r','y',{'F_thx','F_thy','M_th'});

% Check(de)coupling with the step response
figure;
step(T);

u = ones(5001,1);
t = linspace(1e-6,500,5001);              %set time equal to ofx
    simulation

Txy = getIOTransfer(T,'F_thx','y');
Tyy = getIOTransfer(T,'F_thy','y');
Trzy = getIOTransfer(T,'M_th','y');

T2 = T;
save gripper_response.mat -append T2

opt  = stepDataOptions('StepAmplitude',***);
X_P  = step(Txy,t,opt);

opt  = stepDataOptions('StepAmplitude',***);
Y_P  = step(Tyy,t,opt);

opt  = stepDataOptions('StepAmplitude',***);
RZ_P = step(Trzy,t,opt);


figure;
subplot(3,1,1)
plot(t,X_P(:,1))
xlim([0 500])
ylabel('X [m]')
xlabel('time [s]')
title('X displacement')

subplot(3,1,2)
plot(t,Y_P(:,2))
```

```
xlim([0 500])
ylabel('Y [m]')
xlabel('time [s]')
title('Y displacement')

subplot(3,1,3)
plot(t,RZ_P(:,3))
xlim([0 500])
ylabel('Rz [deg]')
xlabel('time [s]')
title('Rz displacement')

temp1 = step(T0,t);
temp2 = step(T,t);

figure;
subplot(3,1,1)
plot(t,temp1(:,1,1),'--')
hold on
plot(t,temp2(:,1,1))
xlim([0 200])
ylabel('X [m]')
xlabel('time [s]')
legend('Step response @ center','Step response @ gripper')
title('X-direction')

subplot(3,1,2)
plot(t,temp1(:,2,2),'--')
hold on
plot(t,temp2(:,2,2))
xlim([0 200])
ylabel('Y [m]')
xlabel('time [s]')
title('Y-direction')

subplot(3,1,3)
plot(t,temp1(:,3,3),'--')
hold on
plot(t,temp2(:,3,3))
xlim([0 200])
ylabel('Rz [deg]')
xlabel('time [s]')
title('Rz-direction')
```

D

Complete results Hs = 1.0m

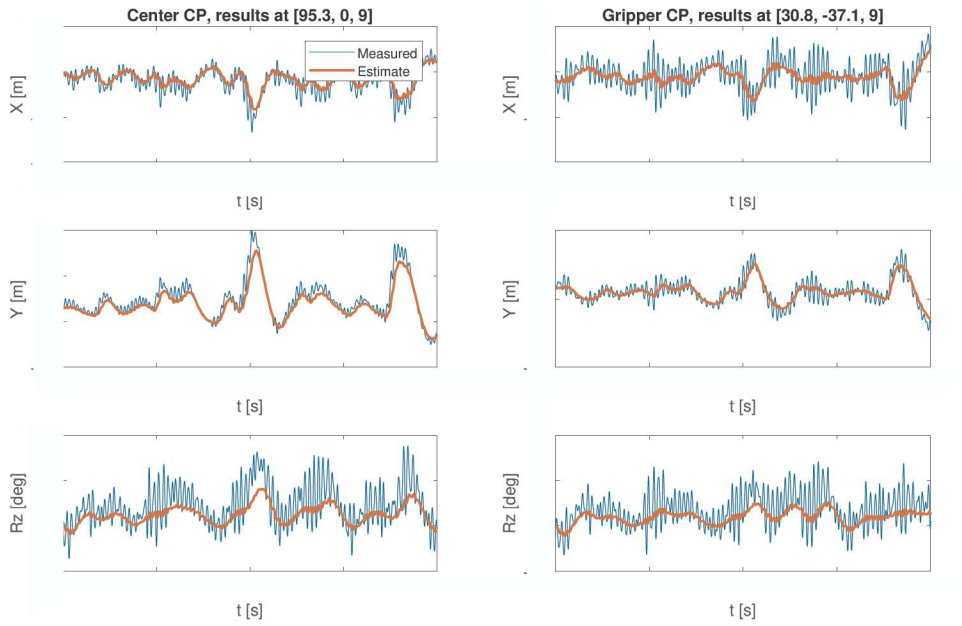

Figure D.1: Time-domain results for Kalman Filter in Hs = 1.0m, 135 deg. Tp = 8s; center control point vs. gripper control point

Figure D.2: Total motions in the horizontal plane during 1h time domain simulation in Hs = 1.0m, wavedir. = 135 deg and Tp = 8s; results obtained at t =

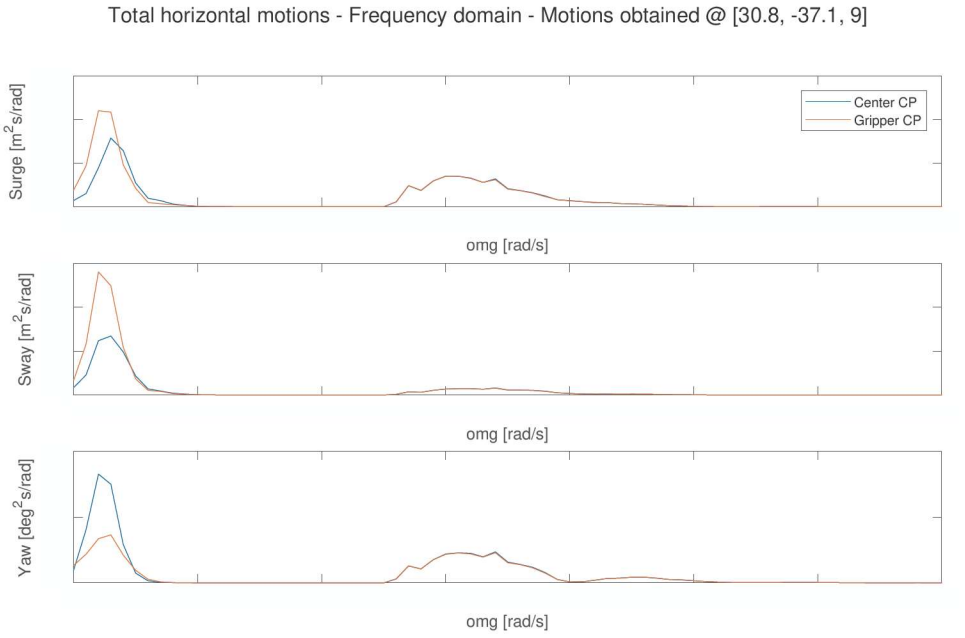

Figure D.3: Total motions during 1h time domain simulation in Hs = 1.0m, wavedir. = 135 deg and Tp = 8s - Frequency domain plots

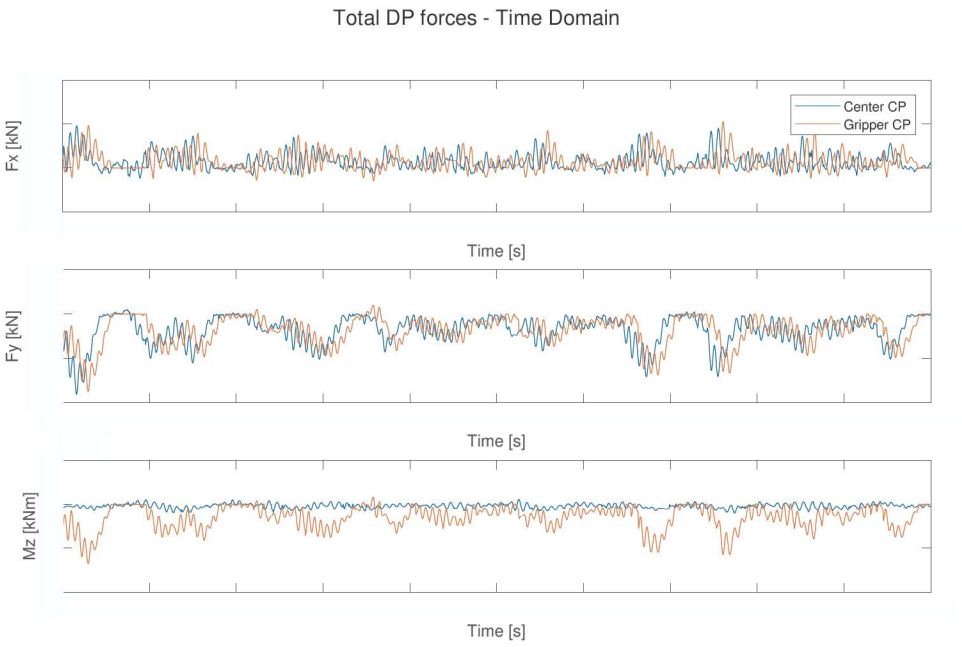

Figure D.4: DP Forces during 1h time domain simulation in Hs = 1.0m, wavedir. = 135 deg and Tp = 8s; results obtained at t = ***

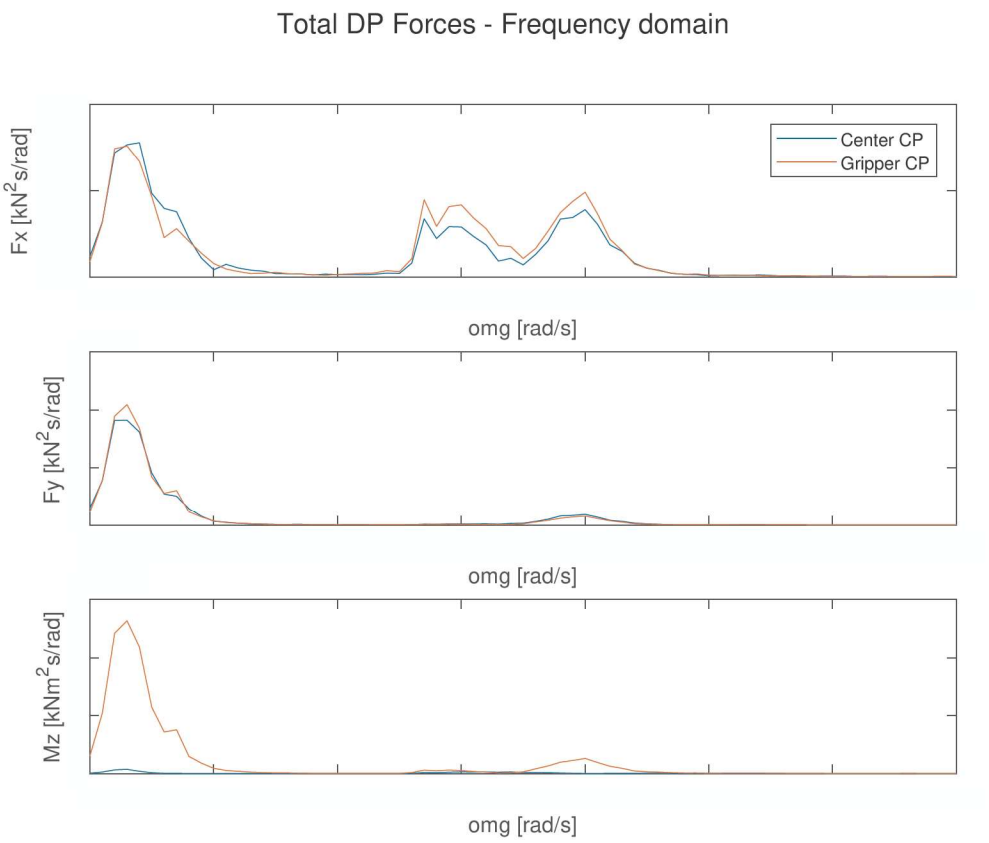

Figure D.5: DP forces during 1h time domain simulation in Hs = 1.0m, wavedir. = 135 deg and Tp = 8s - Frequency domain plots

Figure D.6: Demanded vs. obtained forces during 1h time domain simulation in Hs = 1.0m, wavedir. = 135 deg and Tp = 8s; results obtained at t = ***

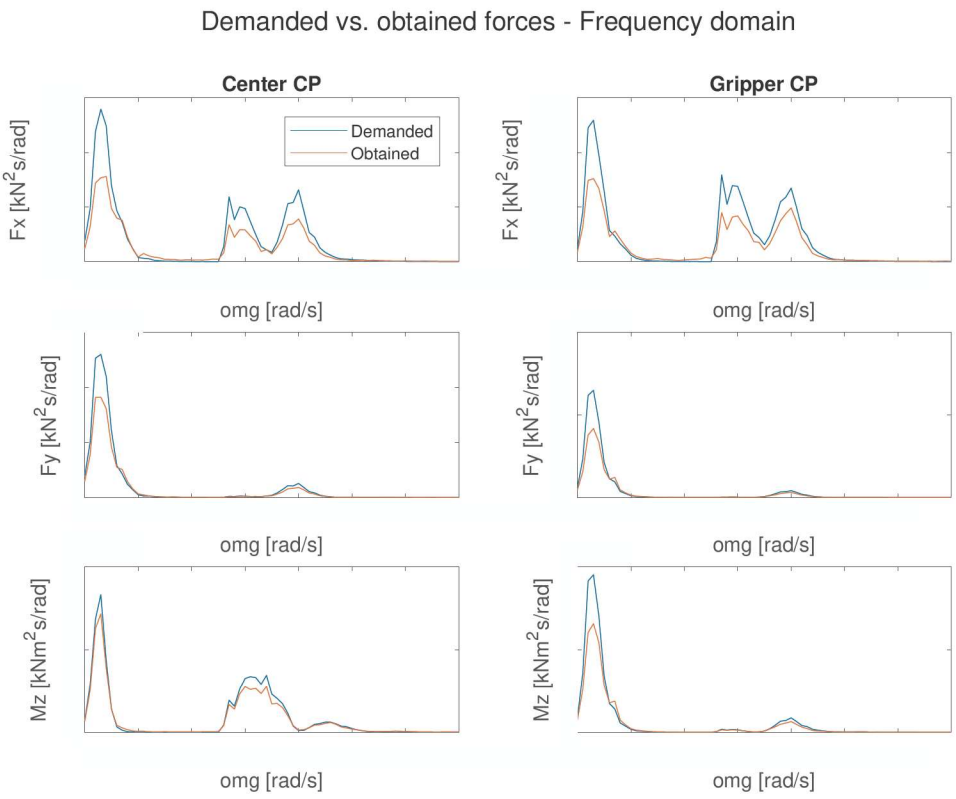

Figure D.7: Demanded vs. obtained forces during 1h time domain simulation in Hs = 1.0m, wavedir. = 135 deg and Tp = 8s - Frequency domain plots

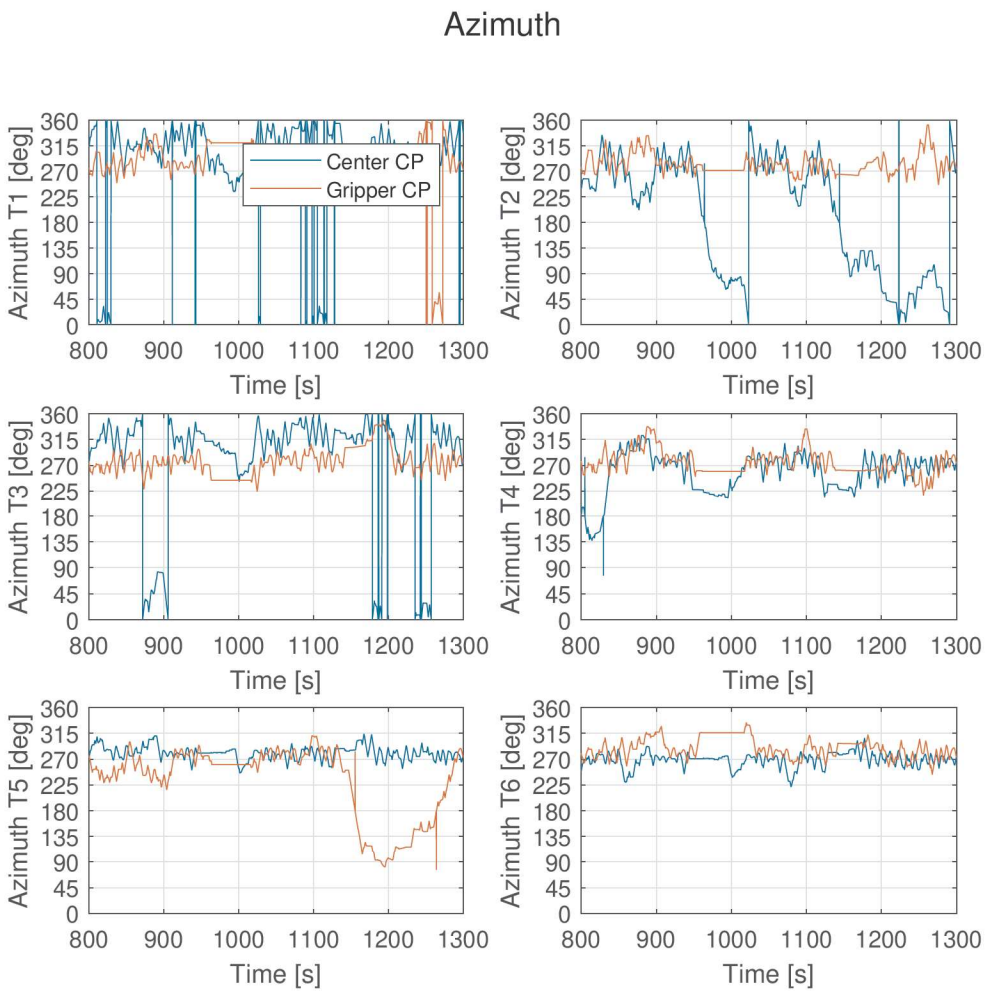

Figure D.8: Azimuth of thrusters during 1h time domain simulation in Hs = 1.0m, wavedir. = 135 deg and Tp = 8s; results obtained at t = ***

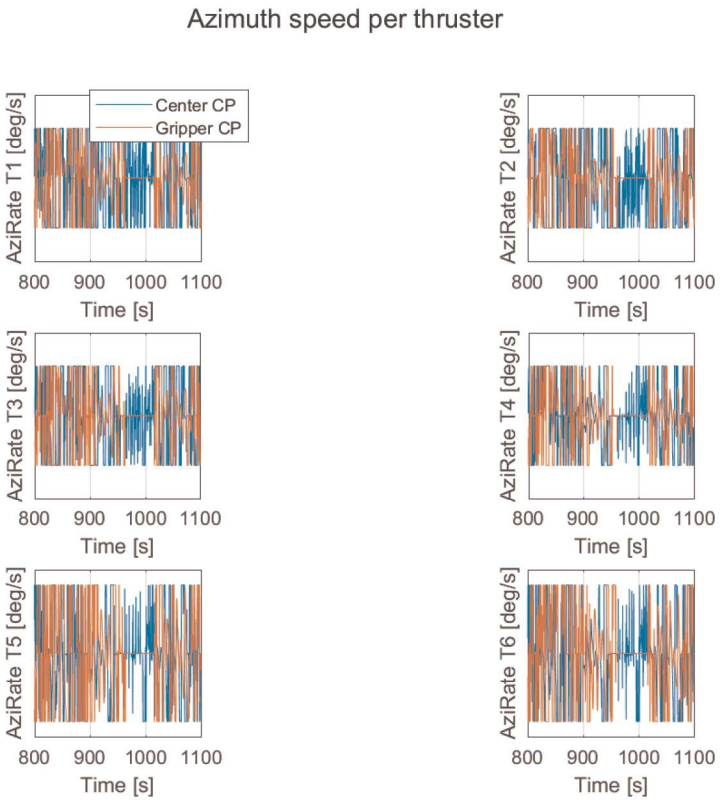

Figure D.9: Azirate of thrusters during 1h time domain simulations, with sea state Hs = 1.0m, 135deg, Tp = 8s - Results obtained at t = ***

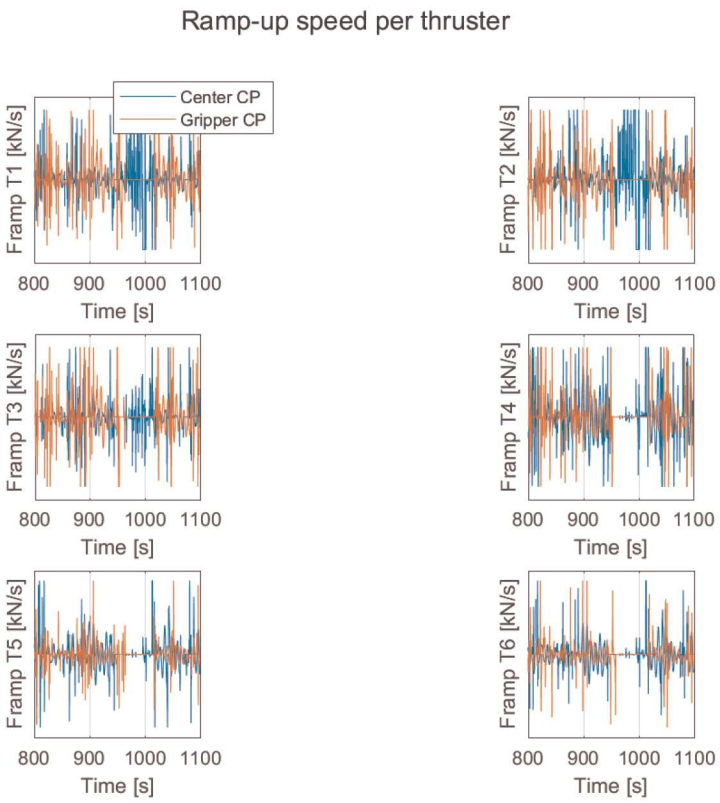

Figure D.10: Ramp up speeds of thrusters during 1h time domain simulations, with sea state Hs = 1.0m, 135deg, Tp = 8s - Results obtained at t = ***

E

Complete results Hs = 2.0m

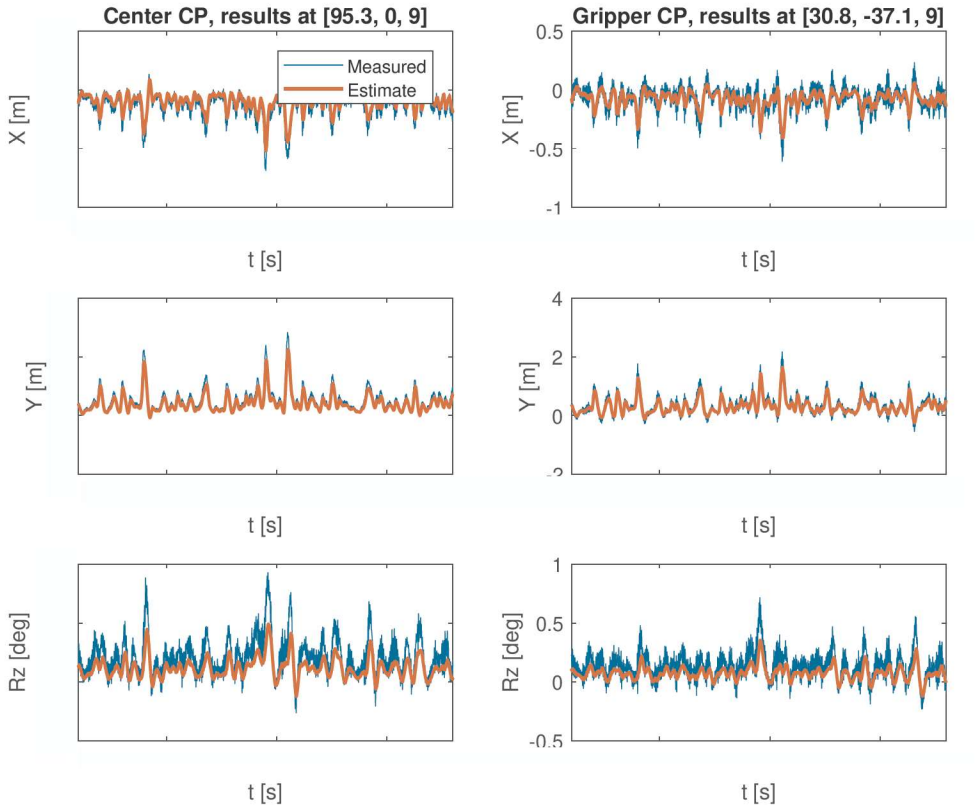

Figure E.1: Time-domain results for Kalman Filter in Hs = 2.0m, 135 deg. Tp = 8s; center control point vs. gripper control point

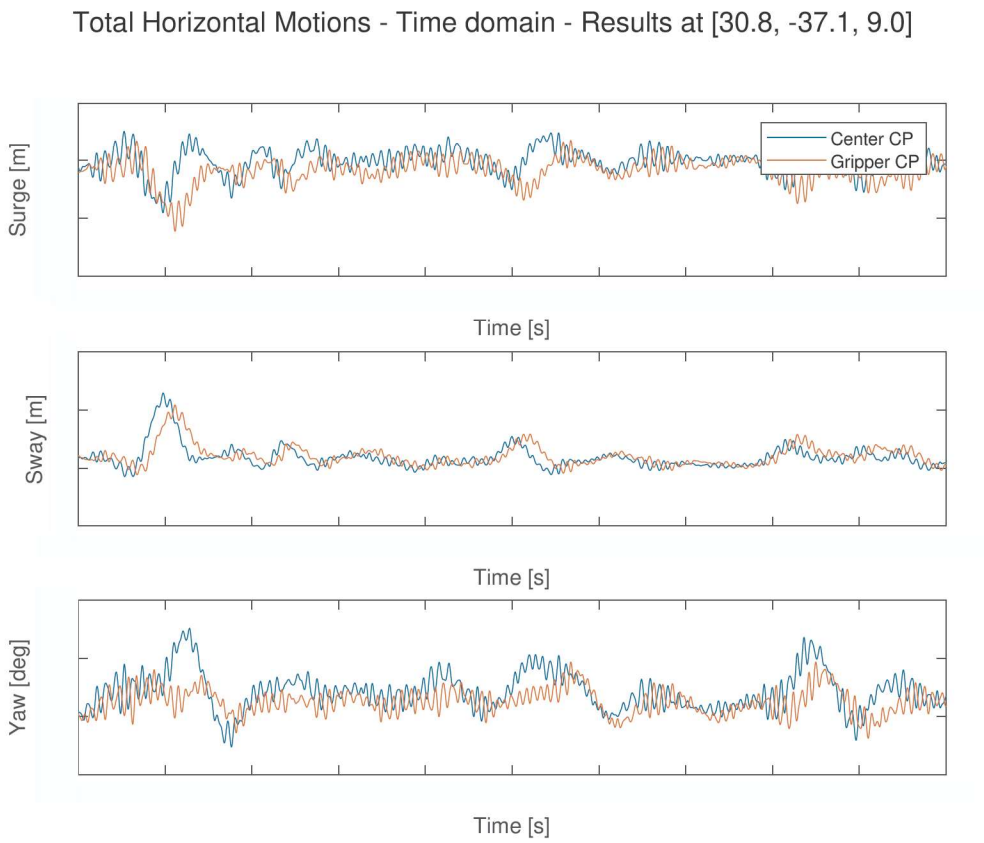

Figure E.2: Total motions in the horizontal plane during 1h time domain simulation in Hs = 2.0m, wavedir. = 135 deg and Tp = 8s; results obtained at t = ***

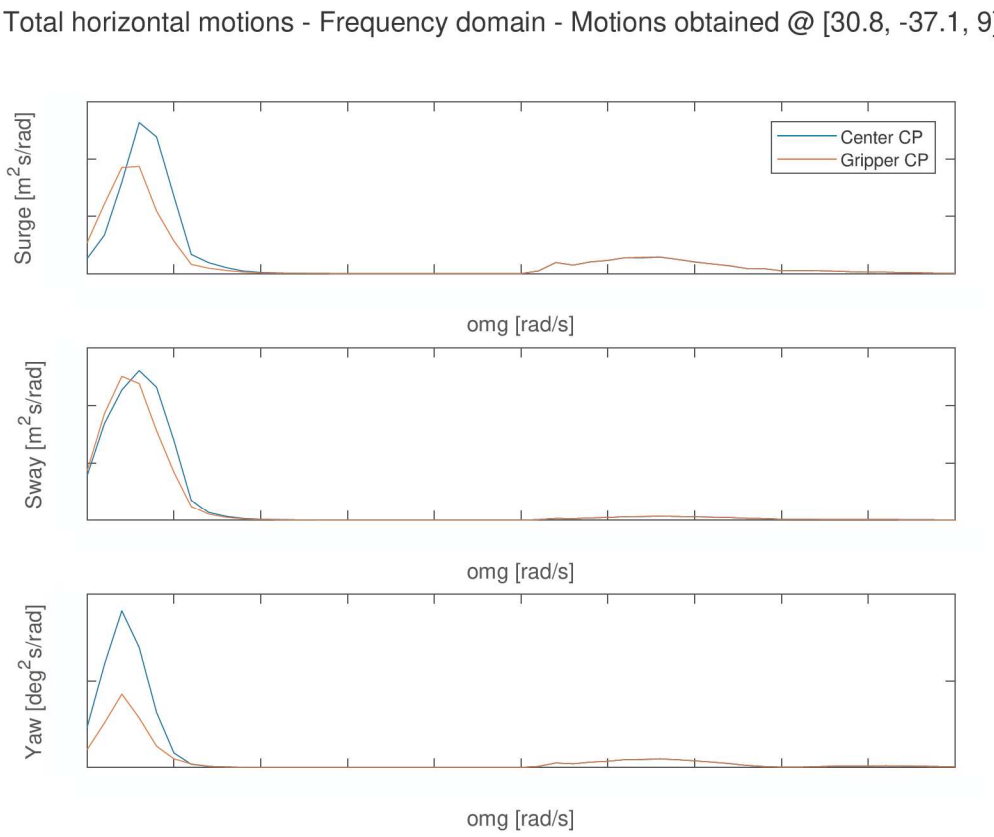

Figure E.3: Total motions during 1h time domain simulation in Hs = 2.0m, wavedir. = 135 deg and Tp = 8s - Frequency domain plots

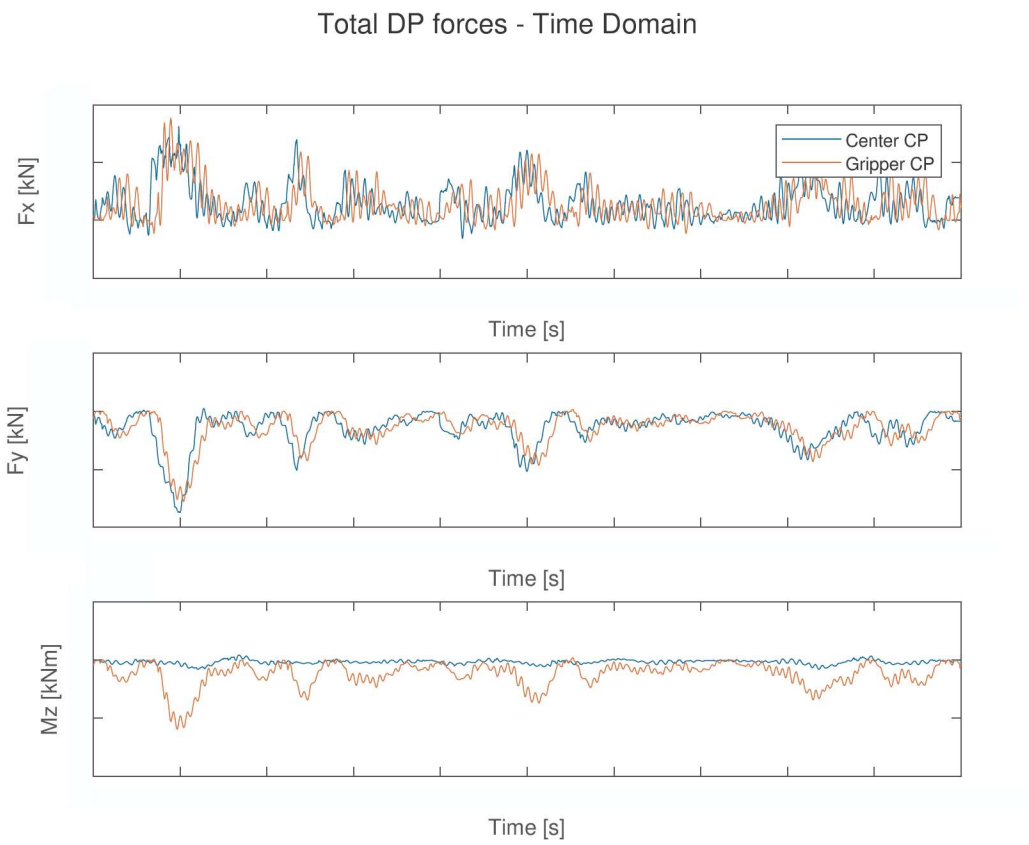

Figure E.4: DP Forces during 1h time domain simulation in Hs = 2.0m, wavedir. = 135 deg and Tp = 8s; results obtained at t = ***

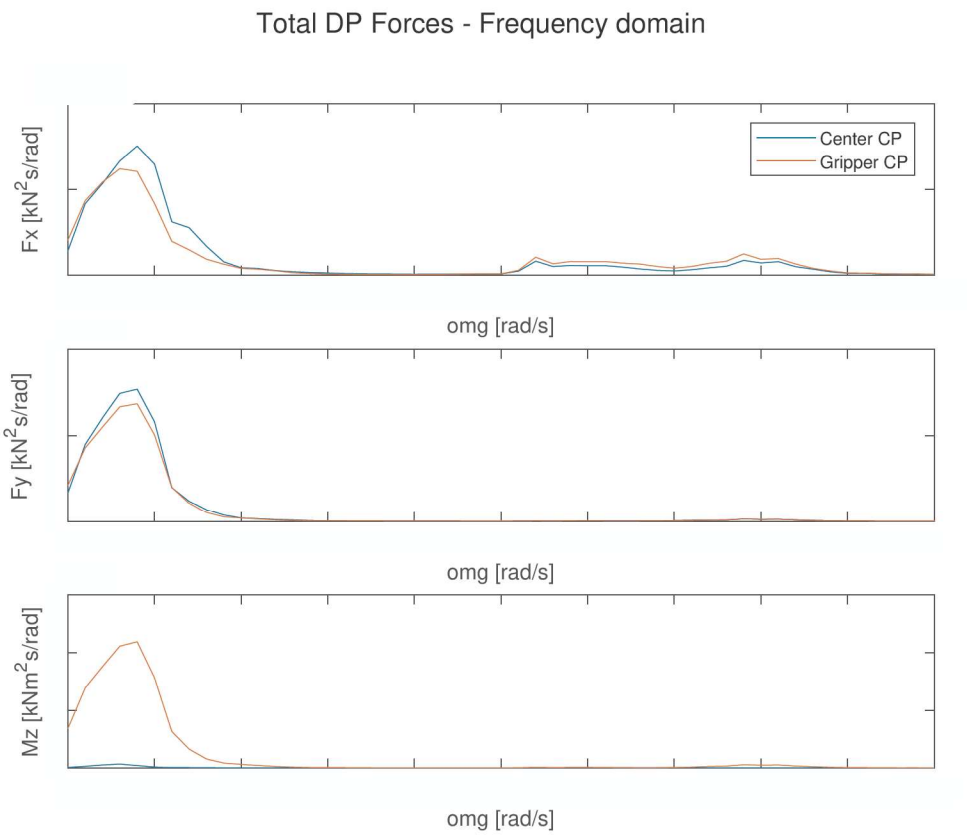

Figure E.5: DP forces during 1h time domain simulation in Hs = 2.0m, wavedir. = 135 deg and Tp = 8s - Frequency domain plots

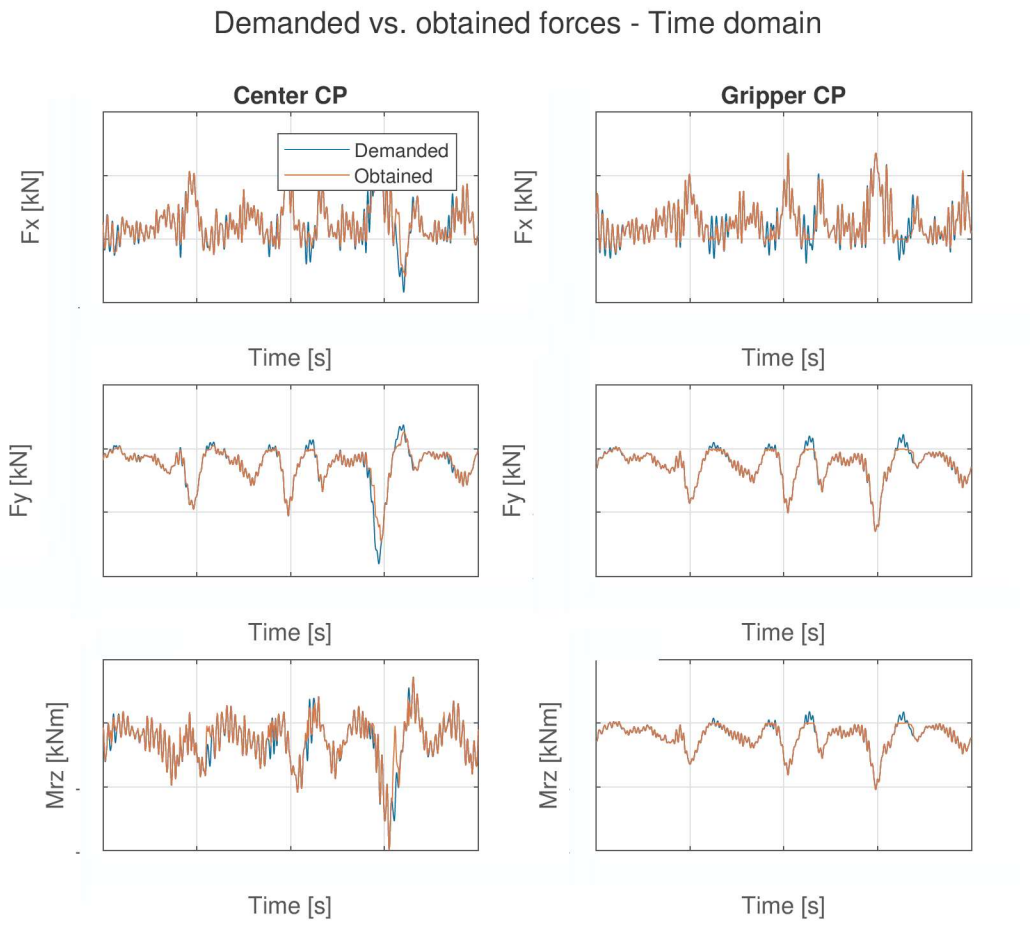

Figure E.6: Demanded vs. obtained forces during 1h time domain simulation in Hs = 2.0m, wavedir. = 135 deg and Tp = 8s; results obtained at t = ***

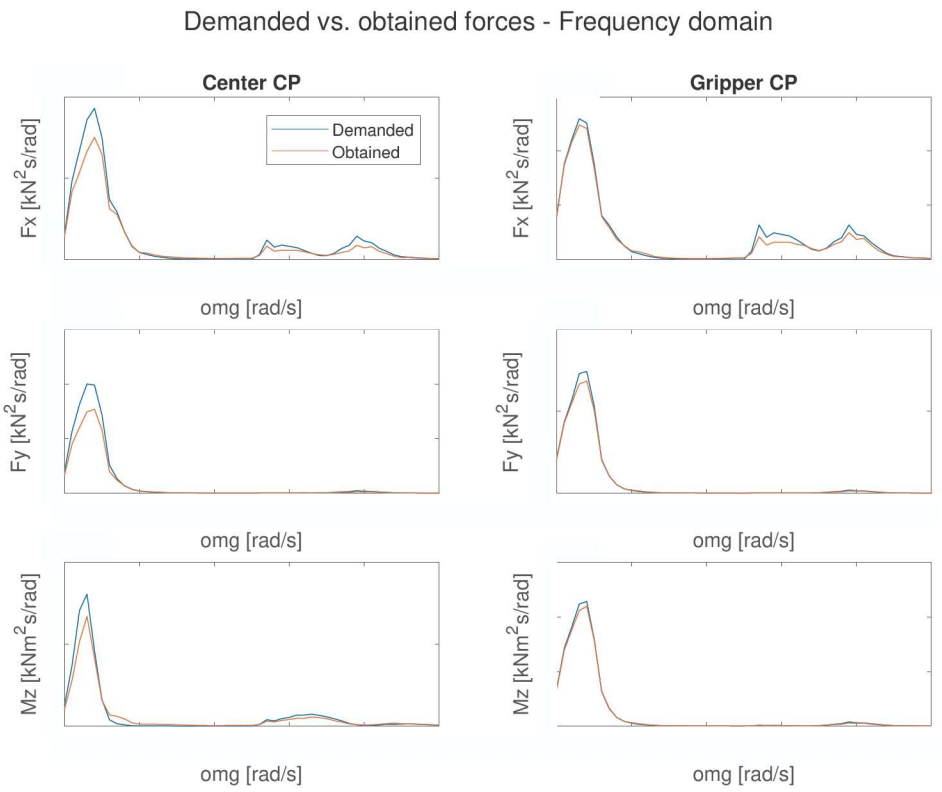

Figure E.7: Demanded vs. obtained forces during 1h time domain simulation in Hs = 2.0m, wavedir. = 135 deg and Tp = 8s - Frequency domain plots

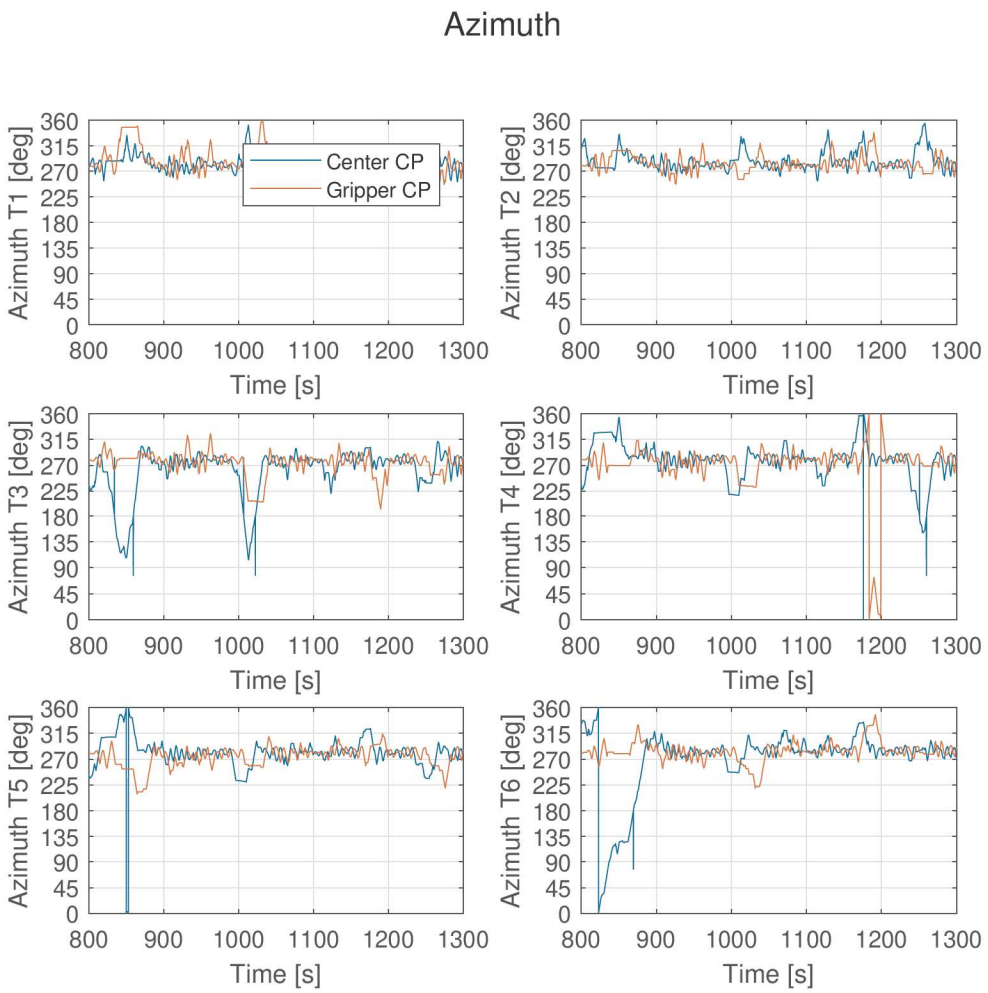

Figure E.8: Azimuth of thrusters during 1h time domain simulation in Hs = 2.0m, wavedir. = 135 deg and Tp = 8s; results obtained at t = [800 1300]

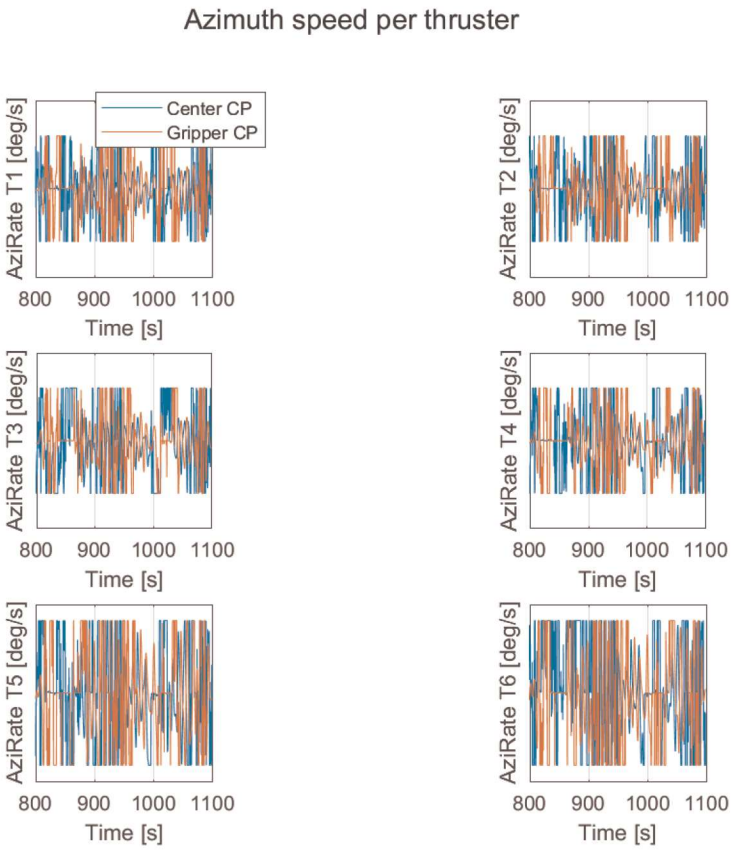

Figure E.9: Azirate of thrusters during 1h time domain simulations, with sea state Hs = 2.0m, 135deg, Tp = 8s - Results obtained at t = [800 1100]

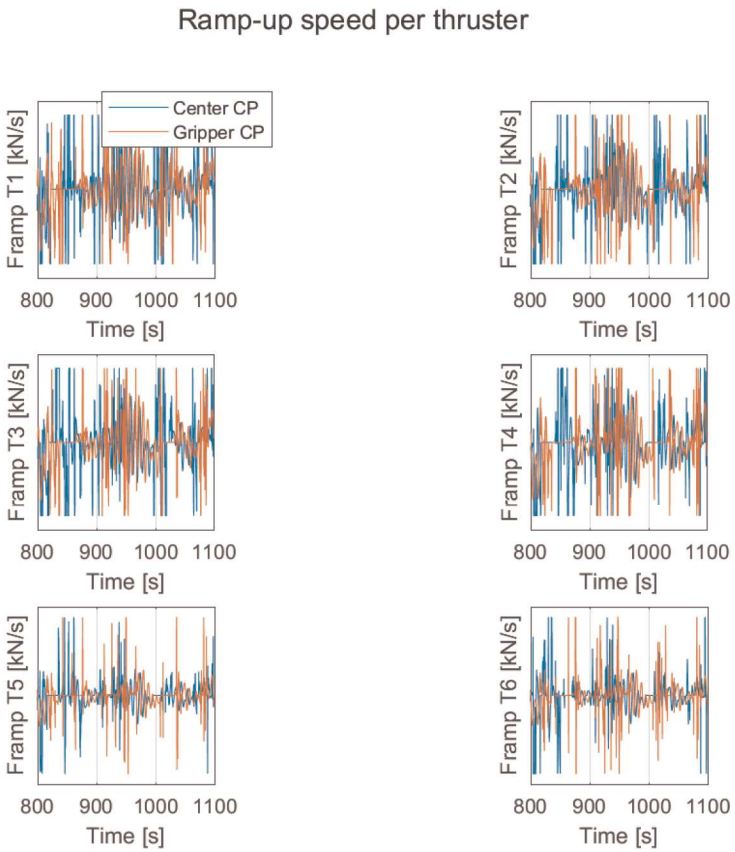

Figure E.10: Ramp up speeds of thrusters during 1h time domain simulations, with sea state Hs = 2.0m, 135deg, Tp = 8s - Results obtained at t = [800 1100]

F

Thruster location overview

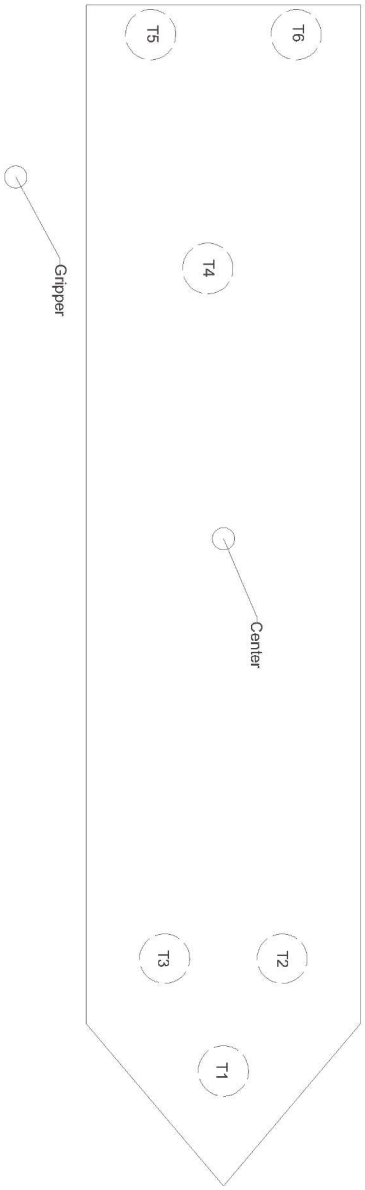

Figure F.1: Thruster layout Aegir

G

Potential theory

G.1. Potential theory

Potential theory is a commonly used theory for problems related to a vessel its dynamic behaviour in waves, with (most of the time) sufficient accuracy for engineering purposes. However, because of the simplifying assumptions in some cases we need to complement the results by adding the effects of viscosity [17]. This section gives an introduction on the concept of the fluid potential and how the hydrodynamic coefficients can be obtained from it. The theory presented here is obtained from the book of Journée and Massie [7].

G.1.1. The fluid potential

In order to describe the fluid flow that is associated with the waves and the motion of the vessel in waves, the pressure of the fluid and its velocity needs to be determined. A velocity potential of a flow, is a mathematical expression or function, which has the property that the derivative of this function at a given point in a certain direction equals the velocity component at that given point in that certain direction. The upcoming section will discuss the concept of this velocity potential.

The first assumption that should be made to apply potential theory, is that the considered flow is in-compressible, which means that the density is assumed to be constant. This assumption leads to a simplification of the mass-conservation statement and turns it into the continuity condition:

$$\frac{\partial u}{\partial x} + \frac{\partial v}{\partial y} + \frac{\partial w}{\partial z} = 0 \tag{G.1}$$

or:

$$\nabla \cdot \mathbf{v} = 0 \tag{G.2}$$

Another assumption that must be made, is that the flow is irrotational, hence:

$$\nabla \times \mathbf{v} = 0 \tag{G.3}$$

Under this assumption, the fluid *potential* $\Phi(t, x, y, z)$ can be defined as a scalar function of position and time. Which means that the velocities can be defined as:

$$u = \frac{\partial \Phi}{\partial x},\ v = \frac{\partial \Phi}{\partial y},\ w = \frac{\partial \Phi}{\partial z} \tag{G.4}$$

or

$$\mathbf{v} = \nabla \Phi \tag{G.5}$$

By using the potential as stated here and substituting it into the Equation G.2, the continuity equation becomes the Laplacian of the potential:

$$\nabla^2 \Phi = \frac{\partial^2 \Phi}{\partial x^2} + \frac{\partial^2 \Phi}{\partial y^2} + \frac{\partial^2 \Phi}{\partial z^2} = 0 \tag{G.6}$$

Together with the Continuity Equation (see Eq. G.2), the conservation of momentum statement form the so-called Navier-Stokes equations:

$$\rho\left(\frac{\partial \mathbf{v}}{\partial t} + \mathbf{v} \cdot \nabla \mathbf{v}\right) = \rho \mathbf{F} - \Delta p + \mu \nabla^2 \mathbf{v} \tag{G.7}$$

Wherein $\mathbf{F} = [0, 0, -g]^T$ are accelerations due to volumetric forces, $p = p(\mathbf{x}, t)$ is the pressure and μ is the viscosity coefficient of the fluid. The Navier-Stokes equations are certain partial differential equations which describe the motion of viscous fluids. However, solving this set of nonlinear, partial differential equations that are formed by Equations G.2 and G.7 is still yet unfeasible. Therefore, the assumption is commonly made to neglect the viscosity, since viscosity is only of importance in the boundary layer of the vessel. By neglecting viscosity, one can disregard the last term of Equation G.7, which results in the *Euler Equations*:

$$\rho(\frac{\partial \mathbf{v}}{\partial t} + \mathbf{v} \cdot \nabla \mathbf{v}) = \rho \mathbf{F} - \Delta p \tag{G.8}$$

The potential can now be calculated by solving the *Laplace Equation* in Equation G.6. This equation can be solved by applying the appropriate boundary conditions, hence it becomes a boundary value problem. With the potential known, the velocities can be calculated. As stated before, to describe the fluid flow the velocities and the pressures need to be calculated. Once the potential is found, the pressure can be calculated by using the Euler Equation, as presented in Equation G.8. Some mathematical manipulation of this equation leads to the Bernoulli equation:

$$\frac{p}{\rho} + \frac{\partial \Phi}{\partial t} + \frac{1}{2}(\mathbf{v})^2 + gz = C \tag{G.9}$$

G.1.2. Boundary conditions

The linear fluid potential that is considered for problems related to a vessel its dynamic behaviour can be seen as a superposition of three potentials:

$$\Phi(x, y, z, t) = \Phi_r + \Phi_w + \Phi_d \tag{G.10}$$

Wherein Φ_r is the radiation potential from the motions of the body in still water, Φ_w is the undisturbed incoming wave potential and Φ_d is the diffraction potential of the waves about the restrained body. Each part of the fluid potential needs to be solved using appropriate boundary conditions. This subsection discusses the applicable boundary conditions to solve the wave potential and the eventual solutions to it.

Continuity condition and Laplace equation

This boundary condition was already introduced in Section G.1.1. It means that under the assumption of the fluid to be incompressible, the Continuity Condition (Eq. G.2) results in the Laplace Equation for potential flows (Eq. G.6).

Sea Bed Boundary Condition

The Sea Bed Boundary Condition states that the vertical velocity of water particles at the seabed is zero:

$$\frac{\partial \Phi}{\partial z} = 0, \quad at\ z = -h \tag{G.11}$$

Wherein h is the water depth.

Free Surface Dynamic Boundary Condition

The Free Surface Dynamic Boundary Condition states that the pressure, p, at the free surface of the fluid ($z = \zeta$), is equal to the atmospheric pressure p_0. This leads to a simplification of the Bernoulli Equation, which will be repeated here in a more general form for clarity:

$$\frac{\partial \Phi}{\partial t} + \frac{1}{2}(u^2 + v^2 + w^2) + \frac{p}{\rho} + gz = C \tag{G.12}$$

An assumption that needs to be made when applying potential theory to ocean waves, is that the slopes of the waves are very small. As a result of the very small slopes assumption, terms in the order of the steepness squared can be neglected. Hence, u,v and w become very small. The constant values, $p_0/p - C$ can be included in $\frac{\partial \Phi}{\partial t}$ without influencing the obtained velocities, which leads to a simplified Bernoulli equation at the free surface:

$$\frac{\partial \Phi}{\partial t} + g\zeta = 0, \quad or\ \frac{\partial^2 \Phi}{\partial t^2} + g\frac{\partial \zeta}{\partial t} = 0, \quad at\ z = \zeta \tag{G.13}$$

Wherein ζ represents the wave elevation. As a result from the fact that the elevation ζ is relatively small, this condition also applies at the sea bed (z=0) and this yields to the linearized form of the free surface boundary condition:

$$\frac{\partial \Phi}{\partial t} + g\zeta = 0, \quad at\ z = 0 \tag{G.14}$$

Kinematic Boundary Condition
The kinematic boundary condition (or: no leak condition) arises from the assumption that the velocity of a water particle at a surface transition equals the velocity of that surface. For waves at the free surface, this means that the vertical velocity of a water particle at the free surface equals the vertical velocity of the free surface itself. The expression for this boundary condition at the free surface is:

$$\frac{\partial \Phi}{\partial z} = \frac{\partial \zeta}{\partial t}, \quad at\ z = \zeta \tag{G.15}$$

This also applies at the sea bed, at $z = 0$, instead of $z = \zeta$ The same boundary condition can be applied at the surface of a body. Hence, the velocity of a water particle at a given point at the surface of a body equals the velocity of this point of the body itself. Mathematically, this can be defined as:

$$\frac{\partial \Phi}{\partial n} = v_n(x, y, z, t) \tag{G.16}$$

Since the The above boundary conditions are sufficient to solve the undisturbed incoming wave potential Φ_w, however two additional boundary conditions are necessary to solve the radiation potential Φ_r.

Radiation Condition
The radiation conditions follows from the assumption that as distance R, away from the oscillating body becomes large, the potential value goes to zero:

$$\lim_{R \to \infty} \Phi = 0 \tag{G.17}$$

Symmetric or Anti-symmetric condition
Since vessels tend to be symmetric with respect to the middle longitudinal plane, one can use this to simplify the potential equations even further:

$$\begin{aligned} \Phi_2(-x, y) &= -\Phi_2(x, y) \\ \Phi_3(-x, y) &= +\Phi_3(x, y) \\ \Phi_4(-x, y) &= -\Phi_4(x, y) \end{aligned} \tag{G.18}$$

G.1.3. Forces and Moments

The hydrodynamic pressures on the surface of the body can be obtained from the linearized Bernoulli equation, using the known velocity potentials. Integration of these pressures in the required direction provides the hydrodynamic force or moment. The forces F and moments M can be obtained by integrating the pressure p over the submerged part of the hull of the vessel S:

$$\begin{aligned} \mathbf{F} &= -\iint_S (p \cdot \mathbf{n}) \cdot dS \\ \mathbf{M} &= -\iint_S p \cdot (\mathbf{r} \times \mathbf{n}) \cdot dS \end{aligned} \tag{G.19}$$

Wherein n is the normal vector that points outwards and r is the position vector to the surface. The pressure p, can be calculated by using the linearized Bernoulli equation as presented in Equation G.13 and can be split into four parts:

$$\begin{aligned} p &= -\rho \frac{\partial \Phi}{\partial t} - \rho g z \\ &= -\rho \left(\frac{\partial \Phi_r}{\partial t} + \frac{\partial \Phi_w}{\partial t} + \frac{\partial \Phi_d}{\partial t} \right) - \rho g z \end{aligned} \tag{G.20}$$

The total forces and moments can therefore be defined as:

$$\begin{aligned} F &= F_r + F_w + F_d + F_s \\ M &= M_r + M_w + M_d + M_s \end{aligned} \tag{G.21}$$

Where F_r and M_r are induced by waves radiated from the oscillating vessel in still water, F_w and M_w are the forces and moments due to waves that approach the vessel, F_d and M_d are due to diffracted waves on the vessel and F_s and M_s are induced by hydrostatic buoyancy in still water.

G.1.4. Wave and diffraction loads

The wave and diffraction terms (Φ_w and Φ_d) can be treated together. Following the method as presented in Section G.1.3, the wave and diffraction loads can be defined by:

$$F_w + F_d = \rho \iint_S \left(\frac{\partial \Phi_w}{\partial t} + \frac{\partial \Phi_d}{\partial t} \right) n \cdot dS \tag{G.22}$$

and:

$$M_w + M_d = \rho \iint_S \left(\frac{\partial \Phi_w}{\partial t} + \frac{\partial \Phi_d}{\partial t} \right) (r \times n) \cdot dS \tag{G.23}$$

For wave and diffraction loads, a restrained vessel is considered with zero forward speed. The kinematic boundary condition (Eq. G.16) for this case therefore simplifies to:

$$\frac{\partial \Phi}{\partial n} = \frac{\partial \Phi_w}{\partial n} + \frac{\partial \Phi_d}{\partial n} = 0 \tag{G.24}$$

Hence:

$$\frac{\partial \Phi_w}{\partial n} = -\frac{\partial \Phi_d}{\partial n} \tag{G.25}$$

When considering regular waves, the linear fluid potential can be written as a space-dependent part, $\phi(x, y, z)$, multiplied by a normalized oscillating velocity, $v(t) = e^{-i\omega t}$, here written in complex form:

$$\Phi(x, y, z, t) = \phi(x, y, z) \cdot e^{-i\omega t} \tag{G.26}$$

A more convenient formulation for the space-dependent potential can be obtained by writing:

$$\phi = -i\omega \sum_{j=0}^{7} \phi_j \zeta_j \tag{G.27}$$

Wherein $j = 0$ is the undisturbed incoming wave, $j = 1,..6$ are the modes of motion of the vessel and $j = 7$ represents the diffracted wave. ζ_j represents the wave elevation for ϕ_0 and ϕ_7, and the motion amplitude of the vessel for $\phi_1, ...\phi_6$.

The space-dependent part of the undisturbed incoming (regular, long-crested) wave potential, ϕ_0, can be defined as:

$$\phi_0 = \frac{\zeta_0 g}{\omega} \cdot \frac{coshk(h_0 + z)}{coshkh} \cdot e^{ik(xcos\mu + ysin\mu)} \tag{G.28}$$

The fluid pressure can be found, by substituting the potential into the Bernoulli equation:

$$\begin{aligned} p(x, y, z; t) &= -\rho \frac{\partial \Phi}{\partial t} \\ &= \rho\omega^2 \left\{ (\phi_0 + \phi_7)\zeta_0 + \sum_{j=1}^{6} \phi_j \zeta_j \right\} \cdot e^{-i\omega t} \end{aligned} \tag{G.29}$$

As a result of this, the first order wave exciting forces and moments in the k-direction, can be defined as follows:

$$\begin{aligned} X_k &= -\iint_{S_0} p n_k \cdot dS_0 \\ &= -\rho\omega^2 e^{-i\omega t} \iint_{S_0} (\phi_0 + \phi_7) n_k \cdot dS_0 \end{aligned} \tag{G.30}$$

Where S_0 is the mean wetted surface of the vessel and n_k are the direction cosine of surface element dS_0 for the *k-mode* of motion. The generalised direction cosines on S_0 are defined as:

$$\begin{aligned} n_1 &= cos(n,x) \\ n_2 &= cos(n,y) \\ n_3 &= cos(n,z) \\ n_4 &= yn_3 - zn_2 \\ n_5 &= zn_1 - xn_3 \\ n_6 &= xn_2 - yf_1 \end{aligned} \tag{G.31}$$

G.1.5. Hydrodynamic Loads

The *hydrodynamic loads* are the loads induced by the fluid that surrounds the oscillating vessel in still water. When the vessel oscillates, waves radiate away from the vessel and take energy from the system. Just like the representation of the total motion, that is a linear superposition of the 6 ship motions, the fluid motions that each of the 6 ship motions induces can be represented as a superposition of 6 radiation potentials:

$$\begin{aligned} \Phi_r(x,y,z,t) &= \sum_{j=1}^{6} \Phi_j(x,y,z,t) \\ &= \sum_{j=1}^{6} \Phi_j(x,y,z) \cdot e^{-i\omega t} \end{aligned} \tag{G.32}$$

Where in the second part of this equation, the space and time dependent potential is again split up in a separate space dependent potential $\phi_j(x,y,z)$ and an oscillatory velocity $v_j(t)$ in the j-direction. Following Equation G.21, the hydrodynamic forces and moments become:

$$F_r = \rho \iint_S (\frac{\partial \Phi_r}{\partial t}) n \cdot dS \tag{G.33}$$

and:

$$M_r = \rho \iint_S (\frac{\partial \Phi_r}{\partial t})(r \times n) \cdot dS \tag{G.34}$$

Following the same method as in Section G.1.4, the oscillating hydrodynamic forces and moments in the *k-direction* are defined as:

$$\begin{aligned} F_k &= -\iint_{S_0} p n_k \cdot S_0 \\ &= -\rho\omega^2 \sum_{j=1}^{6} \zeta_j e^{-i\omega t} \iint_{S_0} \phi_j n_k \cdot dS_0 \end{aligned} \tag{G.35}$$

The hydrodynamic loads can be split into a part which is in phase with acceleration of the velocity, the hydrodynamic mass (or added mass) a_{kj} and a part that is in phase with the velocity of the oscillation, the damping b_{kj}:

$$\begin{aligned} a_{kj} &= -\Re e\left[\rho \iint_{S_0} \phi_j n_k \cdot dS_0\right] \\ b_{kj} &= -\Im m\left[\rho\omega \iint_{S_0} \phi_j n_k \cdot dS_0\right] \end{aligned} \tag{G.36}$$

With symmetry:

$$\begin{aligned} a_{kj} &= a_{jk} \\ b_{kj} &= b_{jk} \end{aligned} \tag{G.37}$$

G.1.6. Hydrostatic loads

The hydrostatic loads are determined by a simple integration of the static pressure:

$$F_s = \rho g \iint_S zn \cdot dS \tag{G.38}$$

and:

$$M_s = \rho g \iint_S z(r \times n) \cdot dS \tag{G.39}$$

G.1.7. Solving potentials

The incoming undisturbed wave potential(ϕ_0) is already known, but a solution to the remaining 7 potentials is still needed. An important result from the previous derivations is that expressions are found, which are independent of time. According to literature ([7] and [36]) the potential ϕ_j at a point (x,y,z) on the vessel its wetted surface, due to a motion in mode j (*j=1,..6*) and the diffraction potential, can be described by a continuous distribution of single sources:

$$\phi_j(x,y,z) = \frac{1}{4\pi} \iint_{S_0} \sigma_j(\hat{x},\hat{y},\hat{z}) \cdot G(x,y,z,\hat{x},\hat{y},\hat{z}) \cdot dS_0 \quad j = 1,..7 \tag{G.40}$$

Wherein ϕ_j is the space-dependent term of the potential function at a given point *(x,y,z)* on the mean wetted surface S_0 on the vessel. $j = 1,..6$ refers to the mode of motion of the vessel and $j = 7$ refers to the diffracted wave.
$\sigma_j(\hat{x},\hat{y},\hat{z})$ represents a source of strength σ at location $(\hat{x},\hat{y},\hat{z})$ on the mean wetted surface of the vessel, S_0, due to a motion of the vessel in the j^{th} *mode*.
At last, $G(x,y,z,\hat{x},\hat{y},\hat{z}$ represents *Green's function* of the 'pulsating' source, $\sigma(\hat{x},\hat{y},\hat{z})$, which is located at a point $(\hat{x},\hat{y},\hat{z})$, with the potential ϕ_j being evaluated at a point (x,y,z).

The boundary condition for the potential, Φ, results in similar conditions for the space dependent terms ϕ. The unknown source strengths are obtained as a result of the kinematic boundary condition:

$$\begin{aligned} \frac{\partial \phi_j}{\partial n} &= n_j \\ &= -\frac{1}{2}\sigma_j(x,y,z) + \frac{1}{4\pi} \iint_{S_0} \sigma_j(\hat{x},\hat{y},\hat{z}) \cdot \frac{\partial G(x,y,z,\hat{x},\hat{y},\hat{z})}{\partial n} \cdot dS_0 \end{aligned} \tag{G.41}$$

Solving Equations G.41 and G.40 will eventually lead to the added mass and damping coefficients and the wave forces. At last, the motions ζ_j can be obtained by solving the following equation of motion:

$$\sum_{j=1}^{6} \{ -\omega^2(m_{kj} + a_{kj}) - i\omega b_{kj} + c_{kj} \} \cdot \zeta_j = X_k \qquad k = 1,..6 \tag{G.42}$$

G.2. Second order wave drift forces

As mentioned before, the most relevant forces for this study are the low frequency or second order wave drift forces. As mentioned in section 2.2 the second order wave drift forces are calculated using WAMIT, which is based on first and second order potential theory. As the first order terms were explained in the previous section, the second order forces will be discussed in this section.
WAMIT calculates the expressions for the first- and second-order forces are derived from direct integration of the fluid pressure over a body boundary [37]. The deduction of the equations is shown here. Just as when determining the hydromechanic coefficients in the previous section, the fluid domain is bounded by the surface of the vessel, the free sea surface, the seabed and the radiation condition. The fluid is inviscid, irrotational, homogeneous and incompressible. Hence, the fluid motion can be described as:

$$\Phi = \epsilon\Phi^{(1)} + \epsilon\Phi^{(2)} + O(\epsilon^3) \tag{G.43}$$

Wherein $\Phi^{(1)}$ is already defined in Equation G.10. $\Phi^{(2)}$ can be defined as the sum of the second-order equivalents of the first-order diffraction potential and undisturbed incoming wave potential:

$$\Phi^{(2)} = \Phi_d^{(2)} + \Phi_w^{(2)} \tag{G.44}$$

The fluid pressure, can be calculated using the full Bernoulli equation (see Equation G.12). Unlike the first order potential method, the second order terms are not neglected anymore. The full Bernoulli is repeated here for clarity:

$$\begin{aligned} p &= -\rho\frac{d\Phi}{dt} - \frac{1}{2}\rho\nabla\Phi\cdot\nabla\Phi - \rho g z \\ &= p^{(0)} + p^{(1)} + p^{(2)} + O(\epsilon^3) \end{aligned} \tag{G.45}$$

Wherein $p^{(0)}$ is the hydrostatic part and $p^{(1)}$ is the first order pressure. These were already discussed in the previous sections. When considering the second order pressure part, $p^{(2)}$ it applies that:

$$p^{(2)} = -\frac{1}{2}\rho(\vec{\nabla}\Phi^{(1)})^2 - \rho\frac{\partial^2\Phi^{(2)}}{\partial t^2} - \rho(\vec{X}^{(1)}\cdot\vec{\nabla}\frac{\partial\Phi^{(1)}}{\partial t}) \tag{G.46}$$

And the forces are calculated again by integrating the pressures, in the same manner as presented in Equation G.19. From this follows that:

$$\begin{aligned} \vec{F}^{(2)} = &-\int\int_{S_0}(p^{(1)}\cdot\vec{N}^{(1)}\cdot dS - \int\int_{S_0}(p^{(2)}\cdot\vec{n})\cdot dS \\ &-\int\int_{S}(p^{(0)}\cdot\vec{N}^{(1)})\cdot dS - \int\int(p^{(}1)\cdot\vec{n})\cdot dS \end{aligned} \tag{G.47}$$

Without going into further more detail, the total second order fluid force is defined as:

$$\begin{aligned} \vec{F}^{(2)} &= m\cdot R^{(1)}\cdot\ddot{\vec{X}}_G^{(1)} \\ &+\int\int_{S_0}\left\{\frac{1}{2}\rho(\vec{\nabla}\Phi^{(1)})^2 + \rho\frac{\partial\Phi^{(2)}}{\partial t} + \rho\vec{X}^{(1)}\cdot\vec{\nabla}\frac{\partial\Phi^{(1)}}{\partial t}\right\}\cdot\vec{n}\cdot dS \\ &-\oint\frac{1}{2}\rho g(\zeta_r^{(1)})^2\cdot\cdot\vec{n}\cdot dl \end{aligned} \tag{G.48}$$